The Effects of Annual Extreme Weather Conditions on the Exchange Flows between Lake Bardawil and the Mediterranean Sea

by

Philipp Bangen

TU Delft

the WEATHER MAKERS holistic engineering

DEME

Dredging, Environmental & Marine Engineering

in partial fulfillment of the requirements for the degree of

Master of Science (M.Sc.)
in Civil Engineering

by
Philipp Bangen
5022045

at
Delft University of Technology
Delft, The Netherlands

30 November 2021

A thesis conducted in:
Department of Coastal Engineering
Faculty of Civil Engineering
Delft University of Technology

Committee:

Prof. dr. ir. S.G.J. (Stefan) Aarninkhof	TU Delft
Dr. ir. Judith Bosboom	TU Delft
Prof. dr. Peter Herman	TU Delft
Ir. Rick van Bentem	The Weather Makers
Ir. Merel Kroeders	DEME Group

Abstract

Lake Bardawil is a hypersaline, shallow coastal lagoon located along the coast of the northern Sinai Peninsula in Egypt. Coastal systems are understood to be hypersaline when the salinity exceeds values of 30 parts per thousand throughout the year.

Being located in the arid climate region of North Africa the lagoon is subject to year-round extreme weather conditions which are dominated by high air temperatures, extreme evaporation rates, and limited precipitation. All the above in combination with the lagoon's shallow bathymetry and restricted freshwater input causes Lake Bardawil to inhibit hypersaline conditions throughout the whole year. For Lake Bardawil this means average salinity values in the order of 42 – 51 parts per thousand.

The here conducted study is the first in the line of five successive studies focusing on three-dimensional hydrodynamics. Making use of the three-dimensional hydrodynamics, the movement of the water and salt through the lagoon is considered. Here the response of the system to the extreme meteorological conditions around Lake Bardawil is investigated. The meteorological forcing causes subtidal flows in coastal waters which are responsible for the propagation of waterborne materials such as salt and pollutants.

The results show that during periods of extreme meteorological forcing the response of the lagoon and its inlets is in line with expectations one might have from literature. During periods and events of high evaporation, the lagoon shows an overall increase in top and bottom layer salinity. Furthermore, the largest compensation flow due to evaporative losses of approximately *34* m^3/s from the Mediterranean Sea into the lagoon is observed. While the lagoon waters act rather inert as shown for the average conditions during the month of April, it is the wind that initiates the motion. Successively the phenomenon of gravitational circulation in the deeper areas around the inlets can be observed with more saline waters propagating towards the inlets, along the bottom layer. At times, these processes cause subtidal velocities up to *0.15 m/s*, which were computed in the inlets.

Crucial for the overall response of Lake Bardawil to meteorological forcing is the complex lagoon geometry and shallowness. Here the tidal divide, on the verge of the western bottleneck to the eastern basin is found to be of great importance. At this location very calm flow conditions are present promoting stagnant waters. The eastern basin with its vast areal extent experiences wind-driven circulations, while the western bottleneck is bound by its narrowness and tide dominance. As a consequence, the western inlet Boughaz 1 can be described as continuously well-mixed, while its eastern counterpart, Boughaz 2, experiences periodic stratification.

The application of system adaptations as proposed by The Weather Makers (TWM) proves to increase the exchange flow with the Mediterranean Sea. Here the dredging of two new inlets as well as dedicated tidal gullies through the lagoon established a more dynamic system where the inner lagoon connectivity is significantly enhanced. This is evident by the widespread presence of Mediterranean waters and the decreased salinity in a broad stretch along the barrier island as well as on the full lagoon scale. However, the lagoon waters in remote locations along the fringes of the large eastern basin remain of high salinity and show still little interaction with the tidal flow.

Acknowledgments

As this work concludes my studies at the TU Delft, I would like to thank all the people that made it possible.

Over the past nine months these were the members of my committee. Here I would like to thank Prof. Stefan Aarninkhof, Dr. Judith Bosboom, Prof. Peter Herman, Merel Kroeders and Rick van Bentem. During these months they gave me guidance and support when it came to tough decisions and the progress of my report. Even with the small bumps towards the end and the close green light decision I felt supported and want to thank everybody by heart for making this research possible and supporting the project.

A special thanks I would like to direct to Rick, who was at any point in time a great help and gave me the right direction and feedback that I needed. Also, I would like to thank the whole team of The Weather Makers for welcoming me in their middle and sharing their stories, knowledge, and ideas with me. Being part of this small and ambitious group of creative minds made the whole experience a joyful ride. I hope we see each other in the future and stay connected.

Furthermore, I would like to thank my family and friends. My parents for their unconditional support over the past six years in academia and for providing me the tranquility one needs when working on something that big for so long.

My friends for taking my mind off things and being aware of the other things out there. Special thanks here go to Peter, Fabian, Julian & Alon from back home, as well as Jessie, Lukas & Robert in Hamburg. Last but not least, much love to Dan, Flo, Rike, Freek & Shawn, and everybody else out there who at times joined me on this last ride.

List of Figures

List of Tables

Contents

1 | Introduction

Lake Bardawil is a hypersaline, shallow coastal lagoon located along the northern coast of the Sinai Peninsula in Egypt. It is connected to the Mediterranean Sea by two artificial inlets which are maintained open by reoccurring dredging operations. Further one natural inlet exists along the eastern end which is silted up during most of the time (Khalil and Shaltout 2006). This region is according to the Köppen-Geiger climate classification model part of the arid climate region of north Africa (Beck et al. 2018). More precisely it can be classified as a BWh climate, where the Mean Annual Temperature (MAT) is higher than 18°C and the Mean Annual Precipitation (MAP) is lower than 5 times $P_{threshold}$. The threshold in precipitation $P_{threshold}$ is defined as two times the MAT for regions where more than 70% of the rain falls during winter (Beck et al., 2018). Since for Lake Bardawil, the precipitation is bound to the winter months, this classification applies (Euroconsult, 1995; Khalil and Shaltout, 2006; Linnersund and Mårtensson, 2008).

For the region around Lake Bardawil the values are *MAT = 21 °C*, *MAP = 100 mm*, and $P_{threshold} = 42$, obtained from the Meteoblue climate data as well as literature sources (Euroconsult, 1995; Linnersund and Mårtensson, 2008).

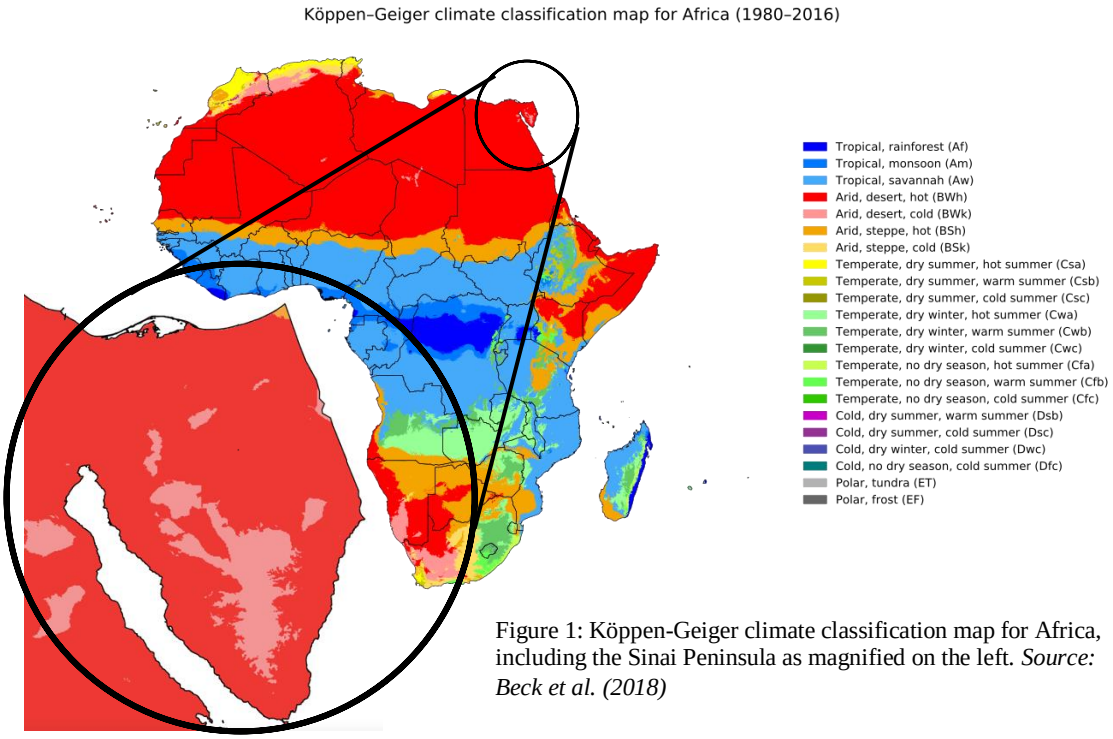

Figure 1: Köppen-Geiger climate classification map for Africa, including the Sinai Peninsula as magnified on the left. *Source: Beck et al. (2018)*

1.1 Problem Description

According to the Köppen-Geiger climate model, Lake Bardawil is subject to continuous high air temperatures and evaporation rates (Ellah and Hussein, 2009). At the same time, the lagoon and its inlets are prone to closure by sedimentation and are subject to regular dredging operations to maintain the exchange between the lagoon and the Mediterranean Sea. Subsequently, the migration of fish in and out of the lagoon is maintained (Abdel-Fattah, Bek, and Negm, 2019; Ellah and Hussein, 2009; Khalil and Shaltout, 2006). The latter is one of the main economic resources of the people living around Lake Bardawil (Lanters, 2016). However, the very shallow bathymetry present in the lagoon ($d_{mean} = 1.3\ m$) causes the tidal flows to dissipate quickly upon entering the lagoon, and very little interaction between the vast volumes of lagoon waters and the Mediterranean waters is observed (van Bentem, 2020; Linnersund and Mårtensson, 2008).

All the above cause for favorable conditions of hypersalinity throughout the whole year with average salinities ranging from *42 – 51 part per thousand (ppt)* and peak salinity values up to *71 ppt* being reached in the summer months of July and August (Egyptian Environmental Affairs Agency (EEAA), 2016; Ellah and Hussein, 2009). This year-round hypersalinity is unfavorable for the fish population and rejuvenation within the lagoon and therewith for the whole ecosystem. As a consequence, of this in combination with overfishing, the fish production at Lake Bardawil decreased drastically over the last decades (El-Shabrawy and Bek, 2019). Lanters (2016) describe this combination of ecological degradation and the lack of economic resources for the communities around Lake Bardawil as “an ecosystem in collapse”.

To stop this collapse from happening and to facilitate the turn-around of the ecosystem, The Weather Makers (TWM) in cooperation with DEME aim to increase the interaction between the Mediterranean Sea and Lake Bardawil with tailor-made engineering solutions by mimicking nature.

Part of this plan is to decrease the overall lagoon salinity which acts as a major constraint for the natural progression of biodiversity and primary production in the lagoon (Khalil and Shaltout, 2006). However, the scarcity of research concerning the three-dimensional hydrodynamics and distribution and propagation of salinity throughout the lagoon and its inlets makes predictions difficult. Furthermore, the effects of annual extreme weather conditions on the lagoon hydrodynamics and the fluxes of waterborne properties such as salinity are not yet well understood. To make sound statements about the effects of interventions on the salinity and therewith on the ecological value of the system, the abovementioned effects of present weather conditions are crucial to be understood.

1.2 Research Objective

The presented work is part of a greater research project carried out by TWM. The scope of this project includes the restoration of Lake Bardawil as a tidal lagoon and establishing a healthy ecosystem that acts as a transitional zone between the Sinai Peninsula and the Mediterranean Sea. Furthermore, it should act, again, as an economic resource for the people living around it. On top of the restoration of the Lake Bardawil ecosystem, the project by TWM and DEME aims at a larger scope to regreen the northern Sinai Peninsula and establish a green and flourishing landmark.
To achieve this goal TWM introduced a 5-step plan in which, using holistic engineering, smart and innovative actions are taken. These steps are

1) the restoration of the aquatic ecosystem of Lake Bardawil, using dedicated dredging interventions to enhance the exchange flows with the Mediterranean Sea
2) the restoration of the wetlands, through (re-)introduction of dehydrated wetlands and salt-tolerant vegetation
3) the reuse of marine sediments, utilizing organic-rich material for fertile soils, cohesive materials for structural works, and granular materials for coastal reinforcement
4) the re-greening of the desert, using freshwater input into the system, and the creation of micro-climates with innovative approaches
5) the restoration of the watershed, by the combined effect of the above-mentioned steps in combination with the choice of strategic deployment locations.

As mentioned before, this research is part of the greater project and will focus on the restoration of the aquatic ecosystem using a three-dimensional hydrodynamic model. It is a follow-up study in the line of hydrodynamic research that has been carried out along the course of the project by van Bentem (2020), Georgiou (2019) & Lanters (2016).
Lanters (2016) looked at the interaction between the lagoon hydrodynamics and the stimulation of fish population to tip over the first stone to natural restoration. The studies by Georgiou (2019) and van Bentem (2020) focused on the tidal inlets, where the former introduced an innovative tidal inlet design to mimic nature and the latter investigated the tidal inlet stability of the current inlets as well as the adapted system according to the innovative tidal inlet design.

As mentioned in the general problem description, little is known about the three-dimensional hydrodynamics and salinity distribution and how they are affected by the occurrences of extreme annual weather conditions such as extreme evaporation periods and stronger wind

conditions. On this matter, Winant and Gutiérrez de Velasco (2003) mentioned the "exist[ence of] a flux of salt toward the ocean, comparable to the flux of salt into the lagoon due to [persistent] evaporation" in the hypersaline, coastal lagoon Laguna San Ignacio in Mexico.
To gain first insight into the hydrodynamic processes and the movement of salt in the lagoon, this research will focus on exactly these periods throughout the year to quantify their effect on the inlet and lagoon hydrodynamics and the salinity distribution in Lake Bardawil. These two parameters are linked by the subtidal flows, which are initiated by non-tidal forcing. This includes the wind-driven and density-driven components. By this, the assessment will provide insight into the dependence between the salinity flows and distribution over the greater lagoon area and the present weather conditions.

The presented research will give insight into the three-dimensional hydrodynamics of a hypersaline, shallow coastal lagoon located in the arid climate region along the north African coast of the Mediterranean Sea. Comparable systems around the world have been subject to hydrodynamic investigations, predominantly focusing on 1D-longitudinal transects, the mere effect of general hydrodynamics on the ecological indicators such as the lagoon flushing rate or using measurement campaigns (David and Kjerfve, 1998; Webster, 2010; Winant and Gutiérrez de Velasco, 2003). Thus, this study takes the next step when modeling the three-dimensional behavior of such systems.
By understanding the way water and salt move through the system, this research will answer the below posed research questions and contributes to closing the knowledge gap on the three-dimensional analysis of hypersaline and shallow coastal lagoons.

1.3 Research Questions

As mentioned above, this study aims at answering the following research questions:

"**How do annual extreme weather conditions affect the subtidal flows present in hypersaline and shallow coastal lagoons using the example case of Lake Bardawil?**"

The following sub-questions are answered to build up the research and to answer the above state question.

- What are the dominant forcing terms for subtidal flows?
- How are the subtidal flows affected by annual extreme weather conditions?
- What are the time scales at which meteorological forcing affects the lagoon hydrodynamics and salinity distribution?
- How is the state of the inlets affected by extreme weather conditions?
- What is the effect of proposed system adaptations on the exchange flows between Lake Bardawil and the Mediterranean Sea during the average conditions (April)?

1.4 Methodology

To investigate the effects of extreme annual weather conditions on the system of Lake Bardawil the study will focus on the subtidal flows and the distribution of salinity in the system. These flows are assumed to affect the residual circulation and thus the circulation of salt inside the lagoon. Further, they are expected to affect the exchange with the shelf sea.

Background study

Before determining the input parameters for the modeling campaign, a thorough investigation of the present data is carried out. This includes an extensive literature study of the current state of knowledge on the system and the available data. In previous studies, the scarcity of available data on the system of Lake Bardawil was mentioned. During the course of this study, it was not yet possible to obtain new data which would improve the detail of this study. Thus, the data review combined previously mentioned data with new findings from the literature. Overall, the scarcity of in-situ data poses difficulties in the model setup and validation.

Research approach

To tackle the above-posed research questions, this study will follow the path as outlined in Figure 2, where the different steps are shortly summarized. As the foundation of this research, a 3D hydrodynamic model is developed in D-Flow FM, which builds upon the 2DH model set up by van Bentem (2020). This model was already further developed in the framework of the research project by TWM; thus, the newest version will be used.

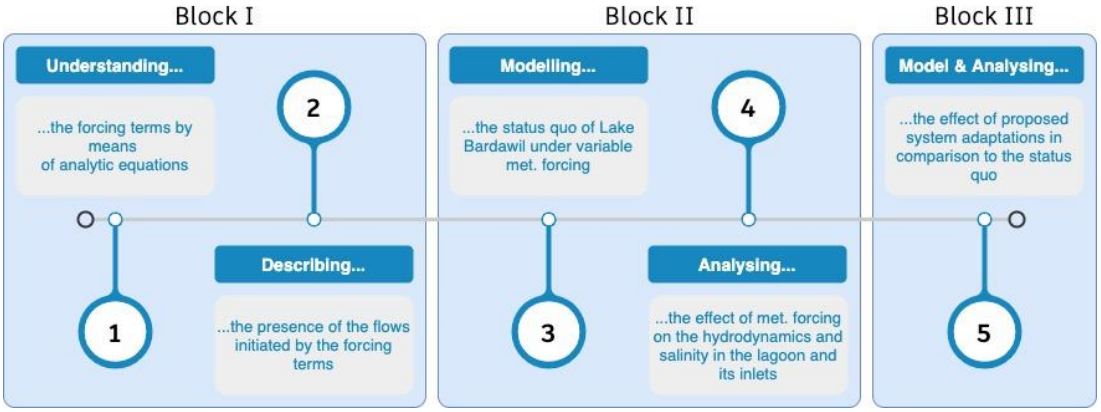

Figure 2: Outline of the research approach

Below a concise description of the different stages and their setting in the larger project is given.

Step 1:

To assess how certain weather events affect the hydrodynamics in the present system of Lake Bardawil, an understanding of the different forcing terms is crucial. This includes the understanding of their theoretical background and how their impact on the system is defined.

Step 2:

Having developed an understanding of the different forcing terms, it is of interest to see how they may affect the three-dimensional system hydrodynamics. By looking at literature, related to the topic of estuarine circulation and residual circulations in coastal waters, a first understanding is derived.

Step 3:

Step 3 of this research involves the setup of a 3D hydrodynamic model of the current state of Lake Bardawil, under variable meteorological forcing using the software package D-Flow FM. The status quo will be assessed by investigating the effect of three distinct weather conditions throughout the year by implementing the current system geometry. The weather conditions to be considered in this study are 1) the annual average conditions (March-April), 2) the annual extreme wind conditions (January-February) and 3) the annual extreme evaporation conditions (July-August).

Step 4:

Step 4 is the analysis and interpretation of the results, obtained from the D-Flow FM model. By looking at the differences in the inlet and lagoon hydrodynamics, conclusions about the effects of the imposed meteorological forcing can be drawn. Further, the inlet and spatial analysis of the lagoon salinity allows for the assessment of how salt propagates in the lagoon.

Step 5:

Step 5 includes the modeling and analysis of the system adaptations, proposed by TWM. Here, the effectiveness of the dedicated dredging interventions is investigated concerning the inlet's hydrodynamics and the overall lagoon salinity distribution.

Validation

A favorable method of validation would be by means of velocity and/or salinity measurements at distinct locations within the lagoon. Comparing the model results with measured data gives a sound idea about the applicability and validity of the model. This was done by Bek and Cowles (2018) using salinity data from the years 1999/2000. Thus, the present model will be validated against the abovementioned model and measurement data as presented in Bek and Cowles (2018).

1.5 Structure of the report

The report is divided into six chapters. Chapter 1 introduces the present research and describes the problem at hand as well as the scientific approach to tackle it.

In Chapter 2 the system of Lake Bardawil is introduced, and a thorough data review is carried out. In addition to that, previous studies regarding Lake Bardawil within the project scope of TWM are summarized, including their main findings.

In Chapter 3 the methodology, including the underlying theory & analytical approach, the key indicators & modeling approach as well as the adaptations of the system geometry, is treated and gives insight into the elements investigated here.

Chapter 4 presents the results from the numerical model for the different simulations. Furthermore, it includes an interpretation of the results based on the underlying theory and knowledge. At last, the validation using the abovementioned data from literature is presented.

Chapter 5 discusses the main points of interest and key indicators. Here a critical discussion regarding the applicability and validity of the chosen approach is carried out.

Chapter 6 concludes this report by answering the research questions and giving recommendations for future research in this field as well as for the system of Lake Bardawil.

2 | Background

2.1 Lake Bardawil: A Unique System

Lake Bardawil is one of the five Egyptian northern coastal lakes, alongside Lake Mariout, Edku, Burullus, and Manzala. Extending from latitude *31°03´ - 31°15´ N* and longitude *32°40´ - 33°32´ E*, Lake Bardawil forms a remarkable feature in the landscape of the northern Sinai Peninsula between the cities of Port Said and El-Arish. Covering a distance of about 80 km along the northern Sinai coast and reaching maximum widths up to 20 km (at the eastern basin), Lake Bardawil covers a total area between *520 km^2* (Ellah and Hussein, 2009) and *685 km^2* (Khalil and Shaltout, 2006). From the domain of the numerical model, the overall lagoon area is determined to be *564 km^2*. The very shallow parts however are not covered by the grid and the overall lagoon area is likely to be changing with the seasons.

While the remaining four lakes are of deltaic origin, being fed by the Nile stream, Lake Bardawil is non-deltaic and of tectonic origin (El Kafrawy et al., 2019). This makes Lake Bardawil unique in its formation and system dynamics.

Being located between Egypt and Israel, historians speculate that Lake Bardawil was on the trail of the Exodus of the Tribes of Israel and is biblically known as the "Red Sea" or "Sea of Reeds". Throughout history, Lake Bardawil took upon different names such as Port Sirbon during the Roman empire. Its current name comes from King Baldwin I, who was a crusader and was killed near El-Arish according to history (El Kafrawy et al., 2019).

Its importance as a socio-economic resource can be dated back to the Early Iron Age and a settlement, called Cassius, during the Hellenistic-Roman times near Mount Cassius on the wide sand bar (El Kafrawy et al., 2019). In more recent times, Lake Bardawil provides fishing grounds for the local communities and is exploited for salt production along the eastern Zaranik protectorate (see Figure 3). Besides the Zaranik protectorate, Lake Bardawil is home to a vast amount of coastal flat sabkhas along the southern shore and playas of silty soil in the west/south-west (Khalil and Shaltout, 2006). The main water body of Lake Bardawil is made up of a large basin towards the east and a narrow, bottleneck-shaped stretch towards the west. It is separated from the Mediterranean Sea by a narrow, concave barrier island (Gat and Levy, 1978).

To maintain its current state, Lake Bardawil is dependent on the water exchange with the adjacent Mediterranean Sea. The water exchange is maintained by three tidal inlets of which two are man-made and one is natural. The two man-made inlets (Boughazes in the following)

are located along the barrier island with Boughaz 1 along the western stretch and Boughaz 2 along the eastern extent (see Figure 3). The natural inlet is located towards the eastern end of Lake Bardawil close to the Zaranik protectorate. While the latter is silted up during most of the year, the former two inlets are being dredged regularly to maintain the sea-lagoon water exchange (Khalil and Shaltout, 2006). Even though maintenance dredging is performed, Lake Bardawil is characterized by a persistent hypersalinity, which hinders ecological growth and hence supports progressive degradation of the local ecosystem (El-Bana et al., 2002).

Figure 3: Location of Lake Bardawil along the Egyptian coast between Port Said in the west and El-Arish in the east. Including details of the Boughazes 1 & 2 as well as the Zaranik Protectorate. *Source: Google Earth*

The Lake Bardawil ecosystem is home to 6 habitat types. These include the open water, mudflats, stabilized sand dunes, mobile sand dunes, salt marshes, and sand hillocks. Furthermore, the distribution of vegetation around and in Lake Bardawil is dominated by the southern shores and islets in the lagoon. These areas are home to large numbers of local species, while the open water body houses 3 species out of the approximately 136 species present. This equals a percentage of about *2.2 %* of the overall vegetation (Khalil and Shaltout, 2006).

2.2 Data Review

2.2.1 Tide

Being located along the south-eastern coast of the Mediterranean Sea, Lake Bardawil is governed by a semi-diurnal, micro-tidal regime (Ellah and Hussein, 2009; Nassar et al., 2018). Micro-tidal coasts are characterized by tidal ranges smaller than *2 m*. As summarized by van

Bentem (2020), tidal range predictions at Lake Bardawil vary slightly in magnitude. The governing tidal constituents around Lake Bardawil are the M2- and S2-components with their respective tidal amplitude of *0.109 m* and *0.063 m* (Lanters, 2016). Table 1 shows a summary of different (spring-neap) tidal ranges as presented by van Bentem (2020) completed with data by Abdel-Fattah, Bek, and Negm (2019).

Table 1: Tidal range present at Lake Bardawil according to literature

	tidal range		source
	neap [m]	spring [m]	
Frihy et al. (2002)	0.3123 (mean)		measured
Khalil and Shaltout (2006)	0.25	0.35	measured
Linnersund and Mårtensson (2008)	≈ 0.30	≈ 0.60	modelled (WxTide)
Ellah and Hussein (2009)	0.25	0.35	literature
Lanters (2016)	0.14	0.37	harm. analysis
Abdel-Fattah et al. (2019)	0.25	0.35	literature

In line with the previous studies that have been carried out by The Weather Makers, the tidal forcing will be applied using the harmonic components as presented by Lanters (2016).

2.2.2 Wind

Wind imposes a surface shear stress on the water body and hence affects the transport of water along its streamline (Bosboom and Stive, 2021). Further, wind-driven circulations in shallow lagoons can have a significant effect on the transport of matter such as salt, contaminants, and fish (larvae) (Miller et al., 1990). Besides the large-scale circulation of the water masses, wind plays a crucial role in the process of evaporation (Ellah and Hussein, 2009).

The wind climate at Lake Bardawil is predominantly made up of moderate north-western winds during the spring and summer months with average wind speeds of about *3.69 – 4.92 m/s* (van Bentem, 2020; Khalil and Shaltout, 2006; Linnersund and Mårtensson, 2008). During the rainy season from October to March the predominant wind direction shifts towards a south-western wind with possible peak wind speed up to *14 m/s* (van Bentem, 2020).

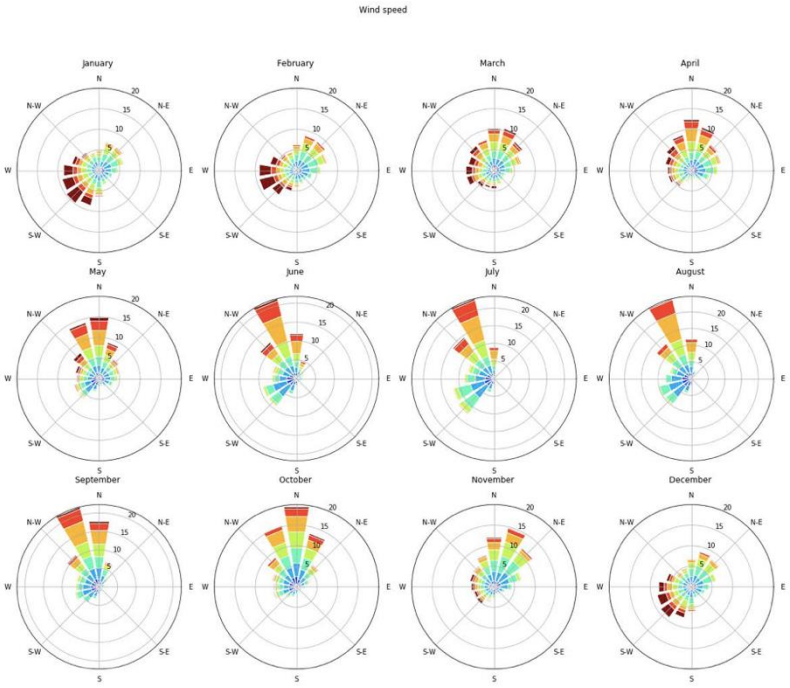

Figure 4: Wind roses for monthly wind climate obtained from Meteoblue data set
Source: van Bentem (2020)

In Figure 4 the wind roses of the monthly wind climate are shown. These were obtained by van Bentem (2020) from a 30-year time series of the Meteoblue data set. This data set provides hourly climate data including wind speed and direction.

In comparison to the previous studies, this study will make use of this hourly wind climate at full resolution in time. In contrast to van Bentem (2020), who used a "representative month with a daily occurring wind pattern", this study aims at investigating the effect of distinct weather conditions throughout the year. To represent the effects accurately it is important to impose a continuous and instantaneous climate. Hence, the full, non-averaged wind data is imposed.

2.2.3 Waves

The wave climate at Lake Bardawil is, similar to the wind climate, predominantly from the N/NW (Georgiou, 2019; Linnersund and Mårtensson, 2008; Nassar et al., 2018). Frihy et al. (2002) examined data from which three wave climate seasons were determined which are: Spring (April-May), Summer (June-September), and Winter (November-March). During spring and summer, the wave data showed rather low waves ($< 1\text{-}1.5\ m$) originating from WNW and NE. The waves during winter might reach stormy conditions with the prevailing wave direction coming from the N, NNW, and NW and maximum measured wave heights of 2.1 m (Frihy et al., 2002; Linnersund and Mårtensson, 2008). Further wave data analysis by

Nassar et al. (2018) paints a similar picture, where *51 %* of the waves approach Lake Bardawil from the NW, further 32% from the N, and only about *5 %* coming from the SE. The wave periods range between 2 to 6 s and are for *98.2 %* of the time below 8 s (Nassar et al., 2018).

As this study focuses on the effects of the local weather conditions at the northern Sinai Peninsula on the lagoon hydrodynamics, the coupled impact with waves will not be included here. On the one hand, previous studies have shown that Lake Bardawil is a tide-dominated system which in addition experiences non-negligible impact by wind forcing and evaporation (Bek and Cowles, 2018; Georgiou, 2019). On the other hand, this is due to computational constraints and is advised to be the subject of separate research.

2.2.4 Climate

The climate along the coast of the northern Sinai can be characterized as semi-arid to arid (Khalil and Shaltout, 2006). In the case of Lake Bardawil, this is governed by very dry weather with temperatures varying between *14°C* in the winter months and *28°C* in the summer months (Khalil and Shaltout, 2006; Linnersund and Mårtensson, 2008). Moreover, the precipitation at Lake Bardawil is limited to the winter months and of relatively small magnitude compared to the evaporation which was already touched upon in the introduction of this report. Linnersund and Mårtensson (2008) present data in which the mean annual precipitation amounts to approximately 100 mm/year. Another crucial component of the present climate is the wind climate present at Lake Bardawil. Figure 5 shows the full annual climate including the air temperature, wind velocity, and wind direction. Further, the three modeling months are shown in more detail, where the clear distinction between peak wind, average, and peak evaporation month becomes evident.

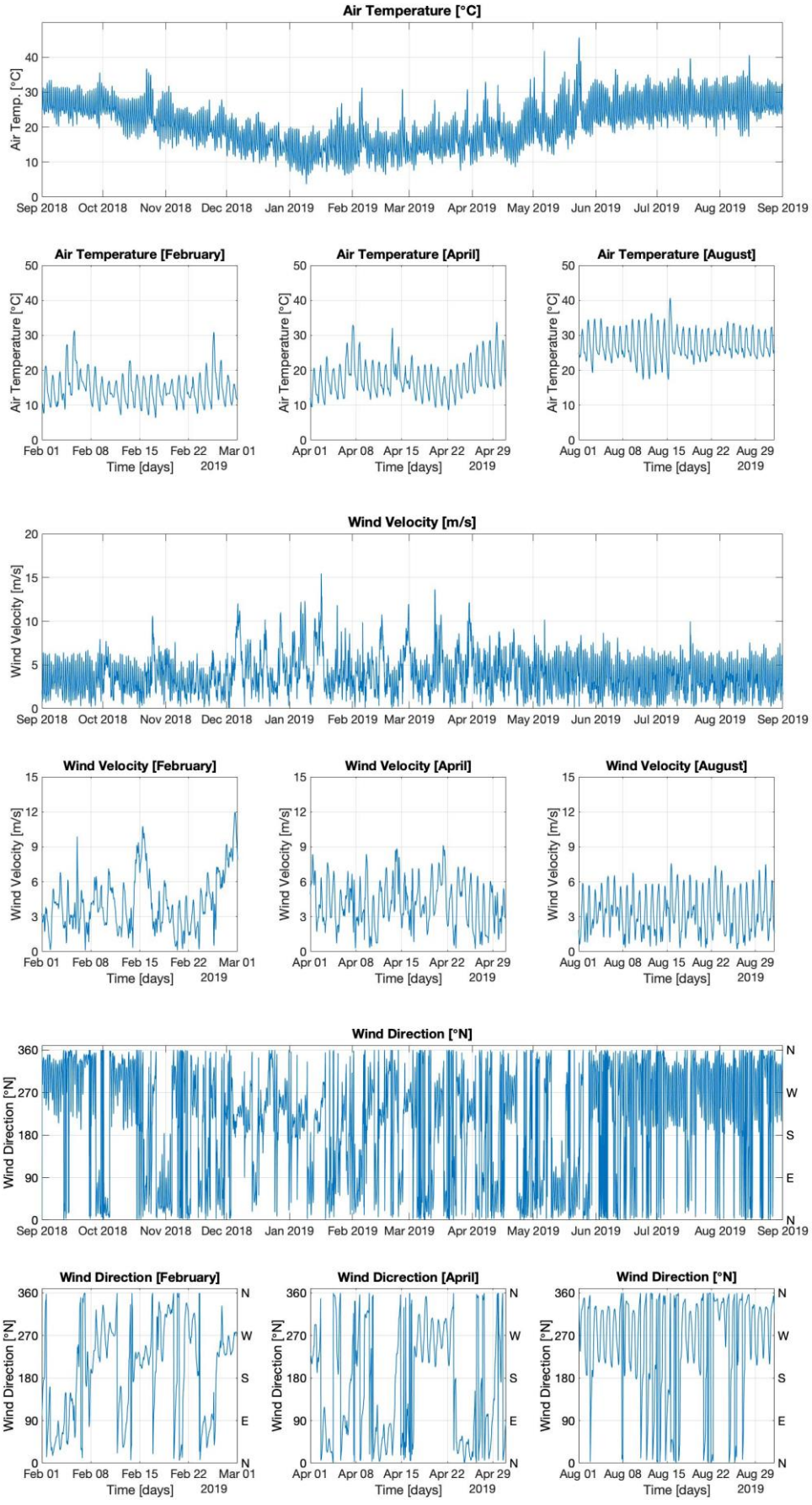

Figure 5: Climate data as recorded and obtained from the Meteoblue data set, including Air Temperature (top), Wind Velocity (mid), and Wind Direction (bottom).

For this study, the Meteoblue data set containing data of the local climate of the northern Sinai Peninsula is used. This set contains hourly climate data which is used to represent the full climate. Figure 5 shows the full year from September 2018 to September 2019 including the data for air temperature, wind velocities, wind directions. Further, the data for the individual simulation periods are shown. The remaining climate parameters such as relative humidity, cloud coverage, and precipitation are shown in Appendix A.

2.2.5 Evaporation

Various information on evaporation around Lake Bardawil has been collected and published over the years. One of the earliest mentions was by Gat and Levy (1978) which was also picked up by Krumgalz et al. (1980). Here evaporation was identified as one of the major contributors to the formation of hypersaline brines in the isolated areas of the lagoon, which remain in the lagoon due to the restricted exchange flow.

Other sources on (more detailed) evaporation rates present daily, monthly, and annual mean values. Figure 6 shows the two most recent studies carried out by Euroconsult (1995) as well as the data presented in Linnersund and Mårtensson (2008) from the unpublished works by the Coastal Research Institute in Egypt. Here the monthly mean evaporation and the mean annual evaporation are presented in *mm*. What can be seen is that, while the annual trend shows a similar behavior, the actual mean annual evaporation rate differs considerably by about *270 mm*. This gives an idea of how sensitive the determination of the evaporation rate is.

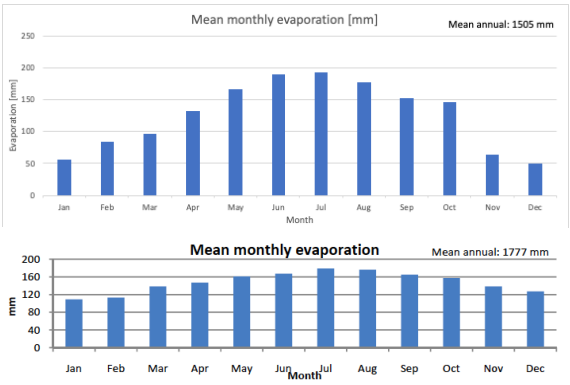

Figure 6: Mean monthly evaporation rates [mm] from Euroconsult, 1995 (top) and the Coastal Research Institute (bottom) as presented by Linnersund & Mårtensson, 2008.

As this study focuses on the investigation of the effect of evaporation on the hydrodynamics, no mean values will be prescribed to prevent averaging of numerous studies and introducing inaccuracies due to data scarcity.

For the determination of evaporation (rates) in this study the climate data provided by the Meteoblue data set will be used. By including data on the air temperature, relative humidity, cloud coverage, and wind D-FLOW FM can compute heat fluxes and the consequential evaporation. Section 3.3.4 will elaborate further on the implementation of evaporation using the heat flux model.

2.2.6 Salinity

Given the nature of a hypersaline lagoon, Lake Bardawil has been subject to several studies regarding the lagoon salinity. These studies include the work carried out by Krumgalz et al. (1980), Ellah and Hussein (2009), and more recently the work by Bek and Cowles (2018).

Figure 7: Map showing the salinity sampling stations as given in Table 1 by Bek & Cowles (2018) throughout Lake Bardawil

With average salinity values ranging from *42* to *50 ppt* throughout the lagoon, Lake Bardawil inhibits large spatial and temporal differences (Egyptian Environmental Affairs Agency (EEAA), 2016). The former is mainly due to the presence of isolated areas and the very shallow bathymetry, while the latter is due to the changing annual weather conditions (Bek and Cowles, 2018; Ellah and Hussein, 2009).

In their work on a three-dimensional circulation model of Lake Bardawil, Bek and Cowles (2018) determined the monthly average surface salinity values and compared them to values from in-situ measurements in the years 1999/2000. The outcomes lie within the abovementioned range from the measurement campaign carried out in the years 2013-2016.

Figure 7 & Figure 8 show the locations for which Bek and Cowles (2018) determined the surface salinity values, the monthly record of the salinity as well the spatial distribution of the monthly average surface salinity.

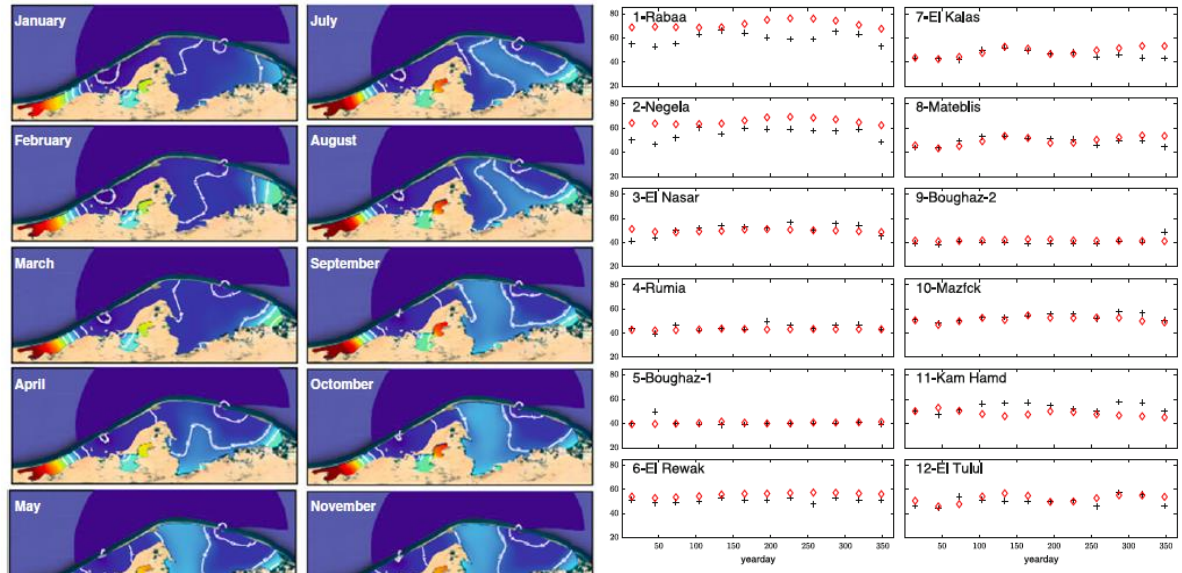

Figure 8: Spatial distribution of the average monthly surface salinity inside Lake Bardawil over the course of a year (left). Computed (red diamonds) and in-situ measured (black crosses) surface salinity values at the stations in Lake Bardawil. *Source: Bek & Cowles, 2018*

2.2.7 Sediment

During the field campaign at the end of 2020 performed by DEME Group sediment samples were obtained. The data reaches from borehole samples on the dry land over samples of the bed material within the lagoon to water samples. Figure 9 shows the sampling locations.

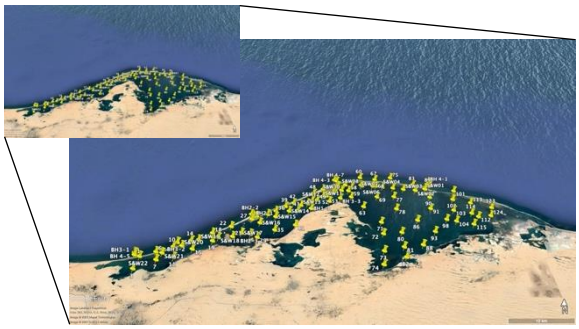

Figure 9: Sampling locations during the field campaign in 2020. Small: all sampling locations, incl. dry land. Large: filtered sampling locations containing data on bed material. *Source: DEME Group*

For this study, the borehole samples on the dry land are not of interest and hence will be left out. The remaining stations are also shown in Figure 9. The data shows that the finest sediment (*O(10)µm*) is found along the calm region in the western bottleneck and eastern basin. The largest sediment is found in the vicinity of the inlets or along the shore of the lagoon. Here the recorded diameter reaches up to *480 µm*. To determine a coherent roughness coefficient according to Manning, a fit-to-data analysis was carried out. For that Manning coefficients for sand were taken from literature and fitted by a polynomial trendline (Arcement and Schneider, 1989). By use of the polynomial function, the Manning coefficient for the measured d_{n50} at the above-shown stations was calculated.

However, as the determination of an accurate roughness coefficient continues to pose difficulties and adds uncertainties to the model it will not be included in this study. Factors such as the grain size but also the bedforms play a crucial role (Barua, 2017; Phillips and Tadayon, 2006). Values for fine to normal sand lay however in the previously mentioned range by Arcement and Schneider (1989). Besides the inaccuracies introduced by the fit-to-data analysis, the relatively scarce amount of sampling points over the extent of the lagoon area requires significant averaging. Hence the D-FLOW FM default setting for the Manning coefficient of $n = 0.023\ s/m^{1/3}$ will be applied (Deltares, 2021).

Appendix D shows the spatial distribution of the Chezy coefficient over the lagoon area for the default setting as well as the applied field data. Furthermore, the reasoning behind the visualization of the Chezy coefficient and the relation between the applied Manning and the plotted Chezy coefficient is briefly given.

2.3 Forcing

2.3.1 Tide

The tidal motion is the main driver of water exchange in systems like Lake Bardawil (Georgiou, 2019). However, analytically quantifying the residual flows initiated by the tidal motion poses difficulties. This is due to the combination of 1) the interaction of the tidal constituents and 2) the interaction with the bathymetry. Whereas the former introduced non-linearities in the tidal wave motion, the latter affects the flow by friction and local velocity gradients. These gradients vary over short distances by means of the bathymetry and so do the hydrodynamics. To consider these effects is "important because they are a persistent feature linked to the local bottom or coastal topography" (Officer, 1976). Expressions from literature are often tidal-averaged solutions for well-mixed systems. Here the assumption of a constant vertical eddy viscosity over the tidal cycle leads to simplifications when determining the residual flow profiles by assuming small tidal residuals (Burchard and Hetland, 2010).

2.3.2 Wind

Wind exerts a surface shear stress on the water body and causes wind-driven currents. This is due to the drag of the water surface by the wind (Bosboom and Stive, 2021).

$$\tau = \rho_{air} C_d U_{10}^2 \quad (1)$$

In which ρ_{air} is the air density, C_d the wind drag coefficient, and U_{10} the wind velocity 10 meters above the ground.

In estuarine studies, this shear stress causes the surface waters to accelerate in the direction of the wind whereas over the depth this effect is reversed. While this gives an idea of how wind exposes a force on the water, the depth effect of the wind-driven flows is discussed in the following section on the underlying theory.

2.3.3 Densities

The effect of horizontal density gradients is the so-called gravitational circulation. Since the denser waters are heavier, they tend to flow along the bottom. Due to the conservation of mass, this will cause a surface flow in the opposite direction. As already mentioned above, these flows usually act on a different time scale than the tidal motion and by this, they cause residual flow along the bottom (Pietrzak, 2020). In the case of Lake Bardawil and given the fact that it is an inverse lagoon, this bottom layer flow is expected to be towards the Mediterranean Sea and hence will cause a net flow and transport.

2.3.4 Evaporation

The evaporation causes a net loss of water and a compensation flow from the Mediterranean Sea into the lagoon. This net inflow can be seen to cause a non-zero velocity through the inlets during times of strong evaporation.

2.4 TWM Studies

In the framework of the Lake Bardawil project, several studies were or are being carried out by The Weather Makers and DEME Group. These studies include the works done by van Bentem (2020), Georgiou (2019) and Lanters (2016). Furthermore, there is currently a study being carried out by Panagopoulos (2022). Here the focus lays on the differentiation between the presented study and work being done by Panagopoulos (2022). For the past studies, a summary and the main findings are presented.

2.4.1 Lanters (2016)

The first study was carried out by Lanters (2016) in cooperation with DEME Group, in which the focus was on the effects of system adaptations "to stimulate the fish population by influencing the hydrodynamics of Lake Bardawil". With Lake Bardawil being a threatened ecosystem by means of its natural but also socio-economical value, the availability and rejuvenation of a healthy fish population are crucial. To do so Lanters (2016) assessed the effect of various system adaptations with respect to three governing key indicators he determined beforehand. These are namely 1) the Tidal Prism, 2) the Depth and 3) the Salinity. The proposed system adaptations include four phases. These phases range from the extension of the existing inlets, over dredging of a new inlet, and channels inside the lagoon to the implementation of sand engines at the downdrift side of the inlets.

As concluded, the adaptation phases affect the flow resistance in the inlets and lead to an increase of the tidal prism by more than *400 %*. In addition to the vast increase in the tidal prism, it was found that the renewal time of the lagoon waters decreases by nearly *300 %*.

In conclusion, it was found that the proposed system adaptations positively impact both the lagoon waters and the chance of an "increase in fish population will help to stabilize the ecology and ecosystem of Lake Bardawil" (Lanters, 2016).

2.4.2 Georgiou (2019)

The study by Georgiou (2019) is a follow-up study on the work done by Lanters (2016). The research focuses on an innovative tidal inlet design to enhance the flows in Boughaz 1. By proposing inlet adaptations which are mimicking nature, it is aimed at improving the inlet functionality and natural behavior of Boughaz 1. The design elements being assessed are the inlet cross-sectional area, the approach channel, and inlet nourishments. By carrying out a numerical modeling campaign in which the individual design elements were assessed, a final design was proposed. For the understanding of the effectiveness of the combined design Georgiou (2019) looked at three hydrodynamic properties: the tidal prism, the flow velocities, and the water levels in the inlet. Adaptations to the approach channel were found to increase the tidal prism at Boughaz 1 by about *10 %*, the flow velocities by *14 %*, and the water level conditions by *25 %*. For the final inlet adaptations, an increase of the tidal prism of Boughaz 1 by *60 %* was found. In line with this increase in the tidal prism, an increase in the maximum ebb and flood velocity was found, amounting to *0.81 m/s* during flood and *0.80 m/s* during ebb. The water levels in Boughaz 1 were found to be *0.40 m*. In conclusion, the study showed that an optimization of the inlet functionality and the natural behavior by means of the proposed adaptations is possible for Boughaz 1. However, further research regarding the morphological behavior is required (Georgiou, 2019).

2.4.3 Van Bentem (2020)

The most recent study within the Lake Bardawil framework of The Weather Makers was conducted by van Bentem (2020). The research focused on the effects of inlet adaptations on the overall inlet stability. To shift from the current unstable system towards a dynamically stable tidal inlet lagoon. The research builds up in phases, where Phase 0 is the initial situation, Phase 1 is the adaptation of Boughaz 1, and Phase 2 includes adaptations in both Boughaz 1&2. The proposed adaptations in this study were a follow-up on the work of Georgiou (2019) and include a deeper inlet cross-sectional area, the dredging of an approach channel, the addition of a nourishment as well as the removal of the present breakwaters. From the 2DH numerical model, it became evident that the system shifts from an unstable tidal inlet system towards a stable tidal inlet system, when including adaptations to both inlets. Furthermore, the system shifts from a sediment importing to a sediment exporting system. Here, crude assumptions had to be made to determine the sediment transport capacity of the inlets. Due to modeling limitations and the fact that only single fraction simulations (*100/300 mu*) were possible, no accurate representation of the erosion/sedimentation pattern inside the lagoon could be obtained.

2.4.4 Panagopoulos (2022)

Alongside the here-treated study, another study is currently being carried out. The study by Panagopoulos focuses on the three-dimensional hydro- and morphodynamics around a tidal inlet in an inverse estuary. Here an in-depth assessment of the interactions between density-driven, curvature-, bathymetry- and Coriolis-induced flows is performed. This will be done using a three-dimensional numerical model for Boughaz 1.
In line with the Lake Bardawil project design adaptations for Boughaz 1 will be proposed with the aim of minimizing the sedimentation around the inlet (Panagopoulos, 2022)

3 | Research Approach

To approach the study and the research subject at hand, the stepwise approach as introduced in section 1.4 can be divided into three blocks. These blocks cover the overall research and divide it into smaller focus areas. These blocks are elaborated on in the following section by means of

1) the underlying theory & key indicators (Block I),
2) the modeling approach (Block II) and
3) the effect of system adaptations (Block III)

The theoretical background introduces an analytical approach from literature which acts as the initiation of the research. In this approach, it is explained how the processes of wind-driven and density-driven flows affect the horizontal velocity profile over the vertical. The modeling approach explains how these processes and the effects of annual extreme weather events are implemented in the numerical model. The section on system adaptations introduces the proposed concept design by TWM and elaborates on the presumed effectiveness with respect to the status quo.

3.1 Underlying Theory

3.1.1 State of Lake Bardawil

It is important to understand Lake Bardawil from an estuarine physics point of view, for which it is important to classify the system by means of its mixing behavior. Due to the net inflow of water, caused by the net loss due to evaporation, enhanced mixing of the sea and lagoon waters can be expected. The classification is done using the diagram presented in Geyer and MacCready (2014). In this diagram, the system is classified by means of a mixing parameter M representing tidal mixing and a freshwater Froude number Fr_f representing the mixing due to freshwater inflow. By including the tidal and freshwater components it displays the effect of tidal mixing in the inlets. In equations 2 & 3 these parameters are shown and their range for the inlets of Lake Bardawil is determined.

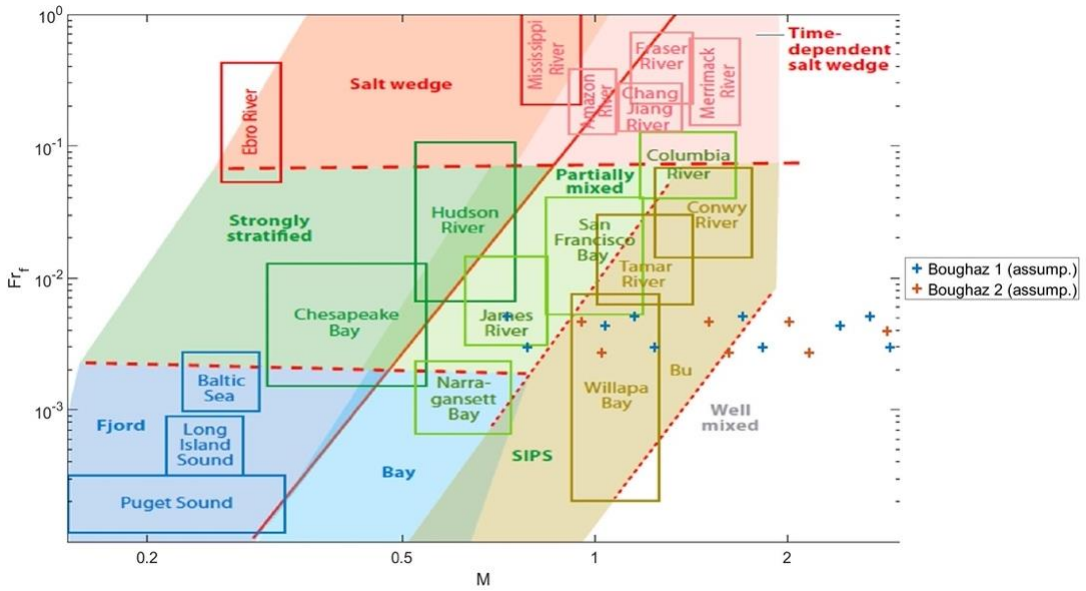

Figure 10: Positioning of Lake Bardawil on the estuarine parameter space as presented by Geyer and MacCready (2014) based on stated assumptions varying over month and spring neap tidal cycle. Blue crosses representing the state of Boughaz 1, orange crosses the state of Boughaz 2.

$$Fr_f = \frac{U_R}{(\beta g s_{ocean} H)^{1/2}} \tag{2}$$

$$M = \sqrt{\left(\frac{C_D U_T^2}{\omega N_0 H^2}\right)} \tag{3}$$

In which U_R is the freshwater flow velocity, β is a scaling coefficient for the salinity/density ($\approx 7.7x10^{-4}$), g the gravitational constant ($= 9.81\ m/s^2$), s_{ocean} the underlying salinity of the ocean/lagoon ($\approx 30\text{-}60\ ppt$), H the water depth ($= 5\text{-}6\ m$), C_D the drag coefficient ($\approx (1\text{-}2.5)x10^{-3}$), U_T the depth-averaged amplitude of the tidal velocity ($\approx 0.3\text{-}0.95\ m/s$), ω the tidal frequency and $N_0 = ((\beta g s_{ocean})/H)^{1/2}$ as the buoyancy frequency.

Given the fact that Lake Bardawil does not receive any surface freshwater runoff, the freshwater Froude number Fr_f is calculated here with the net inflow of water from the Mediterranean Sea to compensate for evaporation (see Appendix B).

For the case of Lake Bardawil, Figure 10 shows the average and the range in which the two inlets (Boughaz 1 & 2) of Lake Bardawil can be found. The large variety in the mixing parameter comes from the combinations of spring-neap tidal velocities as well as the variation of the drag coefficient C_D and salinity values s_{ocean}.

Concluding, the current state of Lake Bardawil and its respective inlets show a range of possible classifications, ranging from partially mixed, over Strain Induced Periodic Stratification (SIPS) to well mixed. SIPS is a state at which the tidal cycle in combination with

present environmental conditions causes temporary stratification of the water column (Simpson et al., 1990).

Here the largest differences in the mixing behavior are observed in line with the spring-neap tidal cycle. During neap tide the here presented initial assessment shows lower mixing parameters for both inlets, placing the inlets within the SIPS. During spring tide both inlets generally show a well-mixed behavior.

3.1.2 Simplified Analytical Expression

The underlying theory is based on the fundamentals of estuarine physics. Estuaries as coastal waters, which have been subject to thorough research, give a good idea about the processes in tidal-influenced coastal waters. It is however of great importance to clearly distinguish between estuaries and coastal lagoons. Whereas the influence of the different forcing terms is assumed to act similarly on lagoons as on estuaries, the dynamics themselves are governed by the absence of riverine input. In addition, the present climate and the geometry of the system are of importance when investigating the dynamics of a lagoon.
The characteristics and hydrodynamics in estuaries were first discussed by Pritchard (1952). In his paper, the definition of an "inverse estuary" for systems like Lake Bardawil was first introduced. Later Officer (1976) and Kjerfve and MaGill (1989) elaborated on the system characteristics and hydrodynamics. While Kjerfve and MaGill (1989) focused in their paper more on the characterization of coastal lagoons through environmental parameters, Officer (1976) carried out a detailed analysis of the hydrodynamics for well-mixed tidal systems.

Looking at systems like Lake Bardawil as an inverse lagoon gives reason to investigate the inlets and their estuarine physics and circulation. Here the freshwater input does not come from a riverine system but the open water. This analysis, following the approach by Officer (1976) and more recently Burchard and Hetland (2010), includes the effects of forcing terms such as wind and density gradients on the water circulation in well-mixed systems in combination with tidal motion. The former mentioned forcing terms cause subtidal flows, which can be of large magnitude and transport significant volumes of water, salt, heat, and other waterborne characteristics (Burchard and Hetland, (2010); Swenson and Chuang, (1983)). This affects the fundamental balances of water, salt, and heat.

As shown by Officer (1976) the non-tidal forcing terms such as wind and densities influence the tidal-averaged horizontal velocity profile over the depth. This is due to the presence of the subtidal flows, which are triggered and maintained by the aforementioned forcing terms. Officer (1976) found a formulation for the effect of these terms in well-mixed systems which is shown below in equation 4. The derivation of equation 4 from the Reynolds-Averaged Navier Stokes Equation (RANSE) is shown in Appendix C.

$$u(z) = \underbrace{\frac{1}{48}\frac{g\lambda h^3}{\rho N_z}(1 - 9n^2 + 8n^3)}_{\text{density-driven}} + \underbrace{\frac{3}{2}v_0(1 - n^2)}_{\text{evap.-driven}} + \underbrace{\frac{1}{4}\frac{h\tau}{\rho N_z}(1 - 4n + 3n^2)}_{\text{wind-driven}} \qquad (4)$$

Here g is the gravitational constant, λ is the horizontal density gradient, h is the water depth, ρ is the water density, N_z the vertical eddy viscosity, n is the depth coordinate *(= z/h)*, v_0 the runoff velocity, and τ the surface shear stress due to the wind.

Figure 11 shows four graphs, in which the vertical velocity profiles according to equation 4 for the two inlets are shown. For these calculations the following assumptions were made 1) a constant horizontal density gradient of $\lambda = 0.015 \frac{kg}{m^3}/m$, based on the mean density in Lake Bardawil and the Mediterranean Sea *(1045 kg/m^3* and *1030 kg/m^3*, respectively*)* and a mean channel length of 1 km, 2) a constant vertical eddy viscosity of N_z *=0.01 m^2/s,* 3) the respective average inlet depths of Boughaz 1 *(= 5 m)* and Boughaz 2 *(= 6 m)*, 4) the runoff velocity v_0 is substituted by the compensation flow velocity u_{comp} for max. and min. evaporation periods and 5) the wind shear stress for average and max. wind conditions (see van Bentem, 2020).

Table 2: Values used for the parameters in equation 4 to carry out the conceptual calculations shown in Figure 11

	Boughaz 1	Boughaz 2
h [m]	5	6
λ [kg/m^3/m]	.015	
N_z [m^2/s]	.01	
$u_{comp,max}$ | $u_{comp,min}$ [10^{-3} m/s]	7.7 | 3.2	7.7 | 3.2
w_{max} | $w_{aver.}$ [m/s]	14 | 4.27	

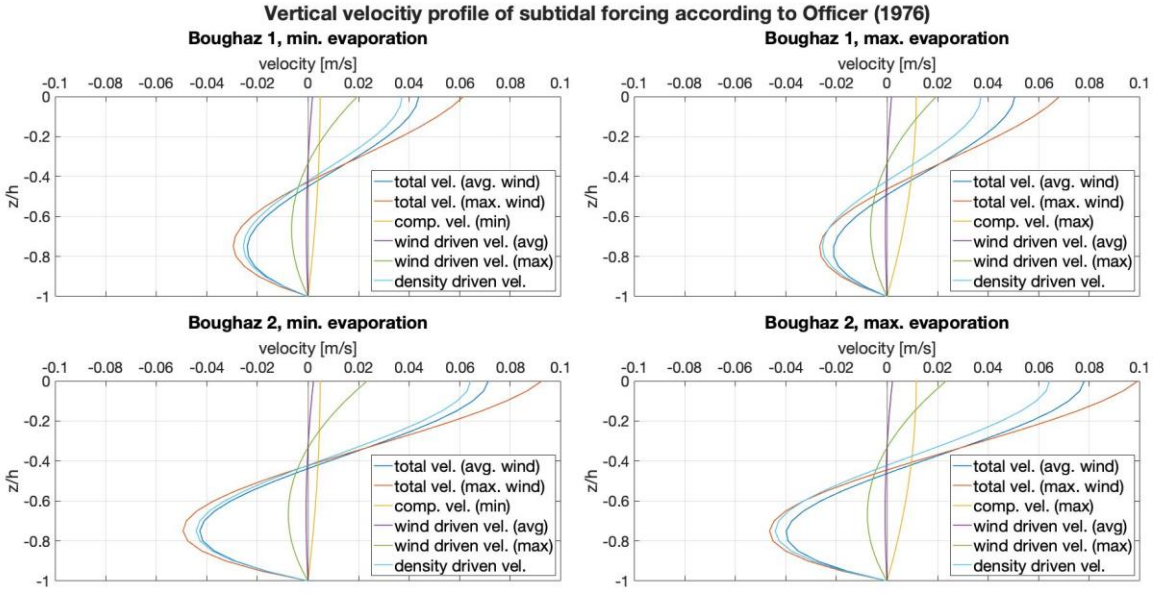

Figure 11: Vertical velocity profiles according to Officer (1976) as presented in Equation 4. Two scenarios of minimum evaporation (February) and maximum evaporation (August) were considered. Top panel is showing the scenarios for Boughaz 1, bottom panel for Boughaz 2.

From Figure 11 it is evident, that the deeper the inlet, the stronger the overall velocity components. While the wind-driven component is rather constant (depth to the power 1), the density-driven component increases significantly from Boughaz 1 ($h = 5\ m$) to Boughaz 2 ($h = 6\ m$). Furthermore, are the total subtidal velocities considered here in an order of magnitude one can expect from literature. Here the subtidal flows can reach values that are an order of magnitude smaller than the present tidal velocities.
Taking the velocities as shown above, which are in the order of $O(10^{-2})$, and comparing them to velocity values determined in previous studies, this ratio holds (van Bentem, 2020).

3.1.3 Water and Salt Balance

The water and salt balance of coastal lagoons are basic but crucial balances that describe the overall flows in a system. By assessing the individual components in these balances, a more thorough understanding and characterization of the lagoon can be obtained. As this study does not aim at setting up a water balance of the system of Lake Bardawil, only the general equations are presented to provide a basic understanding of how certain factors might impact the overall system balances.

From Smith (1994) we obtain the general water balance for coastal lagoons as shown in equation 5.

$$\frac{\Delta V}{\Delta t} = P - E + R + G \pm A \tag{5}$$

In which V is the total volume of the lagoon, P is precipitation, E is evaporation, R is surface runoff, G is groundwater flow and A is an advective gain or loss of water. By the latter, an effective in- or outflow into the considered system is meant.

Equation 6 shows the salt balance derived in Geyer and MacCready (2014) under the assumption of hydrostatic flow and the Boussinesq approximation.

$$\frac{\partial s}{\partial t} + \boldsymbol{u} * \nabla s = \frac{\partial}{\partial z}\left(K \frac{\partial s}{\partial z}\right) \tag{6}$$

In which s is salinity, $\boldsymbol{u}$ is the velocity vector including u, v, w and K is the eddy diffusivity.
Due to changes in the term of evaporation a net inflow (a positive component of A in equation 5) from the Mediterranean is required to restore equilibrium. This is assumed to cause a net inflow of water into the lagoon. Furthermore, evaporation causes the previously mentioned net influx of salt into the water column, and hence it influences the salt balance. Here an increase in local salinity can impact the overall salinity through the horizontal and vertical advection of salt over time.

3.2 Key Indicators

To assess the effect of the varying meteorological conditions on the system this study will consider a number of key indicators. These indicators will focus in the first instance on the tidal inlets and in the second instance on the greater lagoon area. The former is important to be able to understand the impact of the weather on the exchange flows between Lake Bardawil and the Mediterranean Sea. The latter is used to investigate the response of the lagoon salinity over the lagoon area and the effect of the depth varying hydrodynamics.

The indicators regarding the tidal inlets are namely the

- cross-sectional discharge & residual discharge
- cross-sectional velocities
- tidal prism
- top & bottom layer salinity
- cross-sectional salinity distribution

The indicators over the greater lagoon area will be

- evaporative heat flux & evaporation rates
- top & bottom layer salinities
- spatial average salinity distribution

The insights gained by the above-mentioned indicators give a deeper understanding of the system behavior and act supporting when answering the research questions.

The tidal inlet characteristics provide a sound basis of information to quantify the effects of the local weather conditions on the hydrodynamics. Besides that, they provide data that can be compared with the previous studies. It must be kept in mind that changes in the forcing and a new bathymetry influence the results.
Moreover, the full three-dimensional model provides insight into the depth variation of the abovementioned properties and by this deeper insight into the lagoon hydrodynamics.

3.3 Modeling Approach

To assess the effect of the abovementioned forcing terms a 3D numerical model is set up using the software package D-Flow FM. This numerical model for Lake Bardawil builds upon the 2DH hydrodynamic model developed by van Bentem (2020). By extending the model to a 3D model, the effects of the tidal, wind, and density forcing on the depth-varying hydrodynamics can be determined.

In the following section, the main building blocks of the numerical model are introduced and how the forcing is included in the D-Flow FM model. Furthermore, the different model runs are treated in more depth.

3.3.1 The Grid

Horizontal

As this model is an extension of the model by van Bentem (2020) which modeled the 2DH hydrodynamics of the system, a merely similar horizontal grid is used. Here changes around the inlets were included. Figure 12 shows the full model domain as well as a zoom-in on the lagoon area. By including refined, rectangular grids along the inlet and the gullies inside the lagoon, detailed information can be obtained along these locations.

For the modeling scenario of the system interventions, two additional inlets will be included as well as tidal gullies inside the lagoon. Here again refined, rectangular grid cells will be applied.

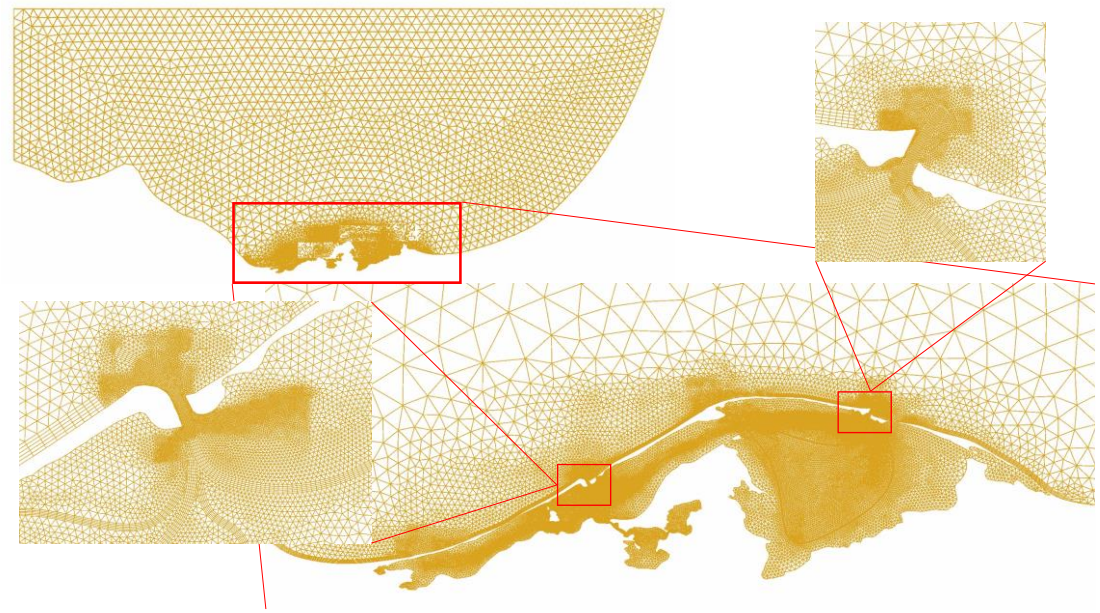

Figure 12: Horizontal Grid of the full modeling domain, a zoom-in on Lake Bardawil, and an additional zoom-in on Boughaz 1 (left) & Boughaz 2 (top right)

Vertical

In the vertical a combination of Z- and Sigma layers is applied (see Deltares (2021)). Here Sigma-layers are scalable layers, which adjust to depth changes. The Z-layers are of fixed thickness. This combination allows for a more detailed resolution in the shallow lagoon area while increasing the layer dimensions towards the deeper waters. As the former is the main area of interest an adequate and accurate layering approach is required. The increasing layer thickness with depth is used to decrease the total number of layers and the computational expense.

Figure 13 shows a schematization of the final vertical layering with a total number of 39 layers in the deepest waters. The upper eight layers are sigma layers followed by a transition to Z-layers. Below the Z-Sigma interface, a maximum growth factor of 1.25 is applied (Kranenburg and Groenenboom, 2021). The main reasons for the application of sigma layers in the top part of the water column are 1) accurate representation of the water level fluctuations and 2) high enough resolution in the shallower parts. In the deeper regions with steeper bed level gradients, the Z-layers allow for an accurate representation of the flow conditions. Here, Sigma-layers introduce a numerical error due to interpolation of the flow properties between the grid cells. The Z-layer model can resolve the flow properties without introducing a numerical error.

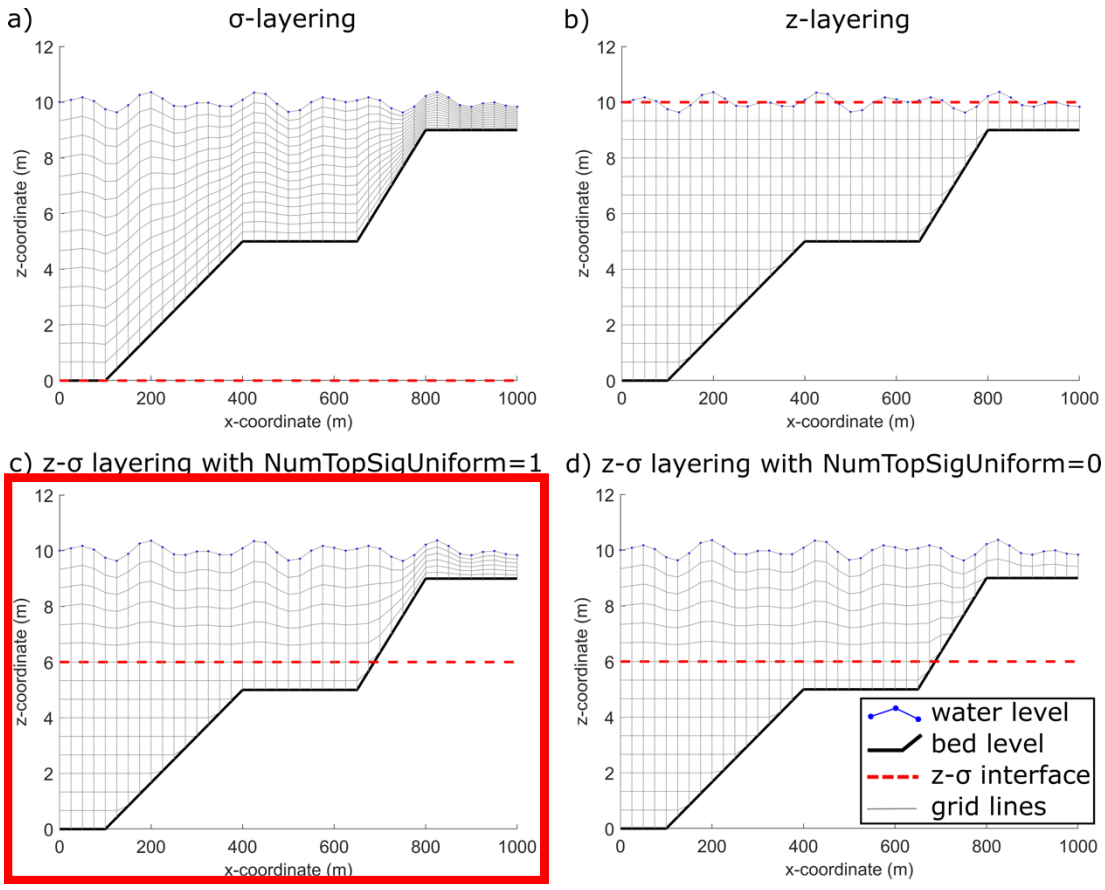

Figure 13: The different options for the vertical grid (layers) in D-FLOW FM. The bottom left figure c) shows the configuration as it is applied in this research using the z-sigma layers. *Source: Deltares, 2021*

3.3.2 The Bathymetry

For the bathymetry, the measured bed level from the field campaign at the end of 2020 by DEME Group will be applied. This new bathymetry introduces more detail, especially along the inlets and to-be-dredged gullies, in comparison to the previously used bathymetries in the works of van Bentem (2020), Georgiou (2019) & Lanters (2016). Table 3 shows the changes in the tidal inlet cross-sectional area from the latest study by van Bentem (2020) to the present study. Here the average values for the cross-sectional area of each model run are included.
Further, an adapted bathymetry will be applied for the simulation of the system interventions. Here the dredging of two additional inlets and tidal gullies will be included as well as the proposed dredging operation in the old inlets.
Figure 14 shows the initial and adapted bathymetry after the implementations of the dredging interventions proposed by The Weather Makers and DEME Group (2021).

Table 3: Average cross-sectional inlet areas [m^2] from the latest study by van Bentem (2020) and the here presented model runs

	Cross-sectional inlet area [m^2]				avg. Δ_{Area}
	van Bentem (2020)	February	April	August	
Boughaz 1	954	1804	1813	1822	190 %
Boughaz 2	1386	1791	1799	1809	130 %

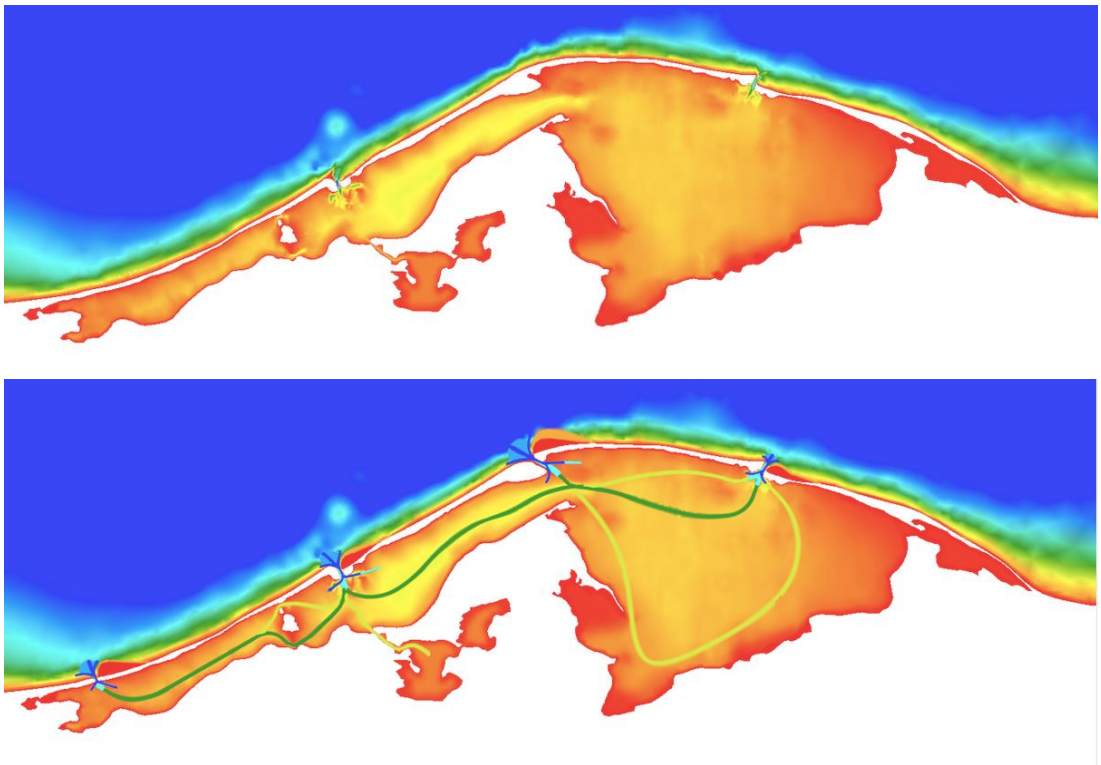

Figure 14: Initial Bathymetry (top) as measured during the field campaign in the end of 2020. The bottom figure shows the adapted bathymetry after the dredging interventions proposed by TWM and DEME Group.

3.3.3 Wind

The wind climate is imposed as a time series uniform over the modeling domain. As mentioned in section 2.2.2 the hourly record of the wind speed U_{10} (at 10 m above the water) and coherent wind direction (°N) is applied. Employing a wind drag coefficient C_d and the widely known formula shown in equation 1, the surface shear stress on the water column by means of wind is determined.

3.3.4 Evaporation

For the model to be able to compute the effect of evaporation on Lake Bardawil, a heat flux model is required. Here D-Flow FM offers three different options, of which the Composite Heat Flux Model is chosen (Deltares, 2021).

This heat flux model requires an external forcing by the meteorological properties of relative humidity [%], air temperature [°C], and cloud coverage [%]. Given the fact that all this data is available for this study, this heat flux model is chosen. An important remark is that to compute heat fluxes also a wind data set needs to be included. This stems from the fact, that wind plays a major role in the heat exchange between the atmosphere and water and hence is inevitable when implementing a heat flux model.

The main reason why the composite heat flux model is applied is that it computes the effective back radiation as well as the convective and evaporative heat losses in the model domain. Further, it allows for free convection in case the environmental parameters of air and water density/temperature are in favor of it (Deltares, 2021).

For the evaporative heat flux (Q_{ev}), EHF in the following, a simple relation to the latent heat of vaporization (L_v) exists, which allows for the computation of the evaporation rates (E).

$$Q_{ev} = L_v * E \tag{7}$$

The latent heat of vaporization is defined as follows

$$L_v = 2.5\ x\ 10^6 - 2.3\ x\ 10^3 T_s \tag{8}$$

in which T_s is the surface water temperature.

3.3.5 Salinity/Density

Changes in density are governed by the water temperature and salinity and are expressed by the equation of state. The equation of state is implicitly computed for every computational time step and the change in density is taken care of accordingly.

The changes in water temperature and salinity are driven by meteorological forcing which is included in the model by means of the heat flux model explained in section 3.3.4.

For the model to be able to accurately represent the changes in density over the modeling period, an initial salinity and temperature are prescribed. This is done by a spatial distribution over the model domain.

The initial temperature and salinity distributions were obtained from a one-year 2DH model run carried out by TWM, which includes the processes of wind and heat flux. Figure 15 shows the initial surface temperature and salinity distribution at the beginning of each modeling period. Here it is shown that the overall water temperature rises from January to July. At the same time, the salinity distribution of the lagoon changes over the months. Here August shows the broadest spread, while January depicts the strongest salinities in the eastern basin. The overall distribution of salinity in the month of January and July is more widespread. This is due to the larger salinity for August and due to the stronger winds for January respectively.

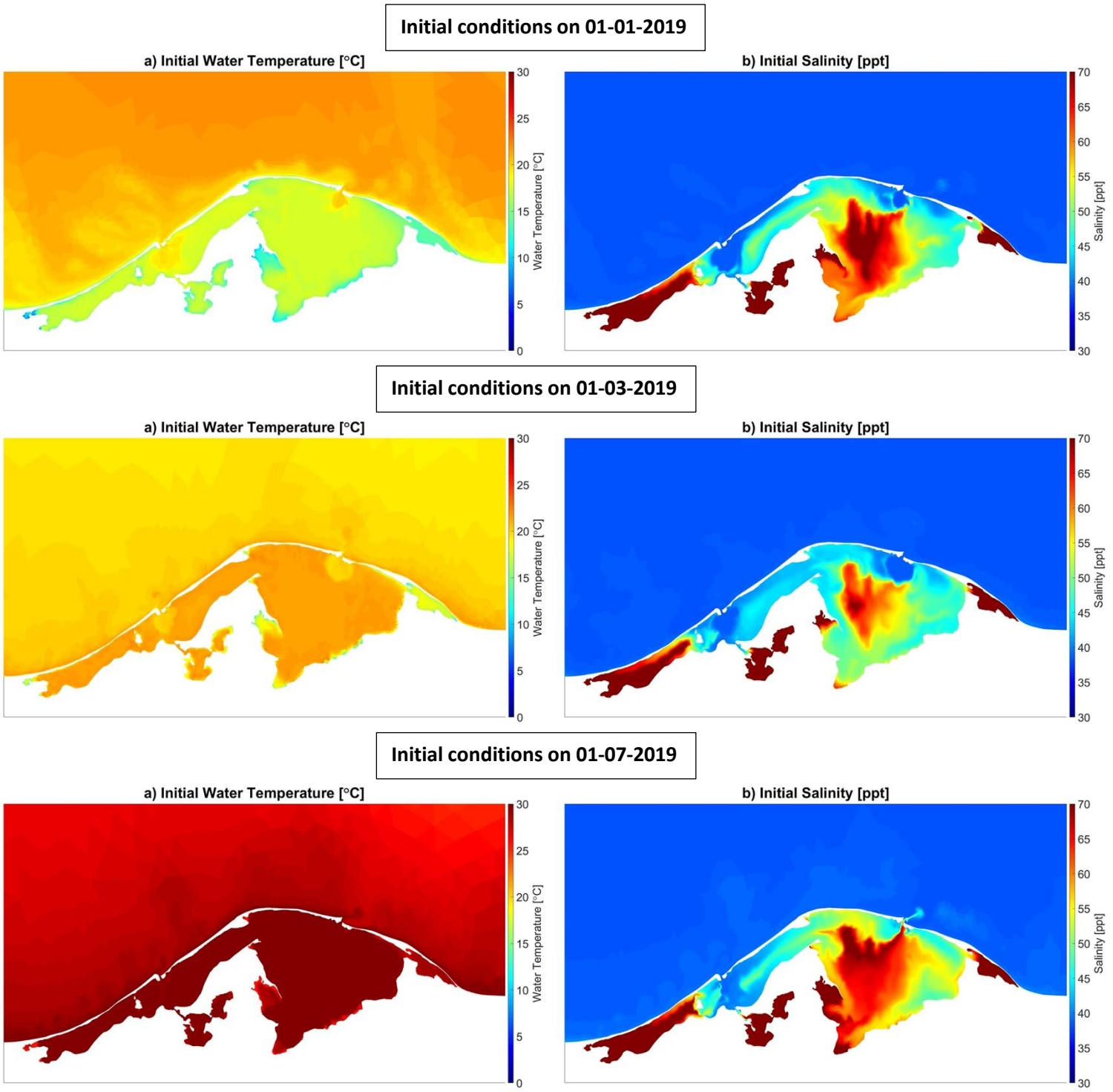

Figure 15: Showing the initial temperature (a) and salinity (b) distribution in Lake Bardawil at the beginning of each simulation period. From top to bottom the initial conditions for the simulation of January/February, March/April and July/August are given.

3.3.6 Model Runs

To gain insight into the 3D hydrodynamics and lagoon salinity and the effect of changing meteorological forcing throughout the year three simulations will be run. The simulations include average meteorological forcing, extreme wind conditions, and extreme evaporation conditions. Further, a simulation with an adapted bathymetry is carried out for the average conditions to investigate the effects of system interventions. This is further elaborated on in section 3.4. Figure 16 gives an overview of the model runs.

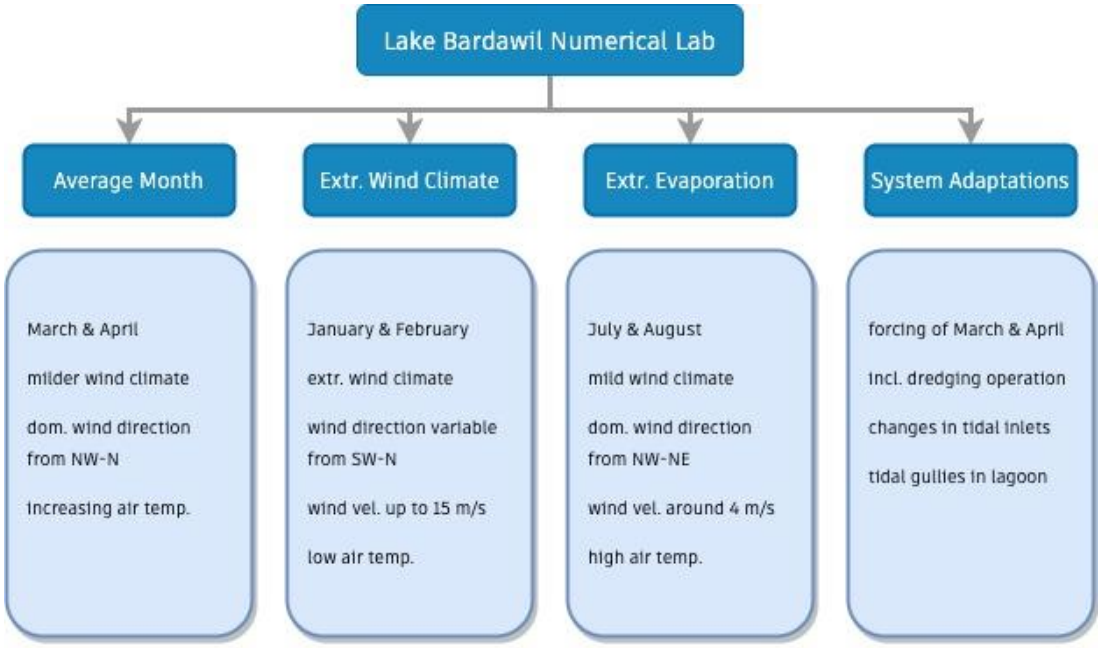

Figure 16: The Lake Bardawil Numerical Lab showing the different modelling runs and their specific characteristics.

By successively approaching the research, a clear understanding of the effect of the meteorological forcing is obtained. Being able to link flow properties to the meteorological forcing is key in understanding the effect of extreme annual weather conditions at Lake Bardawil.
Comparing the two extreme situations of extreme wind and evaporation conditions to an average reference month will give insight into deviations of the flow properties as mentioned in section 3.2 on the key indicators.

The determination of the representative months is done by taking data presented by Ellah and Hussein (2009) and Euroconsult (1995) into account. From this, it is seen that during the month of April average conditions regarding wind and evaporation are present. Peak wind conditions appear during the month of January and February while the peak evaporation conditions are presented during the months of July and August.

3.4 System Adaptations

As part of the greater Lake Bardawil development project, system adaptations by means of dredging operations are proposed by TWM and DEME Group (2021) (see Figure 17). One of the main goals of these adaptations is to increase the water exchange between Lake Bardawil and the Mediterranean Sea to improve the water quality and boost the biodiversity inside and along the lagoon. This includes the creation of varying wetlands and habitats and supporting fish migration farther into the lagoon (see Figure 18).

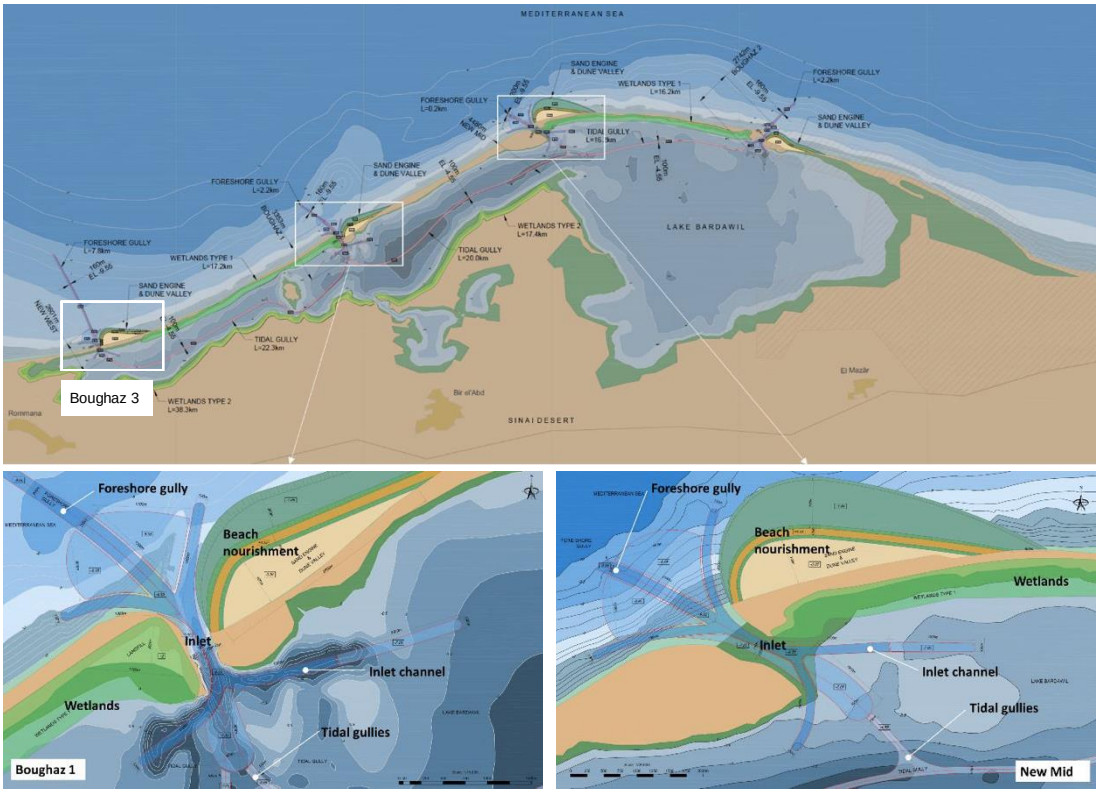

Figure 17: Conceptual design as proposed by TWM in their Extended Summary on the Lake Bardawil Development Project. Top: Overview of the different design aspects along the barrier island, in the inlets, and the lagoon. Bottom: Zoom-In on the proposed inlet design. Left: Showing the adjustments to the existing Boughaz 1. Right: Design of new inlet New Mid or "Boughaz 4". *Source: TWM & DEME Group (2021)*

As shown in the concept design above, the adaptations include the dredging of two new inlets along the barrier island, one in the far western end (Boughaz 3) and one between the existing inlets (Boughaz 4). Besides the new inlets, the old inlets will be adapted by the removal of existing breakwaters and the deepening and widening of the tidal channels. Furthermore, the dredging material is used for the creation of wetland habitats and coastal reinforcement. All the above are visualized in the concept drawings as shown in Figure 17. Below the reasoning for the individual interventions from the Extended Summary on the Lake Bardawil Development Project by TWM and DEME Group (2021) is given and how they are thought of to enhance the overall quality of the present ecosystem.

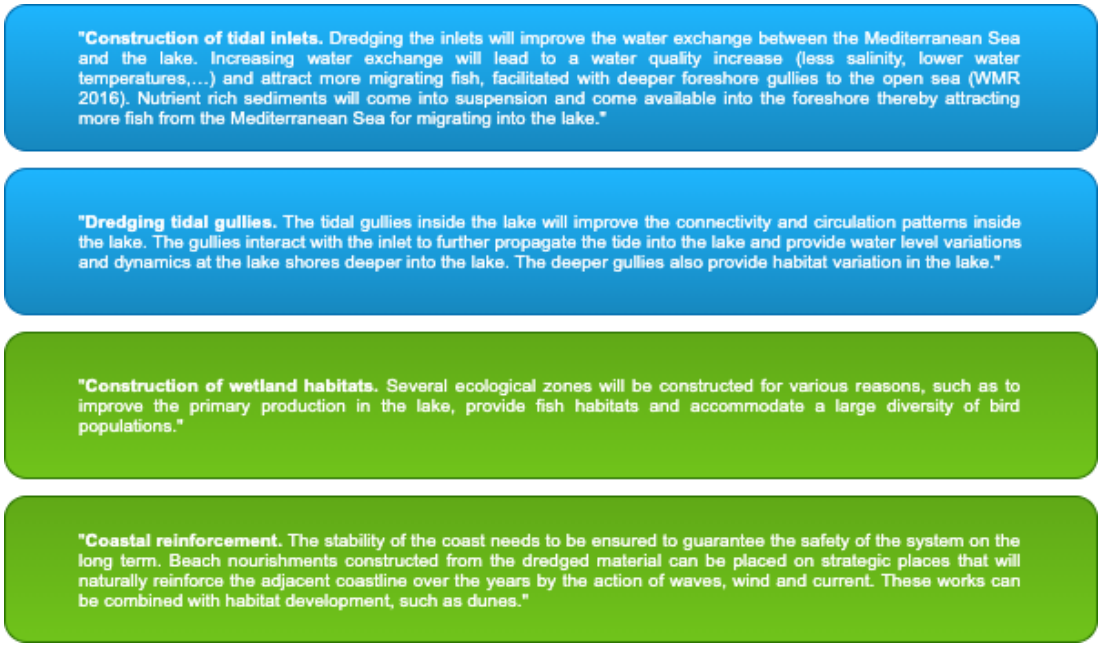

Figure 18: The four blocks of system adaptation to enhance the quality of the Lake Bardawil ecosystem. Including improvements of the aquatic as well as terrestrial parts.

To understand how the concept design impacts the lagoon hydrodynamics and how the adapted bathymetry interacts with meteorological forcing an additional model run will be set up. Here the average weather conditions will be imposed. The results will allow for an investigation of the lagoon response to changes under average conditions. By this, a first assessment of the short-term response can be made, while the investigation of the extreme conditions or even the full annual climate lies out of the scope of the here presented work.

Especially the effect of the dredging and deepening of tidal gullies throughout the lagoon is expected to cause significant changes in the behavior of the water body. As previously mentioned, deeper channels and more space for the gravitational flows might enhance their flow magnitude (Smith, 1994). However, enhanced tidal flows might promote mixing in the inlet and throughout the lagoon.

4 | Results

4.1 Validation

To validate the model, the results are compared to computed and measured data from literature. The validation by means of the comparison of surface salinity values with a previous three-dimensional hydrodynamic model by Bek and Cowles (2018) and the used measured values from 1999/2000 is presented below.

The considered locations for validation are shown in Figure 19. In addition to the locations, the names for the sampling locations are given.

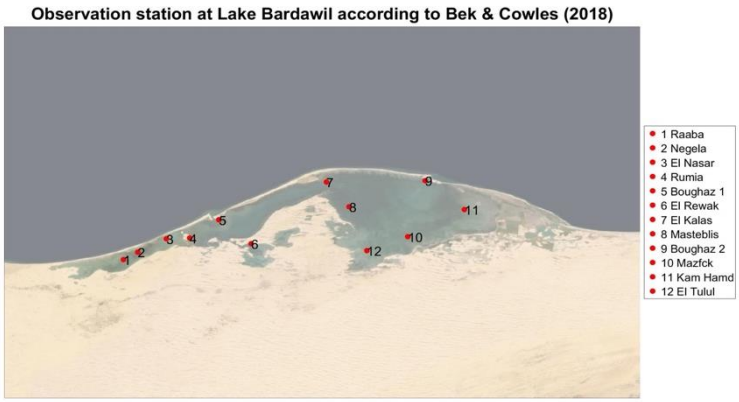

Figure 19: Observation station at Lake Bardawil according to Bek & Cowles (2018)

For these locations (1-12), Figure 20 shows the modeled average surface salinity values against the data from Bek and Cowles (2018). From top to bottom the month of February, April, and August are shown. Overall, it can be concluded that the here presented model aligns fairly well with the values from Bek and Cowles (2018). Especially the stations in the inlets and closest to it resemble the computed and measured values good. The largest differences are found for the stations furthest away from the inlets or in isolated areas. Here the stations of Raaba and Negela in the western end, El Rewak in the pond behind Boughaz 1, and the stations along the edges of the eastern basin are of importance.

For the month of February, the presented model overestimates the measured data in the western end but is in line with the trend observed where towards the western end high salinities are present. In the inlets and the locations close to them, the modeled salinity values align very well with the quantities presented by Bek and Cowles (2018). A very similar image is observed during the month of April and August, whereas the former shows a much better correlation at all stations, except for El Rewak. This station is located in the isolated pond behind Boughaz 1. Especially the stations in the western end and along the southern shore of the basin are rather well represented. This speaks for April as the average month.

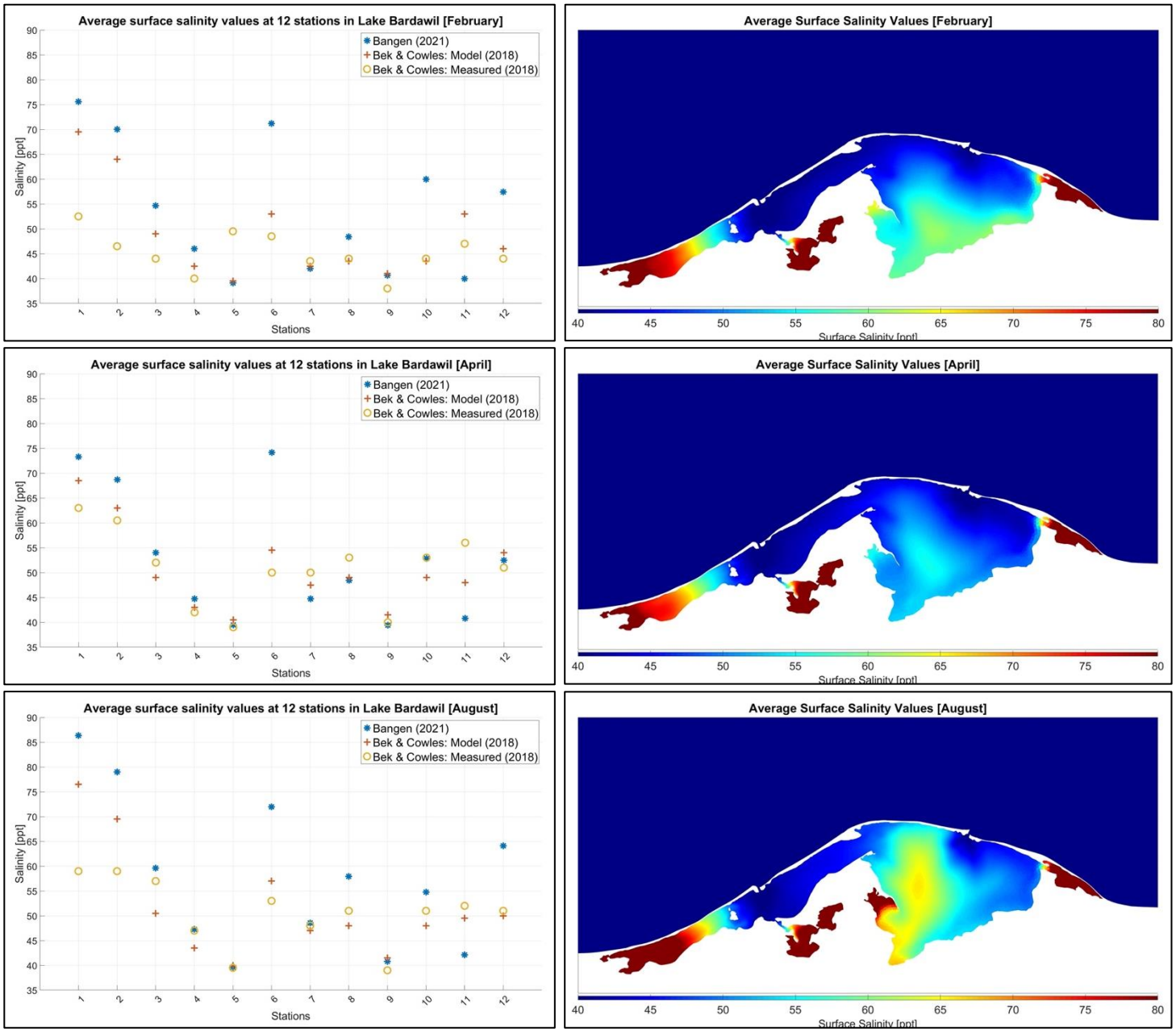

Figure 20: Left showing the average surface salinity values at the stations according to Bek & Cowles (2018) of the presented model and the modeled & measured data mentioned by Bek & Cowles during the months of February, April & August. Right showing the average surface salinity distributions over the whole lagoon area for the months of February, April & August.

For the month of August, the stations in more remote locations show generally some overestimation of the salinity values. However, the trend as seen in the validation data is also observed in the here modelled data. Furthermore, do the eastern stations show a slightly better correlation during the extreme evaporation conditions than they do for the extreme wind conditions.

Overall, it can be said that the trends observed in the data from literature and the here presented results show good correlation. Especially in the locations close to the inlets, where stronger flow conditions are present, the values are equal or differ little. The strong differences between

the modeled and measured data might stem from the initial conditions imposed and the enclosed character of the locations where it is observed. By physical boundaries, the flow conditions in these regions are very calm and evaporation and the consequent salinity increase. Furthermore, does the input data vary in comparison to the data used by Bek and Cowles (2018). This includes the bathymetry, wind climate, and evaporation rates. The evaporation imposed in their model was reconstructed from values found by Ellah and Hussein (2009) whereas the present study imposed an implicit calculation of the evaporation employing a heat flux model. Furthermore, wind is imposed as a time series of spatially uniform wind stress over the model domain. In the model presented here, wind is imposed as a wind velocity with a directional component from which then, by means of a wind drag coefficient the wind shear stress is computed on each cell.

One last point to be raised, and which is likely to be of crucial importance is the period that is simulated in the compared models. While here, periods of two months including initial salinity and temperature distributions were used, the data used for validation was obtained from a four-year simulation. Here the last year was chosen as the output year. This long simulation period allows for certain processes in the lagoon to properly develop, while this is likely not to be the case for the two-month simulations.

Nonetheless, the results show an overall good correlation, considering the differences in the model setup.

4.2 Results – Status Quo

In the following sections the results of the different D-Flow FM model simulations, representing the 'status quo' are presented. These results include the simulations of the average month (April), the months of extreme wind conditions (February), and the extreme evaporation conditions (August) (see Figure 16). To quantify the effect of the different forcing conditions the focus will be on 1) the hydrodynamics in the inlets, 2) the evaporative heat fluxes and evaporation rates and 3) the salinity distribution in the inlets & lagoon. The results presented below show the model output for the second month of the simulation period. This is done to account for the numerical spin-up time and errors introduced by the model.

4.2.1 Hydrodynamics

In the following section, the hydrodynamic properties obtained from the D-FLOW FM model will be presented and discussed. Here the properties for the individual simulations will be treated alongside one another to allow for a direct comparison.

Discharge & Velocity

The discharges and velocities in the tidal inlets are representatives of the exchange flow and the processes governing this flow. Figure 21 shows the time series of the instantaneous and tidal-averaged discharges during the individual simulations of February, April, and August. From this, it is seen that the tidal signal dominates the exchange flow most of the time. Here especially during spring tidal periods the tide dominance is visible, where the tidal-averaged signal for all simulations is found to be around the zero line. During neap tidal periods, distortions of the instantaneous discharge signal can be observed as well as of the tidal-averaged signal, which aligns well with the occurrence of strong meteorological forcing.
Looking at the overall magnitude of the discharges during the different months, only little differences are observed. Here, Table 4 presents the maximum ebb and flood discharges in Boughaz 1 & 2.

Table 4: Showing the max. ebb and flood discharges [m^3/s] through the inlets during the simulation months

		Inlet Discharges [m^3/s]		
		February	April	August
Boughaz 1	$Q_{max,in}$	1879	1877	1850
	$Q_{max,out}$	1710	1673	1628
Boughaz 2	$Q_{max,in}$	2021	1944	2111
	$Q_{max,out}$	2002	1925	1885

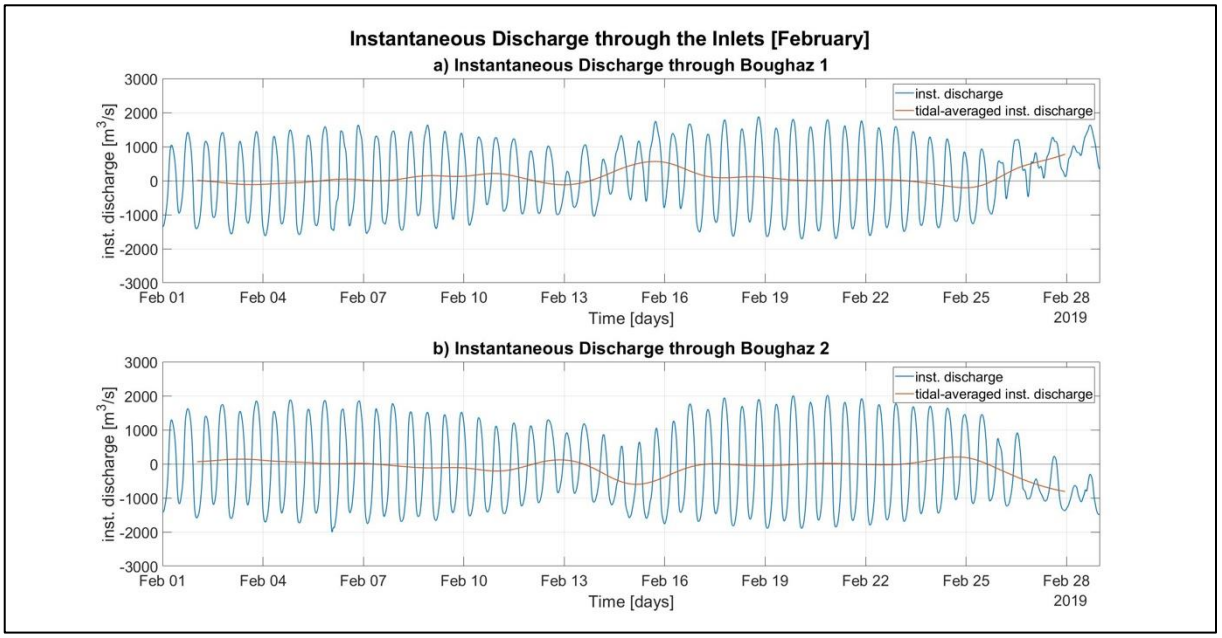

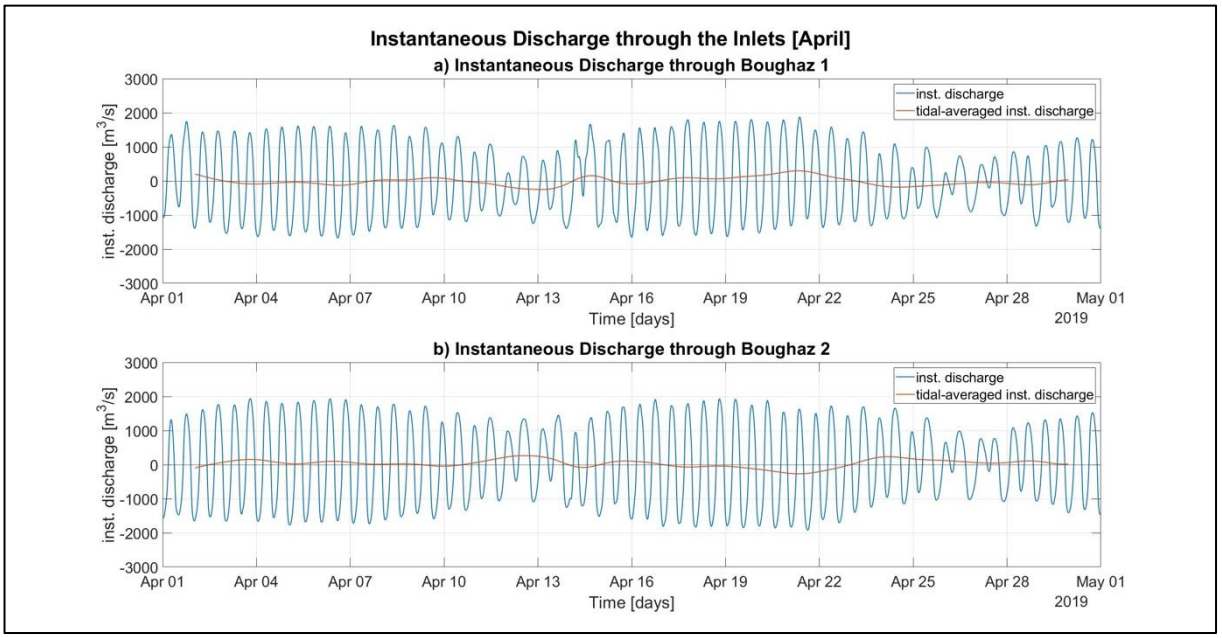

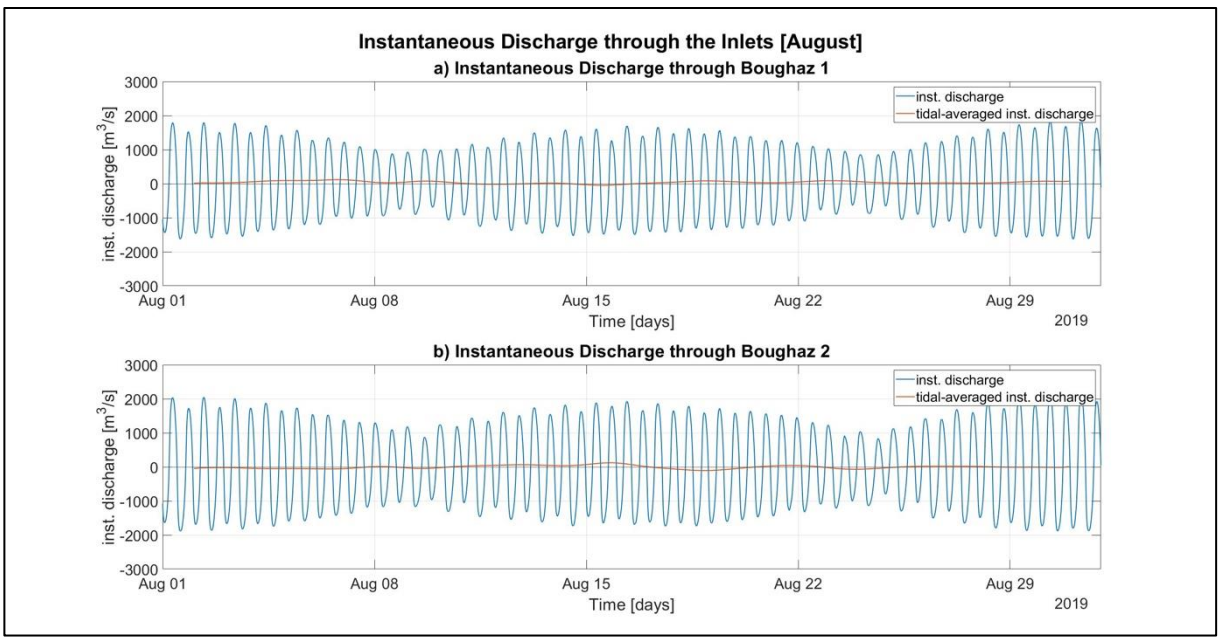

Figure 21: Timeseries of the instantaneous and tidal-averaged discharge [m^3/s] in the inlets during the status quo simulations. From top to bottom the months of February, April, and August are shown.

From the values, it is seen that during all months the flood discharges are larger than the ebb discharges. Where Boughaz 1 experiences in general smaller discharges than Boughaz 2. As a consequence of this Boughaz 1 depicts in general slightly lower flow velocities as presented in Table 5 (and Appendix F). While Boughaz 2 shows overall higher flow velocities, Boughaz 1 experiences rather low velocities during the month of August. Here the maximum ebb and flood velocities are *0.93* and *0.98 m/s*, respectively. Furthermore, is the observed difference between ebb and flood velocity largest in August (*0.05* & *0.09 m/s* for Boughaz 1 & 2) and lowest in February (*0.02* & *0.01 m/s* for Boughaz 1 & 2). During the month of April, these differences amount to *0.05* & *0.01 m/s* for Boughaz 1 & 2 respectively.

Table 5: Showing the max. ebb and flood velocities [m/s] in the inlets during the simulation months

		Inlet Velocities [m/s]		
		February	April	August
Boughaz 1	$U_{max,flood}$	1.01	1.01	0.98
	$U_{max,ebb}$	0.99	0.96	0.93
Boughaz 2	$U_{max,flood}$	1.12	1.08	1.15
	$U_{max,ebb}$	1.13	1.09	1.06

Residual Discharges

Figure 22 is showing the tidal-averaged or residual discharges in the inlets for the individual simulation periods. Here the blue and orange line represent the two inlets Boughaz 1 and 2 respectively while the dashed, black line is the net residual flow in or out of the lagoon. The here shown graphs indicate that during the month of February the largest residuals with values of up to *600 m^3/s* are present. These flows are inversely present in both inlets resulting in a rather small net residual discharge. This net flow shows strong variation around the horizontal axis resulting in an average $Q_{res,net}$ = *+ 8.96 m^3/s* (see Table 6). As for the month of February, the signal for the month of April is rather noisy around the horizontal axis. However, throughout the whole modeling period, clear inflows of water are observed in the signal (see Figure 22) as well as in the average $Q_{res,net}$ = *+ 23.73 m^3/s*.

Table 6: Showing the residual discharges [m^3/s] through the inlets as well as the net residual discharge & the total residual volume [m^3]

	Boughaz 1 [m^3/s]	Boughaz 2 [m^3/s]	$Q_{res,net}$ [m^3/s]	$V_{res,total}$ [10^6 m^3]	$V_{Euroconsult}$ [10^6 m^3]	Δ_{Vol}
February	+ 91.84	- 82.88	+ 8.96	+ 21.7	40.0	*- 45 %*
April	- 12.93	+ 36.66	+ 23.73	+ 61.5	69.3	*- 11 %*
August	+ 38.99	- 4.99	+ 34.16	+ 91.5	97.3	*- 6 %*

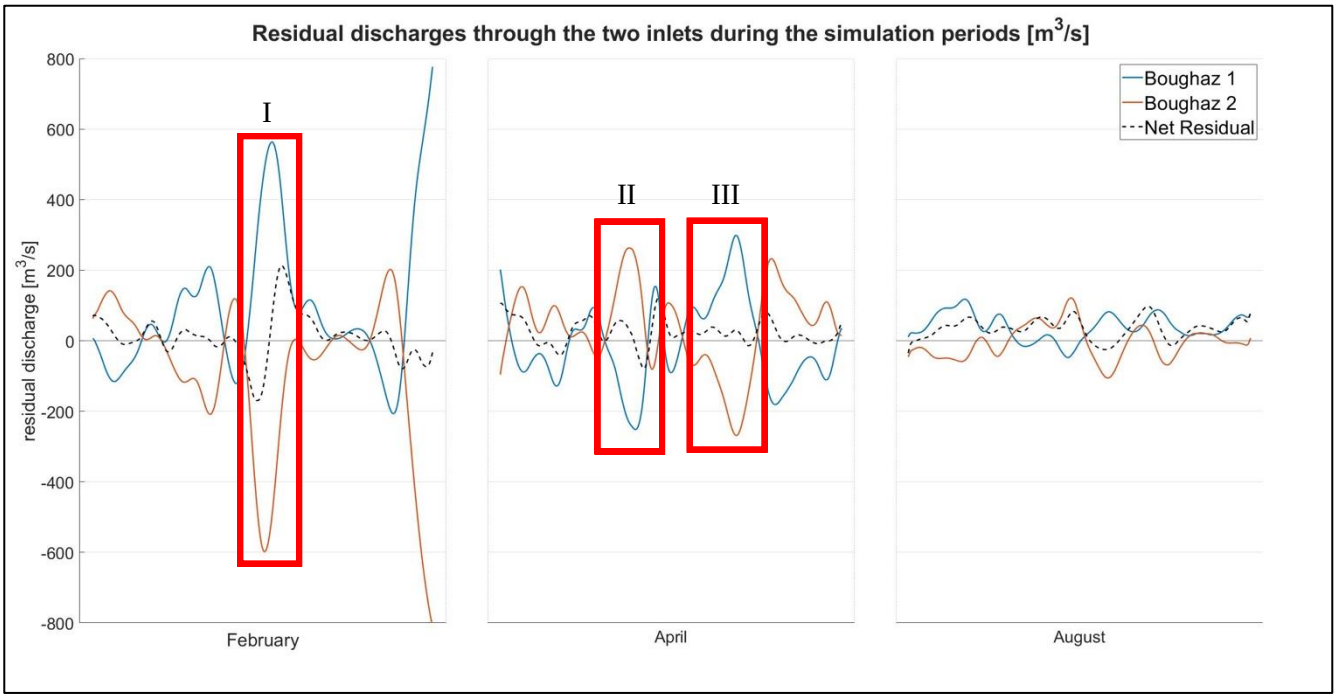

Figure 22: Residual discharges [m^3/s] through the two inlets during the simulations of the status quo. From left to right showing the inlet specific residuals (blue & orange) and net residuals (black) for the months of February, April, August

While the above-described periods experience a clear variation between net in- and outflow at times, the net residual discharges for the month of August do not. Here the calmer wind climate during the extreme evaporation conditions is very well visible in Figure 22. The persistent net residual inflow of $Q_{res,net} = + 34.16\ m^3/s$ leads to a net volume entering the lagoon during August of $V_{res,total} = 91.5x10^6\ m^3$.

The noisy signal during the month of February can be related to strong wind events occurring during this month. Around the peak in residual discharge (I) a strong W-SW wind event occurs (see Figure 5), pushing waters into Boughaz 1 and out of Boughaz 2. The high residual discharge towards the end of February is due to another storm event.
The two events pointed out during the month of April (II & III) are consequences of the present wind climate. Where around these events stronger winds from the NE (II) or W-SW (III) occur (see Figure 5). Here Boughaz 1 experiences a residual inflow during event III and a net outflow during event II. For Boughaz 2 this is the other way around.

Tidal Prism

At last, the tidal prism is considered as a quantity, which is less sensitive to external forcing than the quantities of instantaneous discharge and velocity. By external forcing, the meteorological forcing is meant. This is because the quantity is purely dependent on the cross-sectional inlet area, inlet velocity, and tidal period. Here only the inlet velocity could be altered through the meteorological forcing. Wind can have a short-term impact on this quantity during

extreme conditions. Considering the average tidal prism decreases the impact of short-term extreme events. Furthermore, previous studies pointed out that Lake Bardawil is overall tide-dominated and hence the inlet velocities are largely dependent on the tidal forcing. The average and spring tidal prism are considered and shown in Table 7.

Table 7: Values of the tidal prism [m^3] in the two inlets as well as the total tidal prism during the status quo simulations

	Average Tidal Prism [10^6 m^3]			**Spring Tidal Prism [10^6 m^3]**		
	February	April	August	February	April	August
Boughaz 1	20.38	20.10	20.55	41.77	34.12	29.65
Boughaz 2	24.23	23.46	24.32	61.94	36.98	34.30
Total	**44.61**	**43.56**	**44.87**	**103.71**	**71.10**	**63.95**

From this, it is evident that during the different months, the tidal prism does not change. Taking April as the reference month, we see an increase in the average tidal prism of approx. 2.4 % for February and approx. 3 % for August.

While the average tidal prism values give reasonable volumes, the spring tidal prisms show strong increases. Looking back at the averages during February, the spring tidal prism shows increases by the factor *2 & 2.5* for Boughaz 1 & 2 respectively. For the other months increase factors in the order *1.6 – 1.7* during April and *1.4* during August are observed.

The largest spring tidal prism value is observed for the month of February and decreases towards August, where the minimum is seen.

Interpretation of the Results

The results presented above again support the claim first made by Georgiou (2019) that Lake Bardawil is a tide-dominated system. During all simulation periods, a strong spring-neap tidal pattern is observed. This forms the envelope for the instantaneous discharges as well as for the inlet velocities.

However, during the periods of less energetic tidal flows (neap periods) in combination with stronger meteorological forcing deviations from this pattern are observed. Therefore, the extreme wind conditions, as well as the average conditions, show a clear dependence on the present weather conditions. Here it was also found that the directional component of the wind is crucial in how the inlets respond. While W-SW winds cause a net, residual inflow through Boughaz 1, NE winds cause a net, residual outflow. For Boughaz 2 this is the other way around, whereby NE winds water is pushed into the lagoon and by W-SW winds out of the lagoon. Resulting in a net, residual inflow for the NE winds and a net, residual outflow for the W-SW winds.

Alongside the calming weather conditions, the residual discharges show similar behavior. Here the noise in the residual discharge signal decreases from February to August. The noisy signal during extreme wind conditions (February) is in line with a more dynamic situation where strong and abrupt changes in the forcing and the resulting hydrodynamics are present. The more dynamic conditions are for ones shown by the larger residual discharges in the inlets and will be further supported in the following section on the salinity.
Changing wind directions and velocities cause a large variety in the flow conditions. During the month of August where calm and directional persistent winds are present, this dynamic is not present. As the model only considers water losses due to evaporation, the net loss of water due to the high evaporation rates causes a net residual inflow throughout the whole month. This results in a large net volume of water being transported into the lagoon.

The results for the tidal prism show, at least for the average values, a persistent behavior. This is something to be expected given the dependence on the inlet geometry, the tidal period, and the inlet velocity. While the former two do not vary over the different simulations, the latter was also found in similar ranges. Hence, a good correlation between the three average tidal prisms is expected. The large differences in the spring tidal prism originate from the points in time where strong meteorological forcing significantly alters the tidal signal. Including the discharge amplitude and the coherent duration.
Looking back at the values of the spring tidal prism and the time series of the discharges, the large volumes for February can be appointed to the last days of the month. Here a persistent positive discharge is observed, even during ebb periods. As the tidal prism is determined based on zero-crossings in the discharge signal, the period from February 27th on is not suitable for a sound determination of the tidal prism. However, these values are the ones presented above. Cutting off the time series on February 27th results in a significantly lower spring tidal prism of about $79x10^6\ m^3$. The average tidal prism however is unaffected by it.
This shows that the average tidal prism allows for a more objective assessment of the inlet characteristics, while the spring tidal prism needs to be treated with care. The latter actually can be affected by non-tidal forcing.

4.2.2 Evaporation

In this section, the results of the implemented heat flux model are treated. This is done by presenting the computed Evaporative Heat Flux (EHF) and the following evaporation rates. Here the focus is set on the daily and monthly evaporation rates.

Evaporative Heat Flux

The EHF is the fraction of the overall heat flux model that causes evaporation over the model domain. Here larger, absolute values in EHF mean stronger evaporation rates over the lagoon area.

Figure 23 presents the results for the status quo simulations. Here the blue line depicts the average EHF over the lagoon area while the orange line depicts the wind velocity present at location. The latter is included since the evaporation is largely dependent on the present wind climate. As shown in the graphs for February, the overall EHF is of lower magnitude, hardly surpassing the value of *200 W/m²*. Only during the strong wind events (see markers in top panel of Figure 23) a clear and longer-lasting impact on the EHF is observed. This pattern shows a very good correlation with the wind pattern where around February 16th peak wind velocities are observed.

These observations are also made for the remaining two simulation periods of April and August. Here the more regular signal of the wind during April, up to the daily wind pattern in August is visible in the EHF signal.

For the month of April still some distinct peaks (see markers in mid-panel in Figure 23) can be observed where stronger wind velocities occur. Overall, the signal shows a more regular pattern.

The pattern of the EHF as well as of the wind velocity is most regular during August, where a clear daily pattern is observed. The peaks, which are occurring daily around 2 – 5 pm, reach much larger, absolute values than for the other months. It is not possible to say whether the local maxima, present around August 16th, is caused by the slightly higher wind velocity or by the overall high air temperatures.

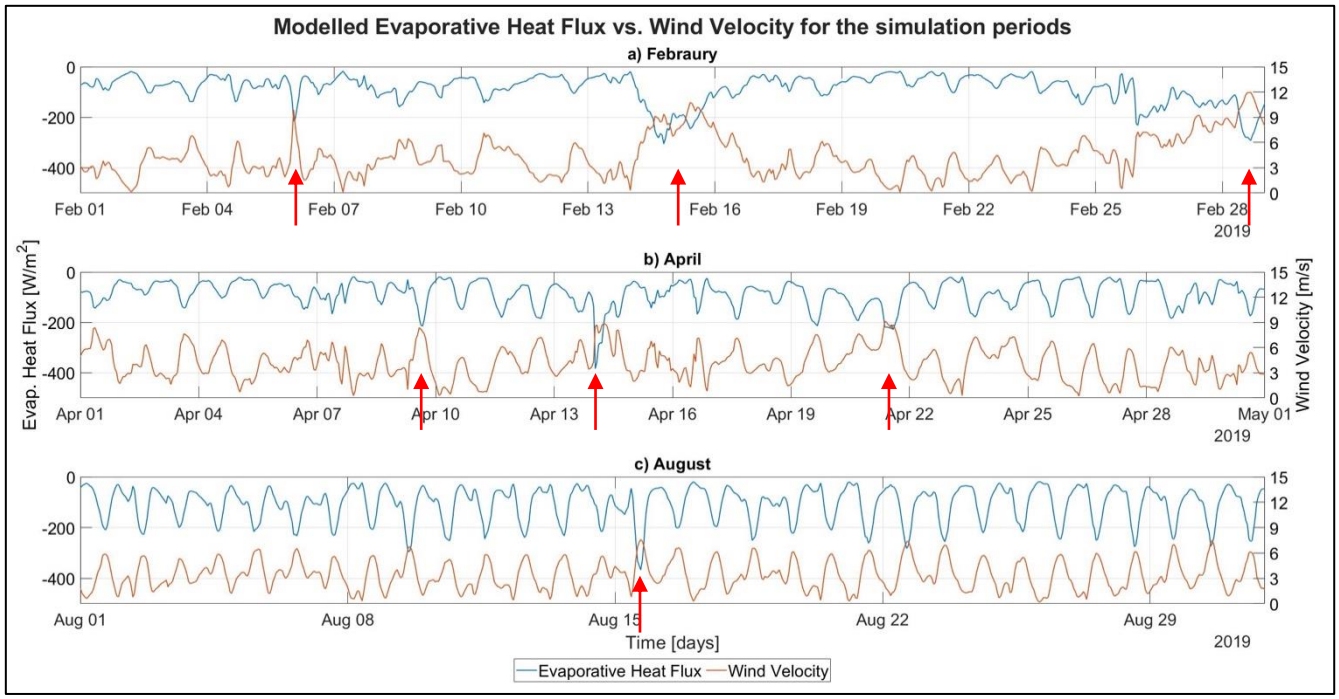

Figure 23: Modelled Evaporative Heat Flux [W/m^2] (blue) and Wind Velocity [m/s] (orange) for the individual month of the status quo simulations. From top to bottom the month of February, April and August are shown.

Evaporation Rates

The evaporation rates in *mm/day* or *mm/month* follow directly from the above presented EHF. By the relation of the EHF and the latent heat of vaporization, which is presented in section 3.3.4, the evaporation rates were computed. Table 8 shows the results from the before mentioned calculation using the modeled EHF and the latent heat of vaporization dependent on the modeled surface water temperature. In addition to that, it shows the evaporated volume of water over the different simulation periods.

Table 8: Showing the daily & monthly evaporation rates [mm] for the status quo simulations as well as the total evaporated volume [m^3]

	February	April	August
Evaporation rate [mm/d]	2.35	2.43	3.26
Evaporation rate [mm/m]	66	73	101
Evaporated Volume [10^6 m^3/month]	37.5	41.3	56.5

As is shown by means of the values a clear increase in daily and monthly evaporation rates is observed. Here during February, these values are lowest with a daily evaporation rate of *2.35 mm* and a monthly evaporation rate of *66 mm*. The values for the average conditions in the month of April amount to *2.43 mm* and *73 mm* for the daily and monthly evaporation

respectively. The peak is reached during the month of August where the daily and monthly evaporation rates equal *3.26 mm* and *101 mm* respectively.

Interpretation of the results

As already pointed out in the previous section when looking at the hydrodynamics, the wind velocity plays a large role in the observed model output. Here is becomes evident, that the evaporative heat fluxes, and hence the evaporation itself scale largely with the wind velocity. While this is clear for the month of February and April, the month of August shows little response to distinct wind events. Here the daily pattern in the EHF can be explained by the calm, daily wind pattern in combination with the very high air and surface water temperatures. The overall regularity during this period promotes steady and high evaporation.

These findings are then also present in the daily and monthly averaged evaporation rates as presented above. The regularity of the weather conditions during August causes high evaporation rates. The heat fluxes as presented during February and April do not allow for such strong evaporation leading to the overall smaller values.

As the system is only experiencing water inflow through the inlets and losses by means of evaporation, these values should be in line. While the overall trend, as just explained, is in line with the data from literature and expectations, the absolute values do differ quite strongly. Comparing the values for the net volume flowing into the lagoon from Table 6 and the evaporation rates as presented in Table 8 clear discrepancies are observed. This matter will be further elaborated in the discussion.

4.2.3 Salinity

In the following section, the results regarding the modeled salinity are presented. Here the focus will at first be on the average lagoon salinities during the different simulation periods and after that on the salinity values in distinct locations. Here namely the inlets as well as one station in between.

Figure 24: Stations for the salinity records. 1) Boughaz 1, 2) Boughaz 2, 3) Bottleneck-Basin

Average Lagoon Salinity

The average lagoon salinity is considered as an objective indicator to assess the overall system response to the varying meteorological forcing. Here Figure 25 shows the time-averaged, spatial distribution of the bottom (a) and surface (b) layer salinity. This is shown for the month of February, April, and August from top to bottom. In addition to the spatial distribution, Table 9 shows the overall surface and bottom layer salinity for the different months. Further, the quantity of Δ_{Sal} is indicating the difference in surface and bottom layer salinity.

Table 9: Average Surface and Bottom Layer Salinities [ppt] during the simulation periods. In addition, the average surface-bottom-salinity difference Δ_{Sal}

	February	April	August
Surface	46.51	45.79	49.74
Bottom	46.75	45.97	50.14
Δ_{Sal}	+ 0.24	+ 0.18	+ 0.39

From Figure 25 it is be seen that during the extreme wind conditions in February the waters along the barrier island depict salinity values up to *43 ppt*, which is lower than for the other months. Here a stretch of these lower salinity values is connecting the two inlets. During April this image is still present, but the salinity along the barrier island is slightly larger and on the verge of the western bottleneck toward the eastern basin a high saline tongue is stretching toward the sand bar.

This tongue is fully developed during the month of August, where a clear separation between the two parts of Lake Bardawil is seen. Further, the reach of the tidal inflow is rather constricted. This is especially visible for Boughaz 2, where the average surface and bottom layer salinity remains in the range of *42-44 ppt*. For the other inlet, this is not the case where

a clear impact of the Mediterranean waters with salinity around *38-39 ppt* is visible. The same behavior holds for the months of February and April, whereas in April a farther reach of the Mediterranean waters is observed. During February, the average salinity values observed in the vicinity of Boughaz 2 are comparably high when looking towards the month of April. Here the most eastern stretch is of interest, where in February high salinity values are observed.

Looking at the differences in surface and bottom layer salinity as shown in Table 9 and the images in Figure 25, an overall increase is observed from surface to bottom. While the values depict an average in time and space, the images give a hint of where the main differences are present. Here the areas where Mediterranean waters and lagoon water oppose each other show the larges differences in surface and bottom salinity. Further, the propagation of the more saline, heavier waters along the bottom and towards the inlets can be observed. Vice versa the less saline and lighter waters propagate further into the lagoon. This is the above-mentioned phenomenon of gravitational circulation. The details shown in Figure 25 depict this process around the eastern inlet, Boughaz 2, where the tidal inflow is more constrained and the bottom waters during February and August show a clear increase in salinity compared to the surface layers.

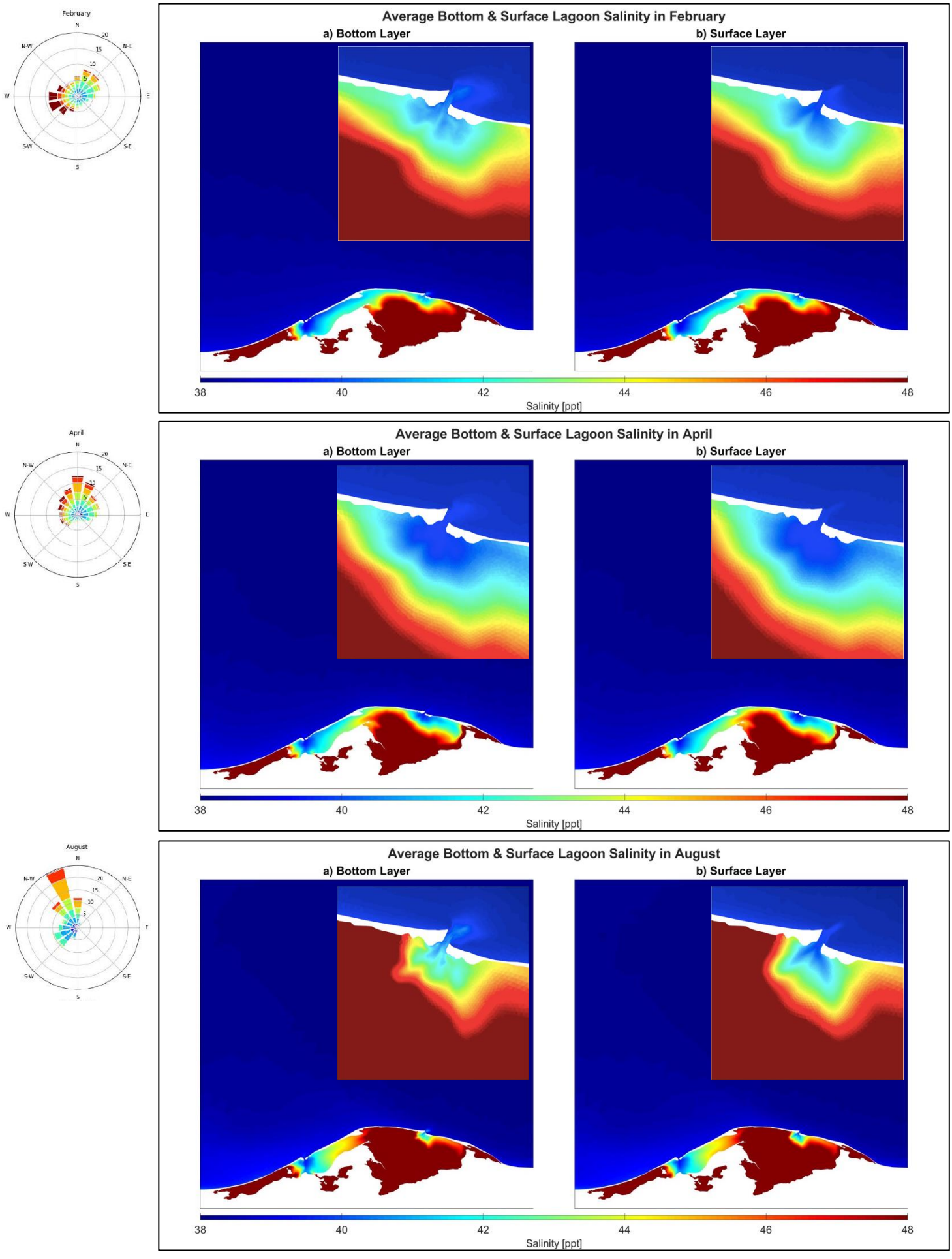

Figure 25: Showing the spatial salinity distribution over the lagoon area, of a) the bottom layer salinity and b) surface layer salinity incl. detail around Boughaz 2. Top to bottom: February, April & August including the wind roses.

Inlet Salinity

As mentioned in the preceding paragraph, the inlets show strong differences in the surface and bottom layer salinity over the different simulation periods. Hence it is important to look at their behavior over time. Therefore, three stations, namely the two inlets, "Boughaz 1" & "Boughaz 2" as well as one station in the inner lagoon "Bottleneck-Basin" were chosen. Figure 26 shows the time series for the month of a) February, b) April and c) August. Here the instantaneous salinity for the bottom and surface layer, are presented.

For the month of February, it is seen that Boughaz 1 is rather uniform in its top and bottom layer salinity. With averages of about *39 ppt,* the waters are of Mediterranean origin, underlining the strong tidal impact in the western inlet. Pronounced peaks around the strong wind event of February 16th show however slight effects of the meteorological forcing on Boughaz 1. The effect of the wind forcing is much more pronounced in the easter inlet, Boughaz 2, and also visible in the inner lagoon station. Here the present W-SW wind (see Appendix E) pushes the waters towards the east resulting in an increase of surface and bottom salinity in Boughaz 2. These waters likely originate from the bottleneck as shown in the bottom plot of a), where a strong decrease in overall salinity appears. These observations are in line with the above presented spatial distribution of the average lagoon salinity, where from west to east an impact of less saline water is seen (see Figure 25a). Hence, the reason for the higher salinities in Boughaz 2 during the period of February is the prevailing wind climate with the occurrence of strong W-SW winds.

For the month of April Boughaz 1 shows more variation in surface and bottom layer salinity. This however does not include distinct peaks. Here the period around April 13th & 25th should be pointed out, where N-NE winds occur, pushing waters from east to west.

This causes an increase in bottom layer salinity in Boughaz 1, which persists even during flood flow (see April 25th – 28th). Boughaz 2 on the contrary shows during most of the month no difference in salinity that is worth mentioning. Only around April 22nd a clear increase in the surface and bottom layer salinity is observed. This follows from the stronger W winds.

From the time series for the inner lagoon station "Bottleneck-Basin", it is seen that after an event of strong evaporation around April 14th (see Figure 23) the inner lagoon salinity increases rapidly and remains at higher salinity. Towards the end of the month, when the overall air temperature increases, and the evaporation rates are of regular and higher magnitude the inner lagoon experiences a constant increase in the surface and bottom layer salinity.

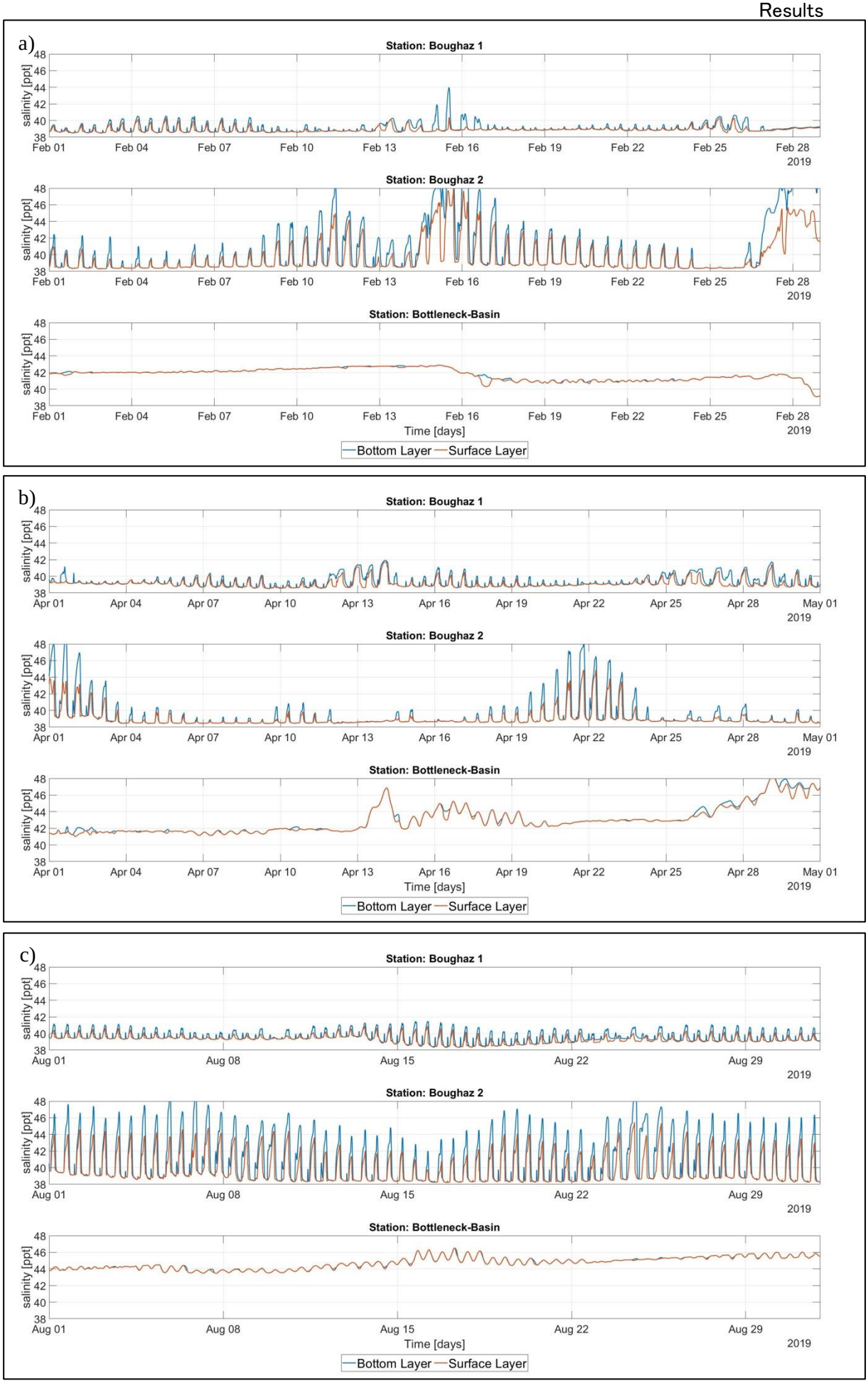

Figure 26: Time series showing the surface (orange) and bottom (blue) layer salinity in the inlets (top & mid panel) and a station on the verge from the bottleneck to the basin. Top to bottom shows the month of a) February, b) April and c) August

The time series for the month of August shows a very regular behavior, just as the above-presented hydrodynamics and evaporation results. Here Boughaz 1, again, depicts lower average bottom salinities than Boughaz 2. While for the former the values are in line with the adjacent Mediterranean Sea, the latter is affected by the lagoon waters. This was also shown by the spatial distribution of the average lagoon salinity in Figure 25c. Further, the amplitude of salinity in Boughaz 2 is much larger reaching up to *46 ppt*. For both, the surface and bottom layer, this strong excursion is seen. This is due to the overall high salinity in the inlet vicinity which is transported with the tide. For the inner lagoon station, high salinity is recorded, where over the course of the simulation it is constantly increasing.

For all simulation periods, it is observed that the inlets are sensitive to the present wind climate, where Boughaz 1 responds stronger to NE winds and Boughaz 2 to W-SW winds. While the W-SW winds cause a decrease in the salinity at the inner lagoon station, pushing waters into the basin, the NE winds show little effect. Here the enhanced evaporation causes a local increase in salinity.

Figure 27 shows the cross-sectional distribution of salinity. This is done for single points in time, where they all present a situation around HW, right after flood. As explained in the section on the average lagoon salinity, Boughaz 1 is in general less affected by the meteorological forcing and is tide dominated. This is shown again by the overall presences of Mediterranean waters in the inlet. Only during the month of April, very weak stratification is observed.
Boughaz 2 on the contrary shows the behavior observed in the average lagoon salinity plots, where during February and August more saline waters along the bottom layer are observed. Here the temporary stratification due to the gravitational circulation is observed.

As the gravitational circulation causes outward directed flow along the bottom layer this is also observed in the velocity signal which is shown in Figure 37 (see Appendix F). Here, beside the geometrical effects of the bathymetry and curvature, a clear outward directed velocity along the areas of high saline water is observed. Reaching values of *– 0.15 m/s* during August.

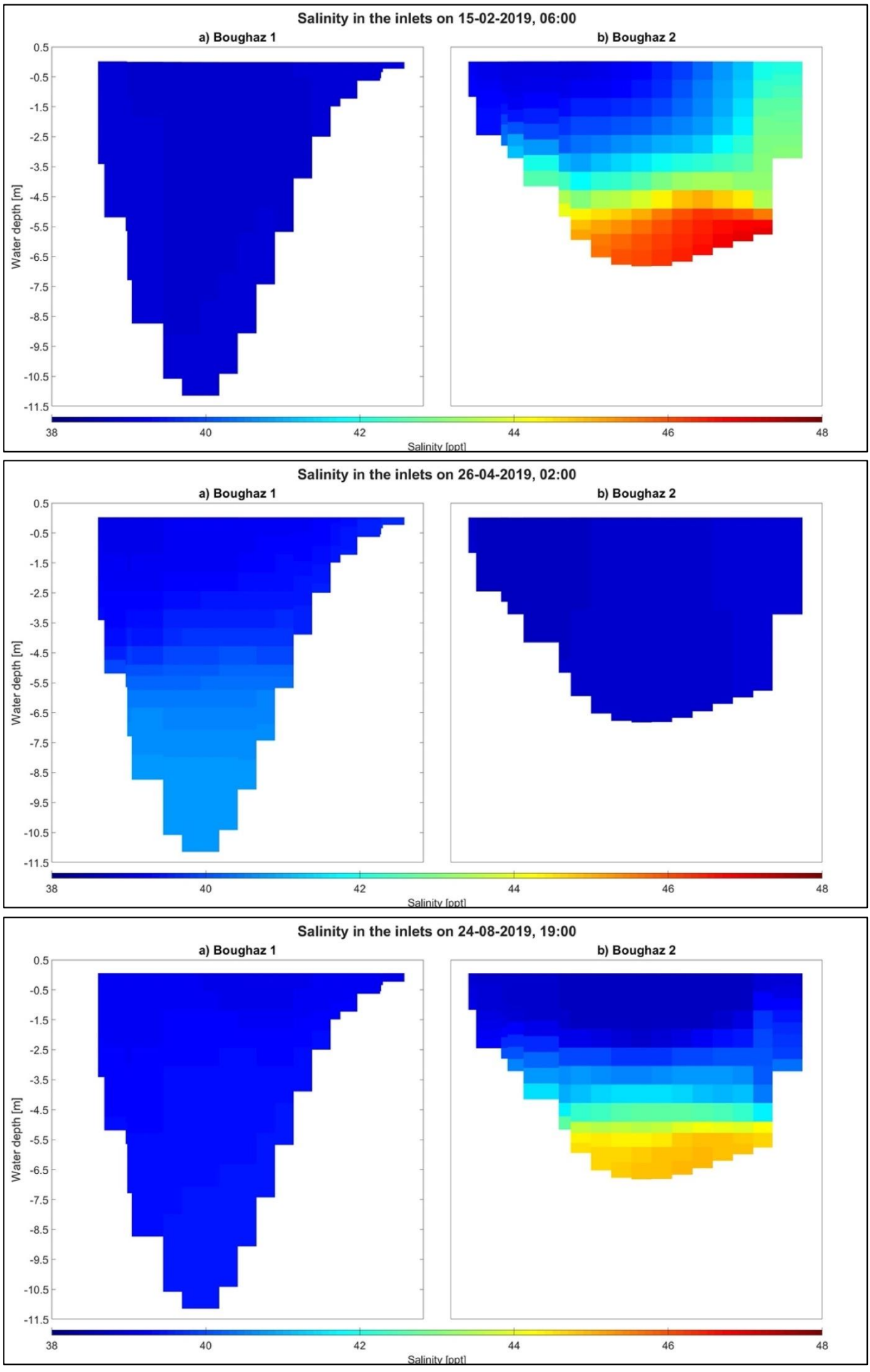

Figure 27: Cross-sectional plot of the inlet salinity [ppt] at individual points in time for February, April, and August (top to bottom). Situations presented always show a point in time after flood.

Interpretation of the results

From the above-presented results, a clear dependence of the salinity distribution over the lagoon area on the present meteorological conditions is observed. Here the extreme wind conditions during February with (strong) NW-SW winds at times, cause a wind-driven circulation as pointed out by Bek and Cowles (2018). This leads to stronger gravitational circulation in the eastern inlet and the overall basin. This supports the importance of wind-driven circulation in shallow lagoons, where the directional component causes a streamlined transport of water masses and hence of waterborne characteristics such as salt.

The average climate depicts a middle ground between the extreme wind and evaporation conditions. Here at times, wind-driven events are observed causing weak, short-term SIPS (mentioned event between April 25th – 28th) in the western inlet, while the eastern inlet mainly experiences tidal straining and the gravitational circulation by the density-driven flows. The observations made for Boughaz 2 show that the inlet is less affected by the average meteorological conditions during the month of April. Here the tidal influence is dominant and causes the waters in the inlet and inlet vicinity to be of Mediterranean origin, inhibiting salinities of *38 – 40 ppt*. For the inner lagoon, it is shown that the overall salinity increases constantly. Here the saline tongue on the verge of the bottleneck to the basin is a distinct feature. Due to the calmer hydrodynamic and meteorological conditions, the waters are prone to evaporation and the following increase in salinity.

During the extreme evaporation conditions, the abovementioned feature is even more pronounced reaching up to the barrier island. The overall regular pattern as described above is in line with findings by van Bentem (2020) where the month of August displayed an average wind climate. This in combination with the tidal forcing causes lagoon waters to be less dynamic than during the other periods. Further, the presence of a tidal divide-like location on the verge of the bottleneck and the basin causes calm conditions leading to strong increases in salinity, as shown for the location in Figure 26c. Much higher salinities in the inner lagoon support the claim that stronger wind-driven circulation is important for a dynamic system. This is not the case during the summer month. Nonetheless does the western inlet show constantly higher bottom than surface layer salinities supporting the presence of gravitational circulation in the inlet over the tidal cycle.

4.3 Results – Adaptations

For the model simulation, including the proposed system adaptations by TWM, the average month was chosen. This is done to get a first understanding of how the additional inlets and deeper tidal gullies influence the lagoon and the old inlets in their characteristics.
From the implemented bathymetry changes, new cross-sectional inlet areas are obtained as shown below.

Table 10: Cross-sectional inlet areas [m^2] after system adaptations

	Cross-sectional inlet area [m^2]			
	Boughaz 1	Boughaz 2	Boughaz 3	Boughaz 4
Old	1813	1799	-	-
New	2147	2995	1273	2831
Diff.	+ 18 %	+ 66 %	+ 100 %	+ 100 %

4.3.1 Hydrodynamics

In the following sections, the hydrodynamics will be discussed. This is done concerning the properties obtained during the status quo simulations. The overall increase in water exchange and flow velocities is evident.

Discharge & Velocity

As for the previous result section, the ebb and flood discharge through the inlets are considered. Therefore Table 11 shows the maximum ebb and flood discharges in the old and new inlets. Figure 28 shows the instantaneous as well as the tidal-averaged discharges. The values of two new inlets, here Boughaz 3 & 4, cannot be compared to any other simulation. Here, the discharge magnitude aligns well with the inlet velocities (see Table 12) and the average cross-sectional inlet area (see Table 10). For the old inlets, the change or increase in the maximum ebb and flood discharge is given below. Here it becomes evident that the adaptations to Boughaz 1 increase the effective discharge by *30 - 40 %* while in Boughaz 2 the maximum discharges almost double (*+ 91 - 95 %*)

Table 11: Showing the max. ebb and flood discharges [m^3/s] through the inlets during the simulation of the system adaptations

		Inlet Dis. [m^3/s]	%
Boughaz 1	$Q_{max,in}$	2427	*+ 29*
	$Q_{max,out}$	2329	*+ 39*
Boughaz 2	$Q_{max,in}$	3723	*+ 91*
	$Q_{max,out}$	3761	*+ 95*

		Inlet Dis. [m^3/s]
Boughaz 3	$Q_{max,in}$	1419
	$Q_{max,out}$	1312
Boughaz 4	$Q_{max,in}$	2813
	$Q_{max,out}$	2722

Furthermore, the overall signal of the instantaneous discharge becomes much more regular as seen in the time series below. This connects to the overall larger discharges and velocities in the inlets, which promote tide dominance and a lesser effect of non-tidal forcing. Only in the western inlets, Boughaz 1 & 3, during the neap tidal period around April 13th clear offsets are visible. These are likely to originate from the strong wind event around that date. Here N-NW wind is pushing water into the western inlets. While Boughaz 3 depicts very small discharge magnitudes, only reaching *1312 m^3/s* and *1419 m^3/s* during ebb and flood respectively, Boughaz 2 exceeds the set limit and increases significantly up to *3761 m^3/s*.

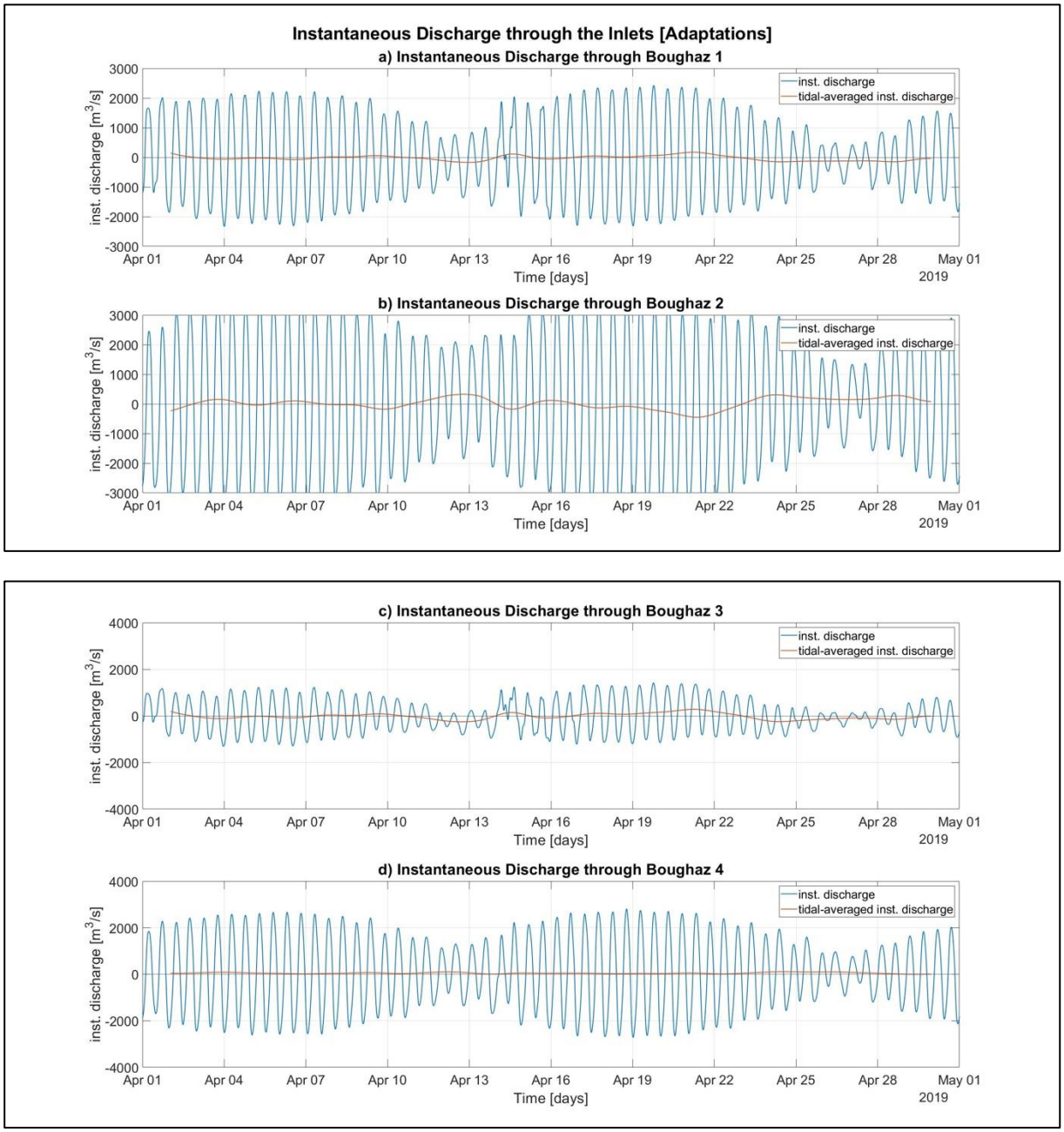

Figure 28: Timeseries of the instantaneous and tidal-averaged discharges [m^3/s] in the inlets during the simulation of the system adaptations. Top panels a) & b) showing the plots for Boughaz 1 & 2, bottom panel c) & d) for Boughaz 3 & 4.

Table 12: Showing the max. ebb and flood velocities [m/s] in the inlets during the simulation of the system adaptations

		Velocity [m/s]
Boughaz 1	$U_{max,flood}$	1.12
	$U_{max,ebb}$	1.11
Boughaz 2	$U_{max,flood}$	1.24
	$U_{max,ebb}$	1.26

		Velocity [m/s]
Boughaz 3	$U_{max,flood}$	1.11
	$U_{max,ebb}$	1.05
Boughaz 4	$U_{max,flood}$	0.98
	$U_{max,ebb}$	0.98

For the inlet velocities, the same behavior is seen. Here all inlets depict maximum ebb and flow velocities of larger magnitude. Here lowest inlet velocities are observed for the new inlet, Boughaz 4. While they are lower than for the other inlets, the equilibrium velocity as previously mentioned is surpassed.

Residual Discharges

Looking at the residual discharges in the inlets, the oval behavior of the old inlets remains the same. The old western inlet has a net, negative residual discharge, and the old easter inlet a net, positive residual discharge. The two new inlets depict the same behavior as their closest neighboring inlet. Meaning that Boughaz 3 inhibits, as Boughaz 1, a net, negative residual discharge, and Boughaz 4 a net, positive residual discharge.

The overall behavior of the system remains the same, where the systemwide net residual discharge amounts to *+ 24.85 m^3/s*. Considering the monthly net inflow following form this residual discharge, the overall volume amounts to *64.4x10^6 m^3*. This is in comparison to the status quo simulation closer to the estimated volume losses by Euroconsult (1995), with an error of *– 7 %*.

Table 13: Showing the residual discharges [m^3/s] through the inlets as well as the net residual discharge & the total residual volume [m^3]

	Boughaz 1 [m^3/s]	Boughaz 2 [m^3/s]	Boughaz 3 [m^3/s]	Boughaz 4 [m^3/s]	$Q_{res,net}$ [m^3/s]	$V_{res,total}$ [10^6 m^3]	$V_{Euroconsult}$ [10^6 m^3]	Δ_{Vol}
Adaptations	- 27.56	+ 24.18	- 22.46	+ 50.69	+ 24.85	+ 64.4	69.3	*- 7 %*
Status Quo	- 12.93	+ 36.66	-	-	+ 23.73	+ 61.5	69.3	*- 11 %*

The time series as shown in Figure 29 depict a very similar behavior as for the status quo simulation, where Boughaz 2 inhibits strong positive residual discharges during NE winds and strong negative residual discharges during W-SW winds.

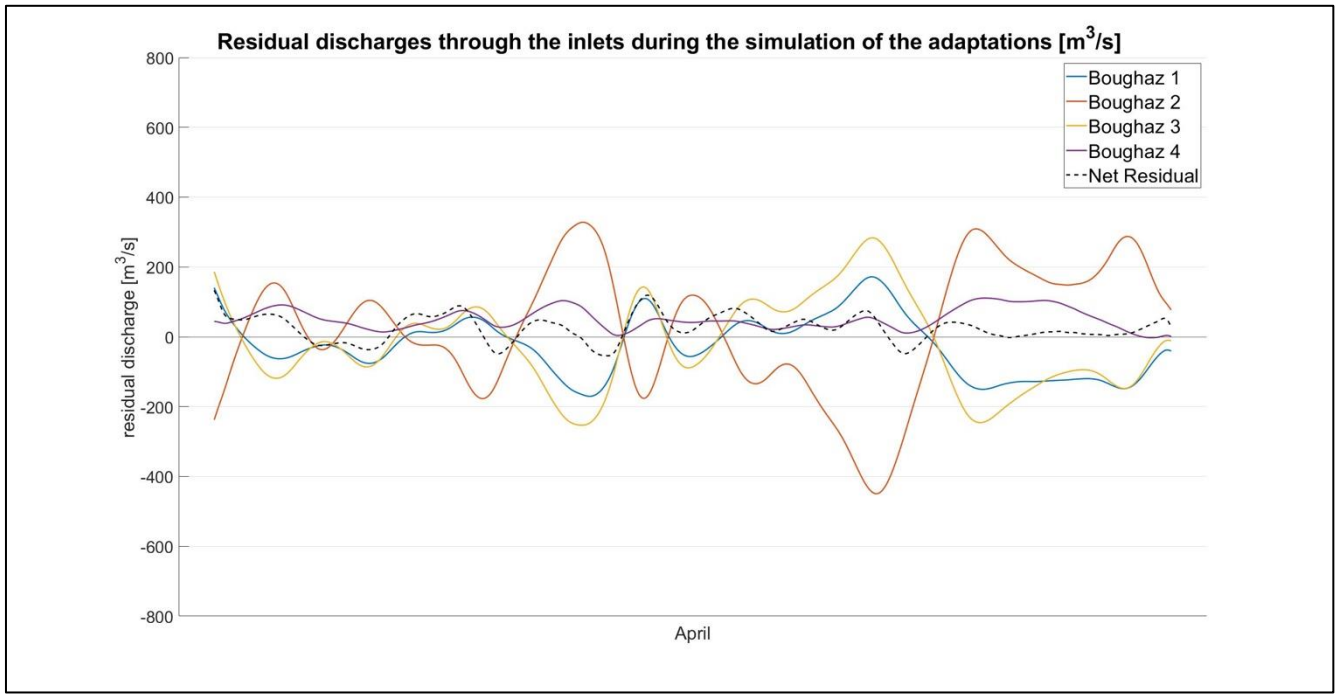

Figure 29: Residual discharges [m^3/s] through the four inlets during the simulations of the adaptations. Showing the inlet specific residuals (blue, orange, yellow, purple) and net residuals (black) for the months of April

Tidal Prism

As presented in Table 14 the tidal prism increases significantly in comparison to the status quo simulations. Here an overall increase of *255 %* was computed for the average tidal prism, leading to much larger volumes of water being exchanged over a tidal cycle. Especially Boughaz 2 experiences a large increase by almost doubling the average tidal prism. In general, the eastern inlets Boughaz 2 & 4, contribute the most to the overall tidal prism (*approx. 67 %*).

Table 14: Values of the tidal prism [m^3] in the four inlets as well as the total tidal prism after the adaptations. In addition, the change concerning the status quo situation is given in %

	Average Tidal Prism [10^6 m^3]				**Spring Tidal Prism [10^6 m^3]**			
	Boughaz 1	Boughaz 2	Boughaz 3	Boughaz 4	Boughaz 1	Boughaz 2	Boughaz 3	Boughaz 4
Adaptations	25.1	43.5	12.6	29.9	39.9	75.5	26.4	42.5
Total	**111.2**				**179.3**			
Change	**+ 255 %**				**+ 252 %**			

Interpretation of the results

From the above-presented results, it can be concluded that the overall system dynamics change significantly. For this, the tidal prism acts as an objective indicator that is less prone to external impacts. The strong increase in the average and spring tidal prism, after the system adaptations were included, speaks for a much stronger interaction between the Mediterranean Sea and Lake Bardawil. Further are the higher velocities in favor of the inlets, when considering the equilibrium inlet velocity that was mentioned earlier and used by van Bentem (2020) for the assessment of the inlet stability and the sediment transport character.
The overall positive and hence inflowing residual flow through the inlets aligns well with certain data from literature. The small offset by 7 % in compensative volume is, considering the uncertainties and simplifications made in this study, in an acceptable range.

4.3.2 Evaporation

Table 15 shows the daily and monthly evaporation rates obtained from the model for the status quo simulation of April as well as for the simulations of the adaptations. Furthermore, the total evaporated volume is given. Overall, it is shown that the number increase after implementing the adaptations. This increase of approximately *8 %* leads to values that are closer to the values from literature ($V_{Euroconsult}$) as shown in Table 13.

Table 15: Daily & monthly evaporation rates for the status quo simulation of April and the adaptations

	April	Adaptations	± %
Evaporation rate [mm/d]	2.43	2.63	+ 8
Evaporation rate [mm/m]	73	79	
Evaporated Volume [10^6 m^3/month]	41.3	44.5	

Interpretation of the results

As shown before, the lagoon wide evaporation increases with the implementation of the system adaptations. This is likely to be related to the larger volumes being exchanged between the Mediterranean Sea and the lagoon. Hereby the covered area is larger and the water levels in the lagoon are higher. This leads to a larger surface area susceptible to evaporation. In combination with the EHF, which is not changing, this leads to the conclusion that the increasing modeled evaporation rate and volume are purely related to the larger surface area covered during the simulation. This is an expected outcome, as the input of the heat flux model does not change.

4.3.3 Salinity

Average Lagoon Salinity

To assess the effect of the system adaptation on the overall lagoon salinity, the same indicators as for the status quo simulation were used. Here Table 16 shows the overall average surface and bottom layer salinity of Lake Bardawil. From this, a clear decrease in the average lagoon salinity due to the adapted bathymetry is seen. By increasing the exchange flows (see section 4.3.1 on the Hydrodynamics) an effective decrease by 10 % can be reached. The bottom layer salinity experiences a slightly larger decrease than the surface layer salinity. Furthermore, does the surface-to-bottom difference in salinity Δ_{Sal} decreases by *50 %* from *0.18 ppt* to *0.09 ppt*.

Table 16: Showing the surface and bottom layer salinity [ppt] for April before and after the adaptations

	April	Adaptations	± %
Surface	45.79	41.12	- 10.2
Bottom	45.97	41.21	- 10.4
Δ_{Sal}	+ 0.18	+ 0.09	

Shifting from the overall average to the spatial distribution of the average layer salinities, strong changes are observed (see Figure 30a). Here the broad stretch of less saline water along the barrier island is a distinct feature. By allowing the Mediterranean waters to travel further into the lagoon the lagoon waters show a strong decrease in salinity. This results in salinities in the range of the adjacent Mediterranean Sea of *38 – 40 ppt*. Furthermore, it indicates stronger connectivity between the different parts of the lagoon after implementing the adaptation proposed by TWM.

As the inlets do not depict significant differences between the surface and bottom layer anymore, a different location was chosen to get a detailed view. Figure 30b shows the zoomed-in view at the channel entrance to the isolated pond behind Boughaz 1. Here the adaptations foresee a deepened channel, which as mentioned above might enhance the density-driven flows. For the considered case this is visible when looking at the excursion of bottom salinity in comparison to the surface salinity. Here the more saline waters propagate towards the inlet, while the less saline surface shows slightly farther propagation into the isolated pond. This is indicated by the two black arrows in Figure 30b.

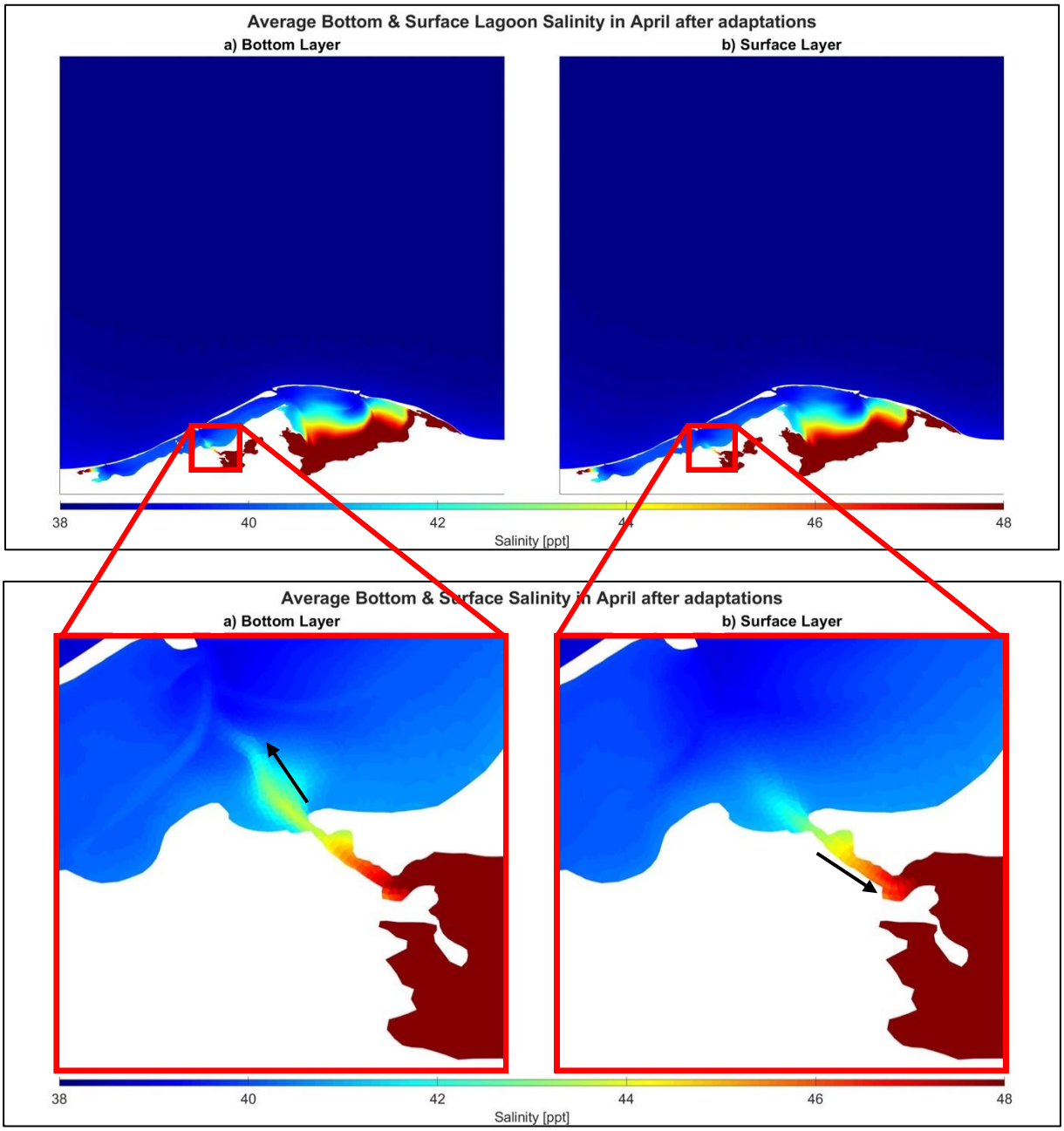

Figure 30: Top: Average bottom and surface layer salinity [ppt] over Lake Bardawil after the adaptations. Bottom: Detail of bottom and surface layer salinity at a location in the western bottleneck.

Inlet Salinity

As for the status quo, the surface and bottom layer salinity in the inlets is considered. This is done to understand how the inlets behave with respect to the meteorological forcing and the changes in bathymetry. As was shown before, the inlets do not depict strong surface-to-bottom differences during the month of April. From the spatial distribution this is already seen, where the average surface and bottom layer salinity are of Mediterranean salinity. Figure 31 displays the time series of the surface and bottom layer salinity at the inlet stations as well as for the bottleneck-basin station.

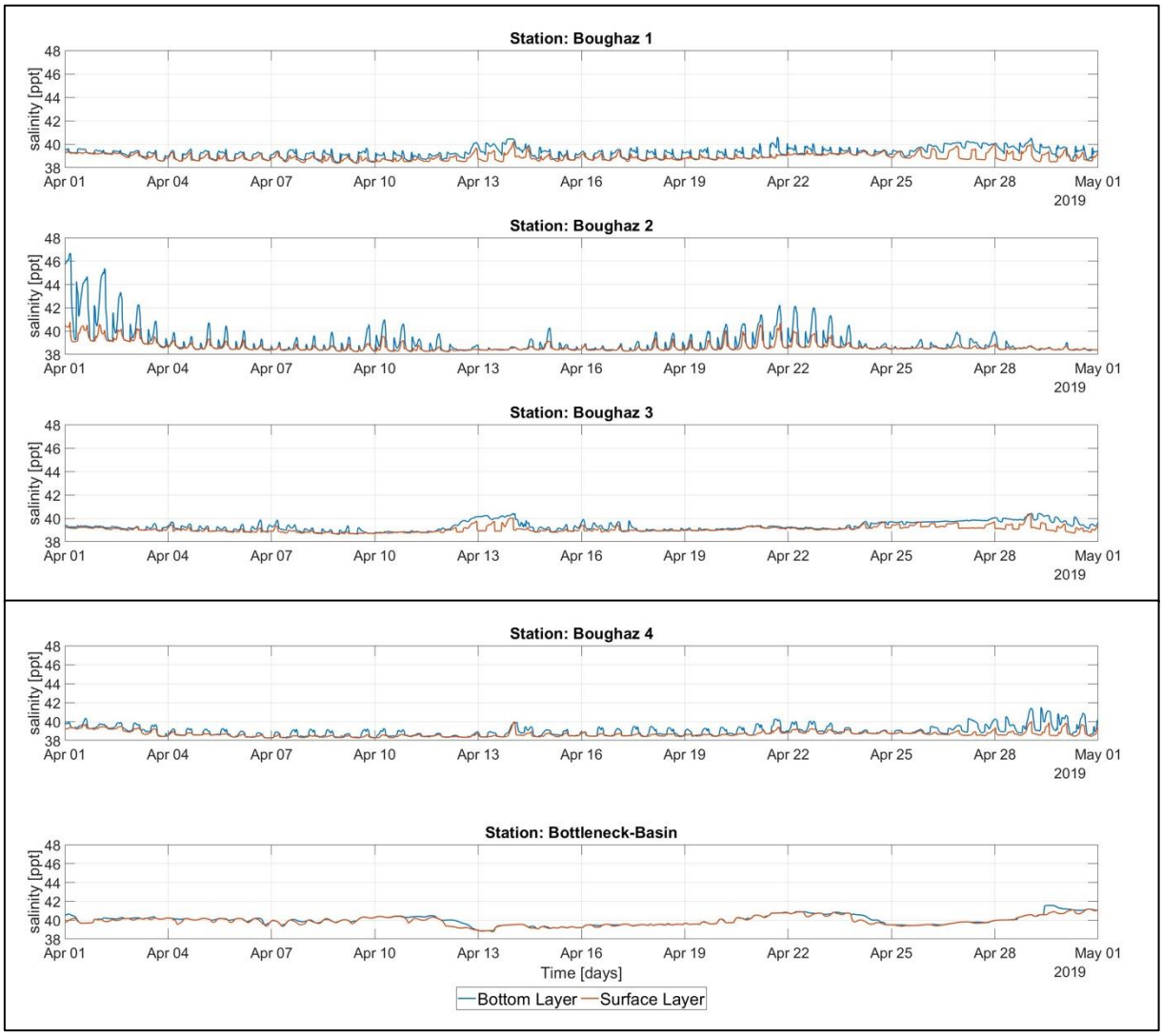

Figure 31: Time series showing the surface (orange) and bottom (blue) layer salinity in the inlets and a station on the verge from the bottleneck to the basin. Top to bottom shows the stations of Boughaz 1 – 4 & Bottleneck-Basin

Table 17: Average layer salinities [ppt] in the considered stations

Layer	Individual Layer salinity in Stations [ppt]				
	Boughaz 1	Boughaz 2	Boughaz 3	Boughaz 4	Bottleneck-Basin
Surface	38.89	38.65	39.06	38.68	39.90
Bottom	39.25	39.02	39.31	38.97	40.00

From the graphs but also the average layer salinity (see Table 17) the overall decrease in salinity is evident. While during the status quo situation the overall lagoon salinities are much higher, here the waters are of Mediterranean origin (salinities around *38-40 ppt*) even at the inner lagoon station “Bottleneck-Basin”.

Furthermore, the signals show a smoother behavior where even during the previously pointed out events, less clear distortions are present. Changes are however observed in Boughaz 1 and coherently Boughaz 3, where around April 13th and April 25th – 28th larger bottom salinities persist even during flood flow.

Interpretation of the results

From the presented results it can be concluded that the system adaptations have a considerable effect on the salinity of Lake Bardawil. Here the clear decrease in the average lagoon salinity speaks for effectiveness. The broad stretch of less saline, Mediterranean waters along the barrier island is a clear indicator for enhanced connectivity. While during the status quo simulations, slowly and hypersaline tongue built out on the verge of the bottleneck to the basin, this feature is not observed anymore. It is countered by the stronger inflow due to the tide and the space given by the deepened channels.

Even in the more isolated areas, as shown in the detailed top view, the effects become visible. Here the less saline waters propagate farther into the lagoon while causing the gravitational circulation to push the more saline, heavier waters towards the inlets.

Only the high saline patches along the fringes of the eastern basin remain. Here the present wind climate with predominantly N-NW winds traps the waters. Meaning that here the wind-driven forcing component still dominates.

4.4 Inlet Classification

In the following section, the classification of the inlets according to the estuarine parameter space for the individual simulation will be presented. Here the determination is done in line with the initial assessment, where the freshwater flow was substituted by the compensative flow through the inlets by means of the evaporative losses in the lagoon. The tidal velocity was chosen as the depth-averaged velocity. For the scenarios modeled, Table 18 shows the freshwater Froude number as well as the mixing parameter during spring and neap tide for the inlets. Figure 32 shows the inlets of the estuarine parameter space.

Table 18: Freshwater Froude No. & Mixing Parameter for the initial assessment and the individual modeling periods including the spring and neap tidal velocities in the inlets.

	Initial Assessment		February		April		August	
	Boughaz 1	Boughaz 2	Boughaz 1	Boughaz 2	Boughaz 1	Boughaz 2	Boughaz 1	Boughaz 2
Fr_f [10^3]	1.9 – 4.2	2.6 – 5.5	9.8	12.6	6.6	8.6	1.3	1.6
M_{neap}	0.73	0.96	1.16	2.64	1.09	1.54	2.03	2.72
M_{spring}	2.89	3.43	3.14	4.38	3.16	4.31	3.05	4.25
Fr_f: Freshwater Froude No.; M_{spring}: Mixing Parameter during spring tide; M_{neap}: Mixing Parameter during neap tide								

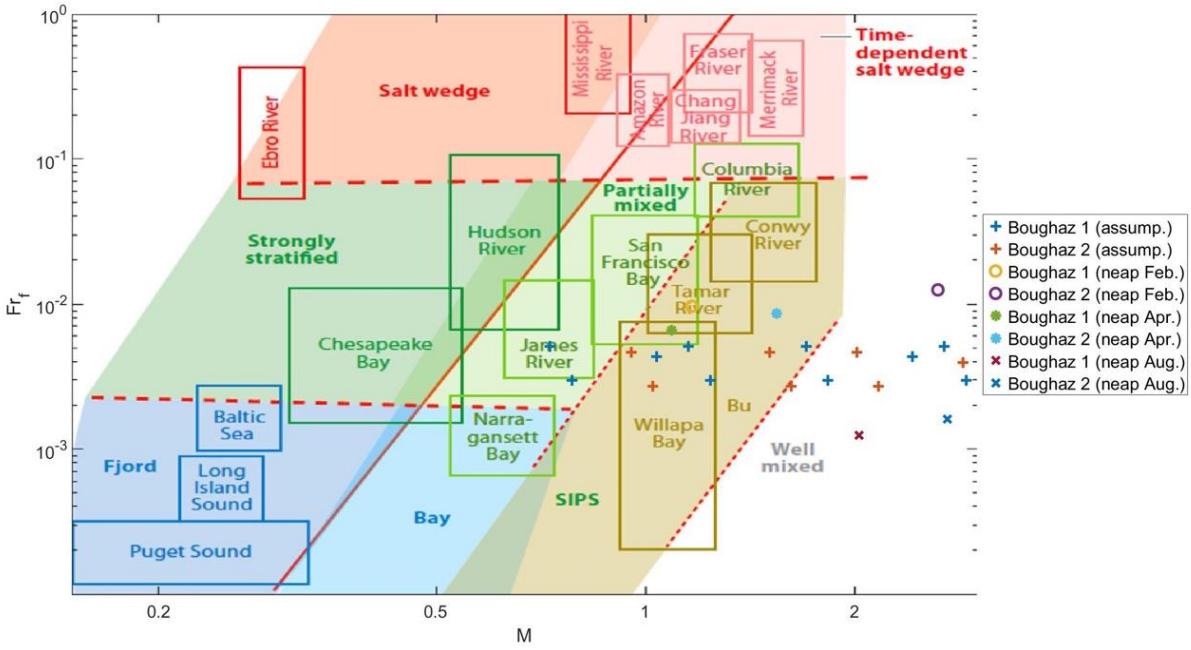

Figure 32: The inlets on the estuarine parameter space according to the modeling results. Here only the neap tidal values are shown since the spring tidal values exceed the space.

4.4.1 Boughaz 1

The western inlet shows throughout the three modeling periods a very similar behavior, where the differences between top and bottom layer salinities are of small and constant nature. With average surface and bottom layer salinities ranging between *38.8 ppt* and *39.5 ppt* respectively, it displays weak stratification (see Table 19). This weak stratification is pronounced during ebb tide and vanishes during flood, which is the phenomenon of tidal straining or ebb-tidal straining.

Table 19: Average surface and bottom layer salinity [ppt] in Boughaz 1 during the simulation periods

	Layer Salinity [ppt]		
	February	April	August
Surface	38.8	39.1	39.3
Bottom	39.1	39.3	39.5
Δ_{Sal}	+ 0.3	+ 0.2	+ 0.2

Considering Boughaz 1 on the estuarine parameter space, it is shown that in line with the initial assessment, it can be classified as a well-mixed system. The freshwater Froude numbers by means of compensative flows for evaporative losses are in the same order of magnitude for the model runs and the initial assessment. The mixing parameters are found in the upper bounds and even exceeding the presented parameter space as shown in Figure 32. Responsible for this strong shift into the well-mixed range are aside from the inlet velocities, the changes in water depth because of the applied bathymetry. Hence the initial system proves to be of very idealized nature, whereas a more thorough analysis showed that Boughaz 1 is purely well-mixed. Here it is however important to say that this evaluation in general, is rather crude by assuming the consistency of the conditions in the location. The, in previous studies mentioned, fast dissipation of the velocities inside the lagoon is cause for persistence of the high salinities within the lagoon.

The phenomenon of ebb-tidal straining persists over all simulation periods. During the month of April and the previously mentioned events around April 13th & 25th (see 4.2.3) however, short-term SIPS can be observed. Here the bottom waters display higher salinity values even during flood flow. This finding is in line with the results presented in Figure 32 where Boughaz 1 is found in the range of SIPS on the estuarine parameter space.

4.4.2 Boughaz 2

As presented in the chapter on the results for the status quo simulations, Boughaz 2 shows a much stronger dependency on the occurrence of extreme weather conditions by means of strong wind and high evaporation events.

Table 20: Average surface and bottom layer salinity [ppt] in Boughaz 2 during the simulation periods

	Layer Salinity [ppt]		
	February	April	August
Surface	39.5	38.9	39.6
Bottom	40.3	39.2	40.8
Δ_{Sal}	+ 0.8	+ 0.3	+ 1.2

Especially during the months chosen, representing the extreme weather conditions, Boughaz 2 displays a large variability in its state, ranging from well-mixed to more pronounced SIPS. This can also be seen by the presented surface and bottom layer salinity in Table 20 and Figure 25, where the bottom layer inhibits higher salinities throughout the month.

During February the shift in the state of the inlet is caused by the occurrence of two consecutive days of very high evaporation forced by W-SW strong winds, which causes the bottom salinities in the inlet to increase significantly and causes SIPS by the combined effect of gravitational circulation over the vertical and wind-driven circulation in the horizontal plane. The very slow response of the inlet promotes the persistence of SIPS for several days.

During April Boughaz 2 displays mostly well-mixed conditions, where only during an event of high evaporation a short-term response in bottom layer salinity is present.

During the month of August, where constantly high evaporation rates occur, Boughaz 2 displays very high salinity values, both in the bottom and surface layer, during ebb flow. These vanish due to tidal straining during flood flow for most time of the month. The strongest ebb-tidal straining occurs during neap tidal periods where the tidal flows are not as energetic. Overall, the salinities recorded in the inlet are much higher than for the other months which is in line with the high evaporation and increased salinity.

The presented results show the strong dependency of the state of Boughaz 2 on the behind lying water body in combination with the local weather conditions. This leads to the conclusion that the response of Boughaz 2 to meteorological forcing is much stronger than for Boughaz 1. Here, especially the prevailing wind direction determines the response of the lagoon and the inlets. Further, a dependence on the spring-neap tidal cycle is observed, whereas the classification of the inlet can be affected beyond the presence of low energetic periods.

5 | Discussion

In the following sections, the overall findings, as laid out above, will be discussed. This is done by addressing the considered key indicators. At last, a short discussion on the extent of the model domain is given, which focuses on the computational aspect of the study.

5.1 Hydrodynamics

The properties of discharge and velocity in this study were considered as the cross-sectional averaged value in the pre-defined inlet cross-sections. This implies a shift away from the previously used depth-averaged approach. Considering the available 3D data, the use is ought to provide a more realistic image of the inlet velocities and overall characteristics. This is because the depth-varying components influence the overall discharge and velocity signal.
Looking at the time series and cross-sectional distribution of the velocities the former gives an overall idea of how the inlets respond during the simulation months. The latter gives more insight into how this velocity is distributed in the cross-section.
As the analysis showed, the considered parameters show a clear response to the meteorological forcing. This was shown in the time series of the instantaneous properties as well as in the residual discharge. Furthermore, the cross-sectional plots showed that at distinct points in time subtidal flows persist over the tidal cycle. This is a strong feature, observed during periods where the meteorological forcing alters the inlet characteristics.
As the focus of this study is on a more general understanding of how extreme meteorological conditions throughout the year affect the hydrodynamics, it comes short in the analysis of the detailed inlet properties. Here the presented 3D data only gives a momentary impression of the conditions in the inlet, from a long series of possible time steps. While these observations support the research on the investigated flows, it would be of interest to look at shorter time frames, during which one forcing is expected to be pronounced. This would mean looking at time scales of for example one tidal cycle only or a distinct storm event. This is thought to provide insight into the more frequent conditions present at Lake Bardawil and the persistence of possible subtidal flows.
From a numerical point of view, the here implemented 3D hydrodynamic model shows stable conditions and results for the discharge and velocity which are in a range that is in line with previous studies. This supports the model itself, whereas the vertical resolution could be increased by changing the model setup itself. This would give increased detail in the inlets

and allow for a more detailed analysis. Here the trade-off between computational expense and required detail is governing the extent to which this refinement of the grid is feasible.

5.2 Tidal Prism

While the average tidal prism for the status quo simulations provides coherent values, the spring tidal prism is significantly varying. As already pointed out in the interpretation of the results, this comes due to the presence of strong wind conditions. These alter the discharge signal in such a way that for a longer period only positive discharges occur. As the zero-crossing approach does not apply during this time, large volumes are computed. As the spring tidal prism is by definition the largest volume between two zero crossings in the discharge signal this very large volume is considered.

By this it shows that the tidal prism is a good indicator when either 1) average values are considered or 2) calm and regular conditions can be expected. The latter means that a clear tide dominance is visible in the discharge signal and no strong distortions are present as observed for April and August.

Furthermore, the results discussed above show that around the end of February, Boughaz 1 experiences solely an inflow, while Boughaz 2 experiences solely an outflow. As in the here chosen determination, absolute values are used, this leads to an overestimation of the tidal prism. By excluding the last days from the tidal prism calculation more realistic values were obtained.

This all shows some limitations and precautions that have to be taken when analyzing a system with regard to the tidal prism. While, on average, this parameter allows for an objective analysis, it is sensitive when looking at individual events or shorter time scales.

With respect to the system adaptations, the tidal prism shows a clear increase, which is one of the main goals of the design. Here the adapted inlets and dredged channels allow for more water to flow in and out of the lagoon during a tidal cycle. Also, it allows for farther propagation of the tidal flow and enhanced gravitational circulation in the channels.

The choice of the average month for the simulation of the adaptations also proves to be of good accuracy. Here the increase from the average tidal prism to the spring tidal prism is similar for the status quo and adaptation simulations.

5.3 Evaporation

The implementation of evaporation in the numerical model was done by the composite heat flux model included in D-Flow FM. The model computes the evaporative heat fluxes at the defined stations and determines the cumulative evaporation over the whole model domain.

The input data required for the heat flux model are the present air temperature, wind velocity, relative humidity, and cloud coverage. Solar radiation is included using the corresponding time of the day at the latitude of the system. Prescribing solar radiation is also possible, for this model however no data on that property was available. By the availability of the hourly recorded values from the Meteoblue data set, the implementation of the heat flux model and the following evaporation is rather straightforward. Considering the implementation of a spatially uniform distribution over a model domain with that extent is likely to introduce inaccuracies or cause for inaccurate representation of important local aspects. By that, especially local changes in the water properties and the susceptibility to evaporation were not accounted for.

This is likely to influence the computed evaporation rates, which showed strong discrepancies when comparing them to values from literature. Here it is found that the property of the EHF depicts very low values along the fringes of Lake Bardawil while in the inner lagoon it showed considerable values. The former is however nothing one would expect when taking the shallowness along the fringes and the large effect of heating of the waters into account. Following equations 10 & 11 an increase in (surface) water temperature would lead to a decrease in the latent heat of vaporization and consequently to an increase in evaporation rates. This however was not observed in the model.

Reasons for this might be found in the just mentioned shallowness along the fringes. Due to periodic dry falling of the cells, the heat flux model dismisses the contribution to evaporation. Here it is worth mentioning that the dry cell threshold was set to 0.05 m, meaning water levels below this value are considered dry. This was done to decrease computational expense. However, in retrospect, it might introduce crucial changes to the here-discussed property of evaporation rates.

Further, the composite heat flux model as implemented by Deltares (2021b) was “calibrated for the North Sea and successfully applied for great lakes”. These are however significantly different systems than Lake Bardawil. As laid out and explained above, the model does calculate considerable evaporation rates across the open water body while discarding the fringes. To resolve this problem an adjusted model could lead to a more accurate determination. Furthermore, a model with a clear focus on modeling evaporation rates at Lake Bardawil would increase the accuracy and strengthen an important but sensitive system variable. Worth mentioning is the lack of reliable/validated data to validate one’s model against.

At last, it must be pointed out, that the compensative volumes due to the residual flows align rather well with the evaporation rates from literature. Here only the month of February is largely underestimated. This points to the possibility, that the determination of the evaporation rates, by the EHF-Latent-Heat ratio presented in section 3.3.4, introduces errors.

While all the above-shown aspects show that the results from the heat flux model inhibit uncertainties and inaccuracies, the implementation of the heat flux model shows an overall satisfying first result. The continuous effect of evaporation causes the average surface salinity values to vary over the different months, where the monthly average aligns well with the data used for validation. Furthermore, the overall trend with the largest evaporation rates during summer is observed.

5.4 Salinity

As mentioned in the introduction of this study, shallow coastal lagoons in (semi-)arid climate regions which are suspect to periods of very high evaporation rates can experience a net influx of salt into the water column following these events. This facilitates a flow of more saline and heavier water along the bottom towards the deeper regions/inlets.

The here presented 3D hydrodynamic model aims at investigating and understanding the behavior of such a coastal lagoon during extreme weather conditions and in specifically the effects on the lagoon salinity over depth.

Generally speaking, the here presented model shows the salinity differences from the surface to the bottom layer and resembles the effects of high evaporation events. The continuously high temperatures during the month of August do not only cause the largest evaporation but clearly show an impact on the lagoon salinity. Either in the monthly averaged value or the spatial distribution. The spatial distribution also shows very well to what extent the inner lagoon waters interact and how strong the impact of the tidal flow is. Hence indicates how 'active' the waters are. By this it is referred to more dynamic flow conditions inside the lagoon.

However, this model is to present knowledge, the first numerical investigation into the 3D behavior of Lake Bardawil considering salinity changes over depth. Hence, the depth-varying results lack validation from in-situ measurements or other numerical simulations. The most recent measurement values, which are presented in section 2.2.6, by the Egyptian Environmental Affairs Agency (EEAA) (2016) only provide general average lagoon salinity values. Nevertheless, the here computed average lagoon salinities show a good correlation laying in the provided range. This data should not be used for validation purposes since it is not sure where the measurements were carried out and the time of the year to which the values relate.

The chosen validation by means of the comparison of surface salinity values shows good resemblance in the regions closer to the inlets while the embayed or isolated areas show over or underestimations in comparison to the measured data from 1999/2000. This shows that there might be processes involved that cannot be modeled by the hydrodynamic model. These might include salt extraction by means of dry falling land or other natural processes one did

not/cannot account for in the scope of this research. However, from literature, it is known that Lake Bardawil is home to vast areas of salt pans where occasional dry falling occurs. These locations are found in the shallow, embayed regions and hence the salinity values could increase drastically.

An overall problem that remains is the lack of reliable data on the salinity in Lake Bardawil. By this, a sound statement regarding the accuracy and validity of the model outcomes continues to be difficult. What however can be said is that the observed values and three-dimensional patterns are in line with the expectation from theory. Here the density-driven patterns around the inlets but also along the entrance channel of the pond behind Boughaz 1 resemble the processes described in the chapter on the underlying theory.

5.5 Salt Fluxes

As this study considers the exchange flows between Lake Bardawil and the Mediterranean Sea (see section on discharges) the quantity of salt fluxes will be discussed briefly. This parameter is not included in the result section due to numerical inaccuracies related to it, however it was considered along the research.
This quantity can be understood as the effective discharge of salt through a pre-defined cross section. In this case, the inlet cross sections of Boughaz 1 & 2.
By investigating the amount of salt being transported over a certain period in relation to the occurrence of extreme conditions is thought to give a good idea of the salt transport capacity of the inlets.
As the time series of the cumulative salt flux in the Boughazes 1 & 2 showed good resemblance with the meteorological forcing and the top and bottom layer time series, it only allows for a qualitative trend analysis rather than a quantitative assessment. The latter is however crucial when volumes should be compared and discussed.
After further consultation with Deltares, this property needs to be treated with care. For once difficulties with the property, in general, were recorded and the implementation in the here used version of D-Flow FM (2021.05) was not finalized. Furthermore, the definition of the velocity and salinity component on the computational grid might introduce numerical inaccuracies. Here the salinity value is defined at the cell center, while the velocity component is defined on the cell face. Meaning that the properties are spatially not aligned and the computation of the salt flux by equation 5 is not accurate. Considering the size of the model domain and the individual grid size this might introduce considerable changes in the salt flux property. Furthermore, this quantity is rather difficult to validate at this point.

If a quantitative analysis of this property is wanted or required, measures to decrease the numerical inaccuracies should be taken. To do so, one could be to further refine the grid in the cross section(s) of interest. This however comes at the expense of computational time and power. Another option would be the setup of an inlet-specific 3D numerical model with the appropriate initial and boundary conditions.

5.6 Inlet Classification

As presented in section 3.1.1 tidal lagoons can be loosely classified using their tendency towards mixing or stratification. The crude analysis of Lake Bardawil showed that the inlets, under idealized assumptions, lay in the range of well-mixed over SIPS to partially mixed systems. The results shown in section 4.4 state that the inlets can, at all times, be classified as well-mixed systems. Even during low-energetic neap tides or calm wind conditions, this is the case. However, the results on the salinity distribution indicate the temporary existence of stratification in the inlets (Boughaz 2) during distinct meteorological conditions. This Strain Induced Periodic Stratification (SIPS) is a distinct feature of estuarine systems, where large amounts of salt are being transported out of the lagoon. Here also the before discussed property of salt fluxes showed strong increases in the cumulative volume.

Thus, this contradiction causes for reevaluation of the inlet classification of Lake Bardawil on the estuarine parameter space. As this space is defined by the freshwater Froude number Fr_f and the Mixing parameter M, the input for these very variables requires a second look. While for Fr_f the values are in the same range as found in the idealized calculation, M overshoots the idealized bound by far. Reasons for this are found in the different depth H and the tidal velocity U_T. Larger depth, as well as larger velocities, cause the mixing parameter to increase significantly.

From this, it has to be acknowledged that for investigating the effects of annual extreme weather conditions on a tide-dominated system, the classification on the estuarine parameter space does not allow for a good representation. This is due to the generalization of the variables involved, where an average of the maximum values is chosen. However, the conditions over individual tidal cycles can differ significantly.

Here it needs to be kept in mind is that this classification is more of a loose, conceptual way to describe (real) estuarine systems. While Lake Bardawil, as a hypersaline, shallow coastal does not necessarily comply with this.

As it was shown in the results the inlets of Lake Bardawil depict variable conditions as a consequence of the imposed forcing. Meaning a general classification is not possible. Considering shorter time scales could allow for the classification of the inlets on the estuarine

parameter space during or following extreme events. While the longer time scales considered promote the impact of the tidal dominance in the calculations.
Shorter time scales would take the highly dynamic nature of tidal inlets into account and allow for a more detailed analysis of the inlet.

5.7 System Adaptations

The system adaptation as proposed by TWM, were modeled and their impact concerning the overall salinity distribution in the lagoon and the inlet characteristics was investigated.
From the above shown results, it can be said that the proposed adaptations by means of two additional tidal inlets and the dredging of tidal gullies through the lagoon have a clear impact on the lagoon waters.
As was shown with the results of the simulation, the overall lagoon salinity decreases, and the stretches where previously high saline waters resided now exchange water with the Mediterranean. Along the barrier island, a stretch of waters is observed which has salinities in the range of the adjacent Mediterranean Sea. However, along the southern shore waters of very high salinity (*>45 ppt*) are still observed, which shows that even after dredging the deeper tidal gullies through the eastern basin, the wind-driven circulation continuously pushes water towards the shores. This observation is in line with the idealized NW wind experiment by Bek and Cowles (2018) where they showed that wind-driven subtidal flows, present in the lagoon push waters towards the southern edge of the basin.
The presence of weak SIPS in Boughaz 1 & 3 towards the end of the month of April shows however a clear effect of the deepened channels through the lagoon. Here more saline waters are being transported towards the inlet, regardless of any pronounced weather event. This complies with literature by Smith (1994) where deeper waters promote density-driven flows facilitating gravitational circulation.
This shows the improved connectivity of the inner lagoon itself and with the Mediterranean Sea where over the course of a month different states of the inlet can be observed as a consequence of meteorological forcing in interaction with the tidal cycle.

5.8 Modelling Aspects

As already mentioned in the discussion on the implementation of evaporation in the model, the model domain influences the quality of the results. The large extent of the overall model domain comes at a high computational expense when including the third dimension. This expense includes time but also storage, which proved to be of importance along with the modeling campaign.

Here, the scarcity in data and the plan of building upon the 2DH model by van Bentem (2020) caused the use of this existing model, in which the boundary conditions were tried and tested throughout the previous modeling campaigns.

However, after experiencing the large increase in computational time and required storage it is smart to decrease the model domain significantly and increase the stability of the boundaries. For the latter, however reliable data needs to be present. Furthermore, it came to attention that a three-dimensional model of the Mediterranean Sea was set up by Deltares, from which new boundary and initial conditions could be obtained.

At last, considering the chosen simulation periods (February, April, August) it can be said that the periods modeled are in line with initial expectations. Here the average month (April) displays a middle ground between the two extreme conditions with rising evaporation rates but also stronger wind events occurring. For the other two months, the results show highly dynamic conditions for the extreme wind conditions and calm conditions during the extreme evaporation conditions.

6 | Conclusion & Recommendations

6.1 Conclusion

This study looked at the effects of annual extreme weather conditions on the hydrodynamics of Lake Bardawil. A hypersaline, shallow coastal lagoon along the coast of the northern Sinai Peninsula in Egypt. Besides being a unique geographical landmark in the Mediterranean Sea along Egypt's northern coast, Lake Bardawil is home to fishing grounds and salt exploitation, important for the communities living around it.

A deeper understanding of the hydrodynamics and the movement of salt through the lagoon allows for tailor-made engineering solutions to restore the ecosystem in decline and enhance exchange flows with the adjacent Mediterranean Sea.

The analysis of the three presented weather conditions during the year, defined as the average month (April), the extreme wind month (February), and the extreme evaporation month (August), answers the initially posed research question on

"How do annual extreme weather conditions affect the subtidal flows present in hypersaline and shallow coastal lagoons using the example case of Lake Bardawil?"

In the following section, the sub-questions are answered subsequently leading up to answering the main research question as shown above.

What are the dominant forcing terms for subtidal flows?

By carrying out a thorough literature study on tidal-influenced coastal waters, the answer was found in the fundamentals of estuarine physics. From research on estuarine systems, where the interaction of water masses with different salinities is present, three forcing terms were determined that can dominate the subtidal/residual flows.

The first one is the bathymetry-induced residual, which stems from the interaction of the tidal flow with the complex bathymetries present in many tidal-influenced systems. Here the presence of deeper tidal channels and shallower (inter-)tidal flats cause flow acceleration and deceleration during ebb and flood. In addition to these simple bathymetrical features, any non-uniformity in the bathymetry causes the flows to deviate from a uniform flow field and hence can cause residual flows.

A second forcing that can have a large impact on the presence of subtidal flows is the wind-driven forcing. Due to the wind drag on the water body, a shear stress is imposed on the surface, which penetrates over the depth and can cause return flows along the bottom. The latter might be enhanced by the geostrophic flows, which stem from the water level set-up due to continuous wind exposure and cause a compensative return flow along the deeper layers.
The triplet is concluded by the density-driven forcing, which is present in systems where horizontal density gradients in combination with tidal flows cause the so-called gravitational circulation. Here the layering of lighter surface waters and heavier bottom waters is the result of opposing flows over the vertical where the heavier and more saline waters move along the bottom. This process is enhanced by the lighter, incoming waters during flood.
Throughout the study, it became evident that, if present, wind-driven flows cause circulation patterns that are dominating the overall lagoon behavior and can act as an initiator for density-driven flows.

How are the subtidal flows affected by annual extreme weather conditions?

The residual discharges in the inlets show a clear response to the different annual weather conditions as applied in this study. During the average conditions (April), where the meteorological forcing represents average wind and evaporation conditions, the residual discharges and velocities in the inlets are of smaller magnitude. Here the overall inlet can be seen in balance, where little distortions of the hydrodynamic properties over the course of the month are seen. Only during very distinct and short-term meteorological forcing, residuals of larger magnitude are observed. The overall behavior throughout the average conditions however depicts a system in balance, where the tidal flow acts as the governing forcing.
During the conditions of extreme wind velocities (February), the two inlets present at Lake Bardawil depict clear residual flows over the month. The presence of these residuals in the inlets is largely dependent on events of very high wind speeds. During these, both inlets depict strong residuals, which however balance each other out. This leads to the smallest residual inflow. This aligns with the lowest evaporation rates. The temporary net inflow during strong wind events can cause complex velocity fields in the inlets, where positive and negative velocities are observed. Here bathymetry-induced flows due to local acceleration-deceleration patterns and the overall geometry are most likely to be the cause of such behavior. For further detail on these flows, one is referred to the study of Panagopoulos (2022).
For the month of peak evaporation (August), the residuals show a very constant behavior, where the inlets depict over the course of the month either inward or outward-directed residuals. In Boughaz 1 the residuals are promoting an inflow by means of an asymmetric tidal signal in an overall tide-dominated inlet. The small, outflowing residuals in Boughaz 2 stem from the strong circulation in the eastern basin, which pushed waters towards the inlet and

promotes density-driven flows along the bottom. On the system scale, these facilitate the largest residual inflow, compensating for the high evaporation rates occurring during August. While short-term events have a short-term impact on the residuals, the long-term phenomenon of evaporation impacts the overall behavior of the residual flows in the inlets.

What are the time scales at which meteorological forcing affects the lagoon hydrodynamics and salinity distribution?

As shown in this study, the timescale on which subtidal flows act is very much dependent on the dynamics and geometry of the system. In the western stretch of Lake Bardawil (Boughaz 1), only a small impact of the meteorological forcing on the subtidal flows is observed. This is limited to short-term NE winds, which only cause short-term responses.
For Boughaz 2, which is the entrance and exit for the waters of the vast water body in the east, the overall response of the inlet to meteorological forcing is much slower. During and after periods of high evaporation the inlet depicts the characteristics of SIPS, where the bottom waters remain of significant higher salinity in comparison to the surface waters. This causes a constant density-driven residual along the bottom layer over the time scale of days. This is also seen by the persistent higher salinities along the bottom after averaging.
For the overall system, it can be concluded that no generalized time scales could be determined for the effect of meteorological forcing. It however can be said is that the water body behind the inlet is of crucial importance for the temporal response of the inlet to extreme meteorological forcing. Here the susceptibility to circulation patterns of the behind lying water body plays a major role which can cause the persistence of density-driven, subtidal flows towards the deeper regions and inlets.

How is the state of the inlets affected by extreme weather conditions?

The state of the inlets as introduced in this study is an indicator of tidal-influenced systems and their characteristics with respect to their mixing/stratifying behavior. For the system of Lake Bardawil, it is concluded that very strong meteorological forcing by means of wind and evaporation can cause a temporary change in the inlet state.
While both Boughazes resemble well-mixed conditions most of the time and are found in that range on the estuarine parameter space, distinct forcing can cause a temporary shift in the state of the inlets. Here the presence of SIPS in Boughaz 2 is the most remarkable observation made. This phenomenon is initiated by W-SW wind conditions in combination with the present hypersaline waters and the successive density-driven flows.
Further, it can be concluded that the inlets show larger susceptibility to changes in the inlet state during neap tidal periods. Here the less energetic tidal environment promotes stronger subtidal flows and the presence of temporary stratification in the inlets.

At last, it was found that the inlets do behave very differently with respect to the annual extreme weather conditions. While Boughaz 1 is in general of well-mixed state, Boughaz 2 is prone to temporary/periodic changes in its state.

What is the effect of proposed system adaptations on the exchange flows between Lake Bardawil and the Mediterranean Sea during the average conditions (April)?

As mentioned in the discussion on the effect of the system adaptations they show an increasing exchange between Lake Bardawil and the Mediterranean Sea. This causes a strong decrease in the average lagoon salinity. Furthermore, the difference in surface and bottom layer salinity at the considered stations showed values in an equal range. Indicating an overall well-mixed system in the vicinity of the inlets and the broad stretch along the barrier island.
The presence of weak stratification in the western inlets but also the eastern inlets at times further shows increased connectivity of the overall lagoon. Here in Boughaz 1 weak stratification was observed, where towards the end of the month weak SIPS/stratification in the western inlets Boughaz 1 & 3 could be seen.
The increased well-mixed state of the inlets speaks for a more dynamic system, where the abovementioned tidal divide is not present anymore and thus the exchange flows between the two lagoon parts (western bottleneck & easter basin) as well as between the lagoon and the Mediterranean Sea are visibly enhanced. On the contrary, the most southern areas in the eastern basin show little changes when observing the spatial salinity distribution. Here the dominant N-NW winds continue to push and trap saline waters into these areas.
Overall, the application of system adaptations enhances the exchange flows between Lake Bardawil and the Mediterranean Sea, which creates more dynamic and favorable conditions for the ecosystem to restore itself.

How do annual extreme weather conditions affect the subtidal flows present in hypersaline and shallow coastal lagoons using the example case of Lake Bardawil?

In conclusion of this study, the here presented results provide a solid base to make a statement on the effects of annual extreme weather conditions on the subtidal flows present in Lake Bardawil.

As laid out in the simulation results of an average month (April), a month of extreme wind conditions (February) and a month of extreme evaporation conditions (August), the lagoon and its inlets depict a large variability according to the present meteorological conditions.
A first conclusion that is made is that the complex geometry of Lake Bardawil plays a major role when it comes to the effect of meteorological forcing on the lagoon and the inlets. Here, geometrical features such as the islet west of Boughaz 1 or the tidal divide on the verge of the

western bottleneck and the eastern basin are of great importance. By their presence, the inner lagoon connectivity is limited. Allowing for subtidal, wind-driven circulation the eastern basin shows much stronger responses to present meteorological conditions, whereas the western stretch does remain largely unaffected in terms of circulation patterns.

The shallowness of Lake Bardawil promotes wind-driven circulation along the streamlines of the prevailing wind which in consequence dominates the response of the lagoon. This is pronounced during periods of high wind velocities and occasional storms in the winter months. But, even during extreme evaporation conditions, wind remains the main driver of subtidal circulation. By imposing surface shear stresses on the shallow lagoon waters, it initiates a circulation which in consequence promotes density-driven flows in the deeper regions around and in the inlets. These flows, causing pronounced subtidal velocity in the inlets, show the significance of the meteorological conditions around systems like Lake Bardawil.

Even though wind governs the subtidal flows in the inner lagoon, the strong evaporation rates throughout the year cause the continuous, residual inflow into the system through the two present inlets. This is in line with the expectation from literature and the system governing water balance. Furthermore, the susceptibility for density-driven flows increases with increasing evaporation rates. Here the vast extent of high salinities causes for stronger density-driven flows in the inlets.

In summary, it is found that extreme weather conditions including very strong wind conditions and extreme evaporation rates, can cause subtidal flows of significant magnitude transporting water and salt in hypersaline and shallow coastal lagoons similar to Lake Bardawil. While the shallow bathymetry is governing for the initial motion of subtidal flows by wind-driven forcing, the hypersaline waters cause density-driven flows in the deeper regions and around the inlets. Here the observed, vertical salinity gradients in the inlets following from density-driven flows are an indicator for that. Further, the inlet geometry can cause complex flow fields during periods of strong winds.

From the greater lagoon area, it was seen that flows observed in the inlets are strongly related to the behind lying water body. Thus, promoting the application of system adaptations to increase the connectivity of the inner lagoon areas with the Mediterranean Sea.

6.2 Recommendations

Data Availability

As repeatedly mentioned in this study, the shortage of data limits the accuracy of the numerical model. This is by means of input data but more importantly by means of validation data.
For the input data, it is recommended to make use of the available open-source data as already done for the climate data. Using data from validated models helps in setting up a sound and stable model. Concerning that, an important aspect are the initial conditions. The here applied 2DH distributions of salinity and temperature showed erroneous values in the remote and isolated areas. By using data from, for example, a 3D Mediterranean Sea model developed by Deltares would allow for better initial conditions as well as redefined boundary conditions.
The latter is important when optimizing the model and decreasing the domain.
At last, the quality of the validation data is crucial when using numerical models. As this study showed the correlation with current validation data ranges between very good to fair. Increasing the accuracy would be possible when extensive local salinity and velocity measurements are available. These would allow for better validation of the three-dimensional results from the presented model.

Long-term Modelling

The differences between the validation data and the modeled data are likely the consequence of the short-term model that was carried out here. As introduced in this study, the subtidal flows which transport waterborne characteristics such as salt act on longer time scales with lower velocities. By modeling over a longer period, these processes are thought to be represented more accurately. This in consequence will lead to more accurate predictions of the overall lagoon data. Foremost concerning the salinity distribution.
Considering the period modeled in the validation data, a four-year period is compared with a two-month period.
Hence it is recommended to set up a long-term model to increase the quality of the results. This model should consider at least a period of two years, to account for the climate effects accordingly.
Furthermore, when assessing the effect of the system adaptations the long-term effect is of crucial interest as here the goal is to provide predictions of the lagoon behavior after implementing the adaptations.

Morphological Modelling

Up to present knowledge, this study was the first in line to look at the depth-varying effects of the annual extreme weather conditions on the hydrodynamics and the transport of salt. As seen in the results, at times strong subtidal velocities can be present in the inlets which concentrate along the bottom layer.
As the inlets are prone to siltation and can currently be characterized as unstable, it would be of interest how these subtidal flows may affect the sediment transport character of the inlets.
As come to attention there is a hybrid model which simplifies the 3D approach by Delft3D and aims at representing morphological changes in a 2DH model by introducing a new sediment transport formulation. While this model is still in calibration it might be, for future purposes, an interesting option when modelling morphological changes in tidal influenced coastal waters similar to Lake Bardawil.

System Adaptations

As the results on the system adaptations show does the system respond rather quick to the introduced measures and shows a beneficial outcome. Since the aim of this study was not to recommend new adaptations but to evaluate the impact of the concept design by TWM, it will not be done here.
However, there are two remarks which can be given:

1) To make sound predictions on the overall lagoon response over time, a long-term model as mentioned above should be considered. Only then clear prediction regarding the salinity distributions can be made.
2) From the results it is seen that the southern extent of the eastern basin requires more attention. From the present knowledge it could be smart to deepen/widen the tidal gullies to facilitate more density-driven flows and enhance the wind-driven flows. The applicability and feasibility of this would however need additional prove by means of the abovementioned long-term model.

References

Abdel-Fattah, Sommer, Mohamed Ali Bek, and Abdelazim M. Negm, eds. 2019. *Egyptian Coastal Lakes and Wetlands: Part I: Characteristics and Hydrodynamics*. 1st ed. 2019. Cham: Springer International Publishing : Imprint: Springer.

Arcement, George J., and Verne R. Schneider. 1989. *Guide for Selecting Manning's Roughness Coefficients for Natural Channels and Flood Plains*. *Report*. 2339. USA: U.S. Department of the Interior. doi: 10.3133/wsp2339.

Barua, Dilip K. 2017. 'Seabed Roughness of Coastal Waters'. Pp. 1–6 in *Encyclopedia of Engineering Geology, Encyclopedia of Earth Sciences Series*, edited by P. Bobrowsky and B. Marker. Cham: Springer International Publishing.

Beck, Hylke, Niklaus Zimmermann, Tim McVicar, Noemi Vergopolan, Alexis Berg, and Eric Wood. 2018. 'Present and Future Köppen-Geiger Climate Classification Maps at 1-Km Resolution'. *Scientific Data* 5:180214. doi: 10.1038/sdata.2018.214.

Bek, M. A., and G. W. Cowles. 2018. 'A Three-Dimensional Circulation Model of Lake Bardawil, Egypt'. Pp. 265–83 in *Egyptian Coastal Lakes and Wetlands: Part I*. Vol. 71, *The Handbook of Environmental Chemistry*, edited by A. M. Negm, Mohamed Ali Bek, and S. Abdel-Fattah. Cham: Springer International Publishing.

van Bentem, Rick. 2020. 'Morphological Response to Lake Bardawil Adaptations - Assessment of Inlet Stability for Multiple System Interventions'. Master Thesis, TU Delft, Netherlands.

Bosboom, Judith, and Marcel Stive. 2021. *Coastal Dynamics*. Delft, Netherlands: TU Delft.

Burchard, Hans, and Robert D. Hetland. 2010. 'Quantifying the Contributions of Tidal Straining and Gravitational Circulation to Residual Circulation in Periodically Stratified Tidal Estuaries'. *Journal of Physical Oceanography* 40(6):1243–62. doi: 10.1175/2010JPO4270.1.

David, Laura, and Björn Kjerfve. 1998. 'Tides and Currents in a Two-Inlet Coastal Lagoon: Laguna de Términos, México'. *Continental Shelf Research* 18:1057–79. doi: 10.1016/S0278-4343(98)00033-8.

Deltares. 2021. 'D-Flow Flexible Mesh - User Manual'.

Egyptian Environmental Affairs Agency (EEAA). 2016. *Summary: Field Trip Results for the Egyptian Lakes Environmental Monitoring Program 'Bardawil Lake'*. *Field Trip Summary*. Ministry of State for Environmental Affairs.

El Kafrawy, Sameh B., Mohamed Ali Bek, and Abdelazim M. Negm. 2019. 'An Overview of the Egyptian Northern Coastal Lakes'. in *Egyptian Coastal Lakes and Wetlands: Part I - Characteristics and Hydrodynamics*. Vol. 71, *The Handbook of Environmental Chemistry*, edited by A. M. Negm, M. A. Bek, and S. Abdel-Fattah. Springer Nature Switzerland.

El-Bana, Magdy, Abdel-Hameid Khedr, Piet Van Hecke, and Jan Bogaert. 2002. 'Vegetation Composition of a Threatened Hypersaline Lake (Lake Bardawil), North Sinai'. *Plant Ecology* 163(1):63–75. doi: 10.1023/A:1020351704409.

Ellah, Radwan, and Maged Hussein. 2009. 'Physical Limnology of Bardawil Lagoon, Egypt'. *American-Eurasian J. Agric. Environ. Sci.* 5.

El-Shabrawy, G. M., and M. A. Bek. 2019. 'Responses of Zooplankton to Long-Term Environmental Changes in the Egyptian Coastal Lakes'. in *Egyptian Coastal Lakes and Wetlands: Part II - Climate Change and Biodiversity, The Handbook of Environmental Chemistry*. Cham: Springer International Publishing : Imprint: Springer.

Euroconsult. 1995. *Bardawil Development Project - Management of the Environmental Parameters. Technical Report*. Netherlands.

Frihy, O. E., A. A. Badr, M. A. Selim, and W. R. El Sayed. 2002. 'Environmental Impacts of El Arish Power Plant on the Mediterranean Coast of Sinai, Egypt'. *Environmental Geology* 42(6):604–11. doi: 10.1007/s00254-002-0563-6.

Gat, J. R., and Y. Levy. 1978. 'Isotope Hydrology of Inland Sabkhas in the Bardawil Area, Sinai: Hydrology of Sabkhas'. *Limnology and Oceanography* 23(5):841–50. doi: 10.4319/lo.1978.23.5.0841.

Georgiou, M. 2019. 'Innovative Tidal Inlet Design - Design Methodology for Boughaz 1 Inlet, Lake Bardawil'. Master Thesis, TU Delft, Netherlands.

Geyer, W. Rockwell, and Parker MacCready. 2014. 'The Estuarine Circulation'. *Annual Review of Fluid Mechanics* 46(1):175–97. doi: 10.1146/annurev-fluid-010313-141302.

Khalil, Magdy, and Kamal Shaltout. 2006. *Lake Bardawil and Zaranik Protected Area*.

Kjerfve, Björn, and K. MaGill. 1989. 'Geographic and Hydrodynamic Characteristics of Shallow Coastal Lagoons'. *Marine Geology - MAR GEOLOGY* 88:187–99. doi: 10.1016/0025-3227(89)90097-2.

Kranenburg, Wouter, and Julien Groenenboom. 2021. 'Correspondance on the 3D Modelling of Coastal Lagoons with Delft3D FM'.

Krumgalz, Boris, Hava Hornung, and Oton Oren. 1980. 'The Study of a Natural Hypersaline Lagoon in a Desert Area (the Bardawil Lagoon in Northern Sinai)'. *Estuarine and Coastal Marine Science* 10:403–15. doi: 10.1016/S0302-3524(80)80120-4.

Lanters, M. J. C. 2016. 'A Hydrological Design of Lake Bardawil: Geometric Adaptations to Enhance Ecological Values'. Master Thesis, TU Delft, Netherlands.

Linnersund, Jonas, and Erik Mårtensson. 2008. 'Hydrodynamic Modelling and Estimation of Exchange Rates for Bardawil Lagoon, Egypt. An Investigation of Governing Forces and Physical Processes Using Numerical Models.' Master Thesis, Lund University, Sweden.

Miller, John M., Leonard J. Pietrafesa, Ned P. Smith, and FAO, eds. 1990. *Principles of Hydraulic Management of Coastal Lagoons for Aquaculture and Fisheries*. Rome: Food and Agriculture Organization of the United Nations.

Nassar, Karim, Wael Elham Mahmod, Ali Masria, Hassan Fath, and Kazuo Nadaoka. 2018. 'Numerical Simulation of Shoreline Responses in the Vicinity of the Western

Artificial Inlet of the Bardawil Lagoon, Sinai Peninsula, Egypt'. *Applied Ocean Research* 74:87–101. doi: 10.1016/j.apor.2018.02.015.

Officer, Charles B. 1976. *Physical Oceanography of Estuaries (and Associated Coastal Waters)*. New York: Wiley.

Panagopoulos, Loukianos. 2022. 'Working Title: Investigation of Secondary Flows in Tidal Inlet Design. Case Study: Lake Bardawil, Egypt'. Master Thesis, TU Delft, Netherlands.

Phillips, Jeff V., and Saeid Tadayon. 2006. *Selection of Manning's Roughness Coefficient for Natural and Constructed Vegetated and Non-Vegetated Channels, and Vegetation Maintenance Plan Guidelines for Vegetated Channels in Central Arizona - Scientific Investigations Report 2006-5108. Scientific Investigations Report*. 5108. U.S. Department of the Interior.

Pietrzak, Julie. 2020. *Reader for CIE5325: An Introduction to Coastal and Basin-Scale Physical Oceanography for Civil and Offshore Engineers*. Delft: TU Delft.

Pritchard, D. W. 1952. 'Estuarine Hydrography'. Pp. 243–80 in Vol. 1, *Advances in Geophysics*, edited by H. E. Landsberg. Elsevier.

Simpson, J. H., J. Brown, J. Matthews, and G. Allen. 1990. 'Tidal Straining, Density Currents, and Stirring in the Control of Estuarine Stratification'. *Estuaries* 13(2):125–32. doi: 10.2307/1351581.

Smith, N. P. 1994. 'Water, Salt and Heat Balance of Coastal Lagoons'. in *Coastal Lagoon Processes, Elsevier Oceanography Series*, edited by B. Kjerfve. Amsterdam, The Netherlands: Elsevier Science Publisher B.V.

Swenson, Erick M., and Wen-Ssn Chuang. 1983. 'Tidal and Subtidal Water Volume Exchange in an Estuarine System'. *Estuarine, Coastal and Shelf Science* 16(3):229–40. doi: https://doi.org/10.1016/0272-7714(83)90142-7.

The Weather Makers and DEME Group. 2021. 'Lake Bardawil Development Project - Extended Summary'.

Webster, Ian T. 2010. 'The Hydrodynamics and Salinity Regime of a Coastal Lagoon – The Coorong, Australia – Seasonal to Multi-Decadal Timescales'. *Estuarine, Coastal and Shelf Science* 90(4):264–74. doi: 10.1016/j.ecss.2010.09.007.

Winant, Clinton D., and Guillermo Gutiérrez de Velasco. 2003. 'Tidal Dynamics and Residual Circulation in a Well-Mixed Inverse Estuary'. *Journal of Physical Oceanography* 33(7):1365–79. doi: 10.1175/1520-0485(2003)033<1365:TDARCI>2.0.CO;2.

Appendix

A. Climate Data

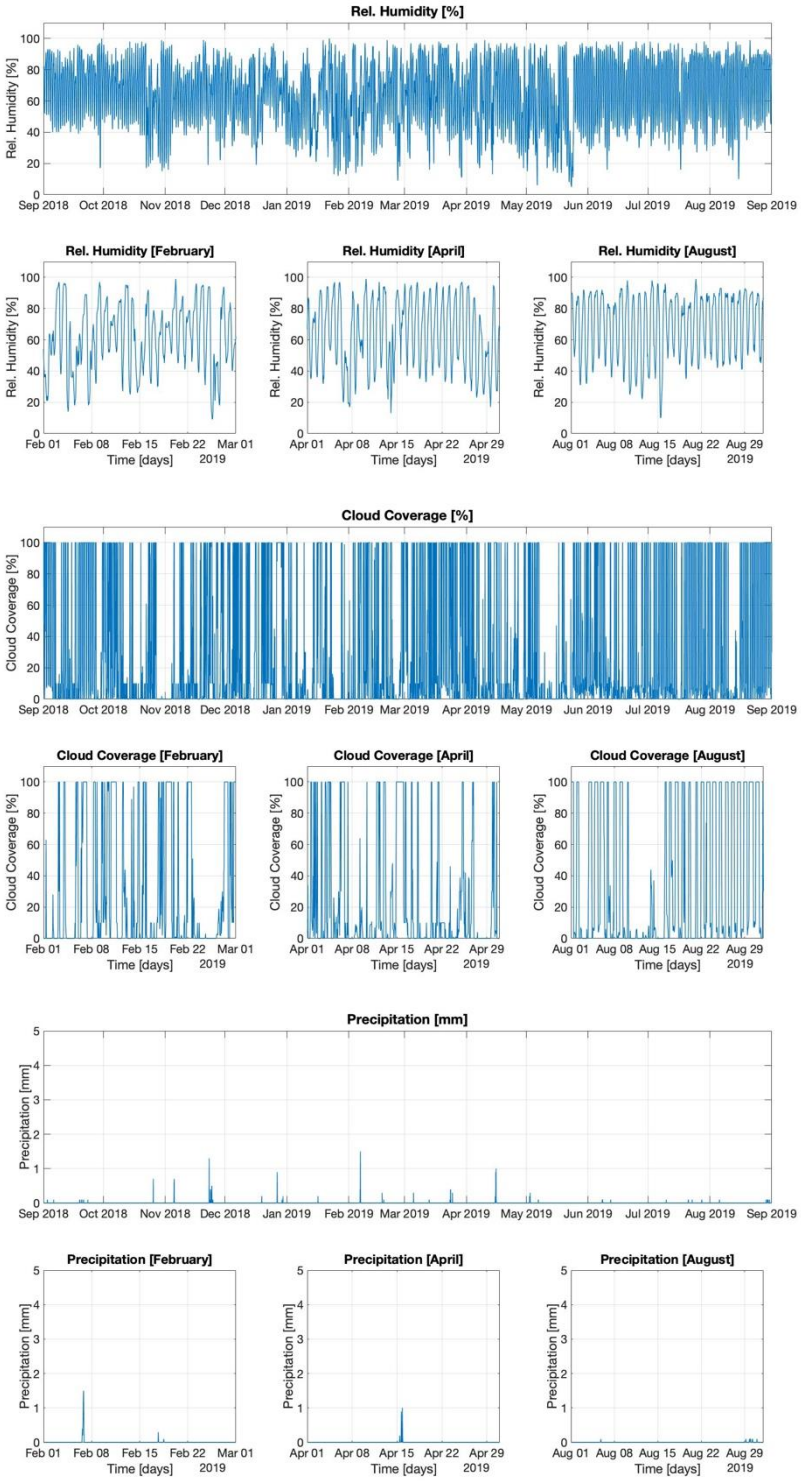

Figure 33: Remaining climate data including the relative humidity [%], cloud coverage [%] and precipitation [mm]

B. Determination of freshwater Froude number

To get a first idea of how the inlets of Lake Bardawil are situated within the regimes for estuaries, as shown in Figure 10, the freshwater Froude number is determined here. This is, as already mentioned before, done based on the compensation flow from the Mediterranean Sea into the lagoon due to the net loss of water by evaporation.

To find the freshwater Froude number, equation 2 needs to be resolved, including some assumptions. The calculation is shown below.

$$Fr_f = \frac{U_R}{(\beta g s_{ocean} H)^{1/2}}$$

In here the freshwater flow velocity U_R following from the river runoff is substituted by the compensation flow velocity U_{comp}. β is a scaling coefficient for the salinity (≈ 7.7x10^{-4}), g the gravitational constant (= 9.81 m/s^2), s_{ocean} the underlying salinity of the ocean/lagoon (≈ 45 ppt) and H the water depth. To determine $U_{comp.}$ the following assumptions are made

- evaporation takes place evenly over the whole lagoon area
- the evaporation rates of February, April, and August are taken as representatives for the minimum, average and maximum conditions
- the compensation flow appears proportionately through Boughaz 1 & 2, meaning the velocities are equal

$$Q_{comp,tot,j} = E_{lagoon,j}$$

In which E_{lagoon} is the net loss of water by evaporation taken from Khalil and Shaltout (2006) in m^3. The coherent velocity is determined as follows

$$U_{comp,tot,j} = \frac{E_{lagoon,j}}{A_{tot}}$$

The compensation flow velocities in the respective inlet are then calculated by

$$U_{comp,i,j} = U_{comp,tot,j}/2$$

The freshwater Froude number is then calculated for the respective inlet and the respective month. The input values and results of these calculations are shown in Table 21.

Table 21: Results from the calculations of the freshwater Froude Number for the two inlets Boughaz 1 & Boughaz 2

	Parameters	February	April	August
Input	β [-]	$7.7x10^{-4}$		
	g [m/s^2]	9.81		
	$H_{Boughaz1}$ | $H_{Boughaz2}$ [m]	5 | 6		
	s_{ocean} [ppt]	30	45	60
	$E_{lagoon,j}$ [m^3]	$40.04x10^6$	$69.30x10^6$	$97.34x10^6$
	$A_{Boughaz1}$ | $A_{Boughaz2}$ [m^2]	954 | 1386		
	A_{tot} [m^2]	2340		
Results	$U_{comp,tot}$ [m/s]	$6.4x10^{-3}$	$11.4x10^{-3}$	$15.5x10^{-3}$
	$U_{comp,Boughaz1}$ [m/s]	$3.2x10^{-3}$	$5.7x10^{-3}$	$7.7x10^{-3}$
	$U_{comp,Boughaz2}$ [m/s]	$3.2x10^{-3}$	$5.7x10^{-3}$	$7.7x10^{-3}$
	$Fr_{f,Boughaz1}$	**$3.0x10^{-3}$**	**$4.4x10^{-3}$**	**$5.1x10^{-3}$**
	$Fr_{f,Boughaz2}$	**$2.8x10^{-3}$**	**$4.0x10^{-3}$**	**$4.7x10^{-3}$**

C. Derivation of the vertical velocity profile

To come to the expression as presented by Officer (1976) the starting point are the Reynolds averaged Navier Stokes Equations (RANSE). Being interested in the depth-dependent horizontal velocity profile the horizontal momentum balance of the RANSE reduces to the following expression, under the assumptions of neglecting the inertial terms

$$\frac{\partial p}{\partial x} = \rho N_z \frac{\partial^2 u}{\partial z^2}$$

Here the left-hand side represents the horizontal pressure term which is balanced by the horizontal velocity term on the right-hand side. The pressure term is composed of the barotropic pressure due to the surface elevation and the baroclinic pressure term due to the present density differences. Hence the left-hand side can be written as

$$\frac{\partial p}{\partial x} = -\rho g \frac{\partial \zeta}{\partial x} + gz \frac{\partial \rho}{\partial x} = -\rho g i + g\lambda z$$

In which $i = \partial\zeta/\partial x$ and represents the water surface slope and $\lambda = \partial\rho/\partial x$ which represents the horizontal density gradient.

Combining the two equations shown above we obtain the following second-order differential equation

$$\frac{\partial^2 u}{\partial z^2} = -\frac{gi}{N_z} + \frac{g\lambda}{\rho N_z} z$$

By imposing zero-velocity boundary conditions at the surface as well as at the bottom the solution to the second-order differential equation is

$$u = \frac{gi}{2N_z}(h^2 - z^2) - \frac{g\lambda}{6\rho N_z}(h^3 - z^3)$$

For estuaries, where the freshwater runoff r needs to balance the integral of the above-shown velocity the expression becomes

$$r = \frac{gi}{3N_z} h^3 - \frac{g\lambda}{8\rho N_z} h^4$$

Now, considering the fact that r often is very small we can find a solution for *i* in relation to the horizontal density gradient, being $i = \frac{3}{8}\frac{\lambda h}{\rho}$. Following this, the horizontal density-driven velocity profile equates to

$$u = \frac{1}{48}\frac{g\lambda h^3}{\rho N_z}(8n^3 - 9n^2 + 1)$$

Including the effect of wind by means of its depth effect

$$\tau = -\rho N_z \frac{\partial u}{\partial z}$$

The above-mentioned equation extents to

$$u(z) = \frac{gi}{2N_z}(h^2 - z^2) - \frac{g\lambda}{6\rho N_z}(h^3 - z^3) + \frac{\tau}{\rho N_z}(h - z)$$

Following the same procedure as above we end up with the expression as shown in equation 4.

$$u(z) = \frac{1}{48}\frac{g\lambda h^3}{\rho N_z}(1 - 9n^2 + 8n^3) + \frac{3}{2}v_0(1 - n^2) + \frac{1}{4}\frac{h\tau}{\rho N_z}(1 - 4n + 3n^2)$$

In which $n = z/h$.

D. Spatial Roughness Distribution

As mentioned in section 2.2.7 this appendix will briefly elaborate on the spatial distribution of the bed roughness. It will also give a brief insight into the relationship between the Manning and visualized Chezy coefficient.

Figure 34 shows the two scenarios in which the left assumes the default setting with a Manning coefficient of $n = 0.023\ s/m^{1/3}$ and the right plot shows the roughness after including the field data.

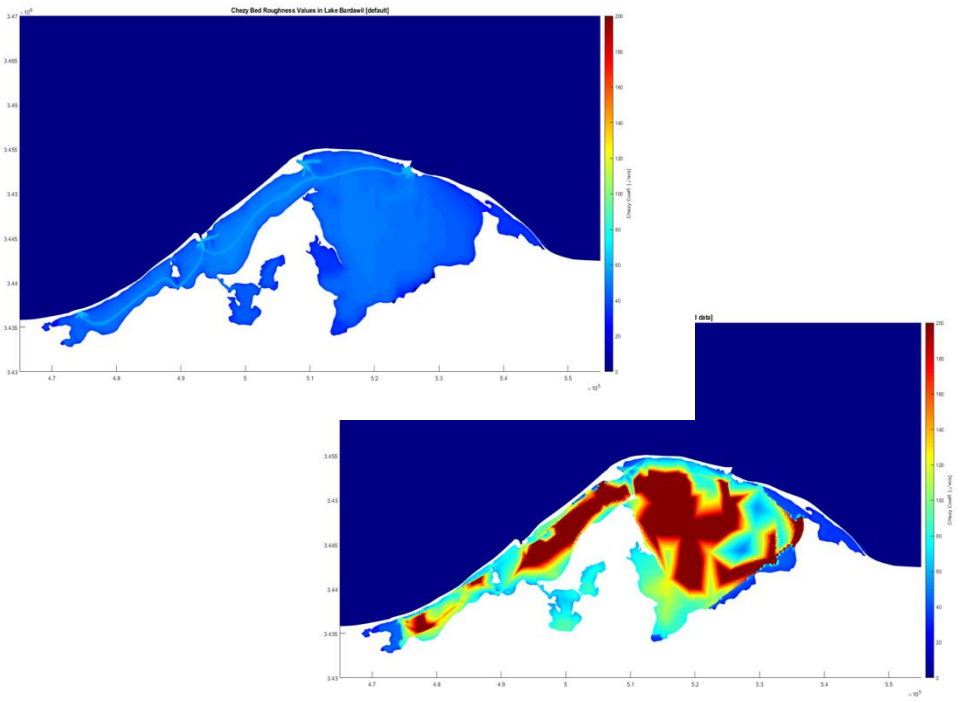

Figure 34: Spatial Distribution of the Chezy Roughness Coefficient over the lagoon area. Left: Default setting with a comp. Manning Coefficient of n = 0.023. Right: Applied field data and its coherent Chezy Coefficients over the lagoon area.

As visible in Figure 34 the default setting applies a rather uniform bed roughness, which is in line with the fact that an initial roughness coefficient is applied. This is then adjusted according to the local conditions, meaning taking the local water depth into account. This causes variations in especially the very shallow areas. Overall, however, the here shown Chezy values are in the range of *40* to *60* $m^{1/2}/s$. These are common values for sandy environments where the lower values appear along the fringes of the lagoon, representing rougher conditions.

For the case where a spatially varying roughness distribution was applied using the fit-to-data analysis, much larger differences are visible. While along the shoreline the values are in the expected range, in the inner lagoon the Chezy values exceed *200* $m^{1/2}/s$, which is not realistic.

The reason for the good fit along the shores of the eastern basin is that along the shores the data coverage is low and hence the default value is applied. The large values in the inner basin and along the bottleneck towards the west stem from the fact that here the combination of fine sediments as well as deeper waters is dominant. The equation below shows how the Chezy values are determined from the Manning values in the numerical model (Deltares 2021).

$$C = \frac{H^{\frac{1}{6}}}{n}$$

In which C is the Chezy coefficient [$m^{1/2}/s$], H is the local water depth [m] and n is the Manning value [$s/m^{1/3}$].

Low Manning values, originating from finer sediments and greater depth, cause significant increases in the Chezy values. When imposing the default value for the Manning coefficient only the local water depth influences the coherent Chezy coefficient, leading to a much more balanced picture. The large values create a false reality and hence the spatial roughness distribution will not be applied for this model.

E. Wind Direction during simulation periods

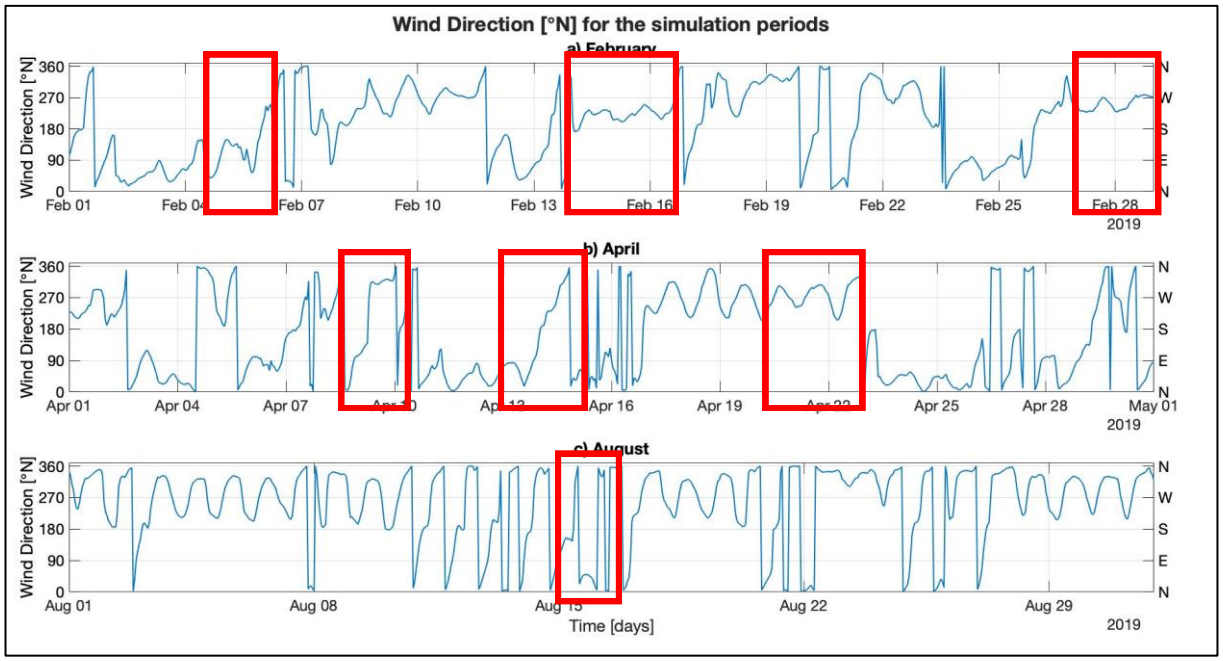

Figure 35: Showing the time series for the wind direction during the simulation periods at Lake Bardawil. Top to bottom showing the data for February, April & August.

Figure 35 shows the time series of the wind direction over the simulation period. Here the markers indicate the events as shown in Figure 23 where strong evaporation occurs, and the wind velocity reaches local maxima.

It is worth mentioning that the low and high values both depict wind directions that are predominantly originating from the north while shifts toward the east and west are present. During the month of February, where the highest wind velocities but also the most dynamic wind climate is expected, a larger variety in the directions is observed. Here more persistent winds coming from the southwest are present as also mentioned by van Bentem (2020). During the month of April already some periods of daily wind patterns can be observed (e.g. around April 18th to April 22nd). In August this daily pattern can be observed more frequently, resembling calmer wind conditions with a certain consistency.

F. Inlet Velocities

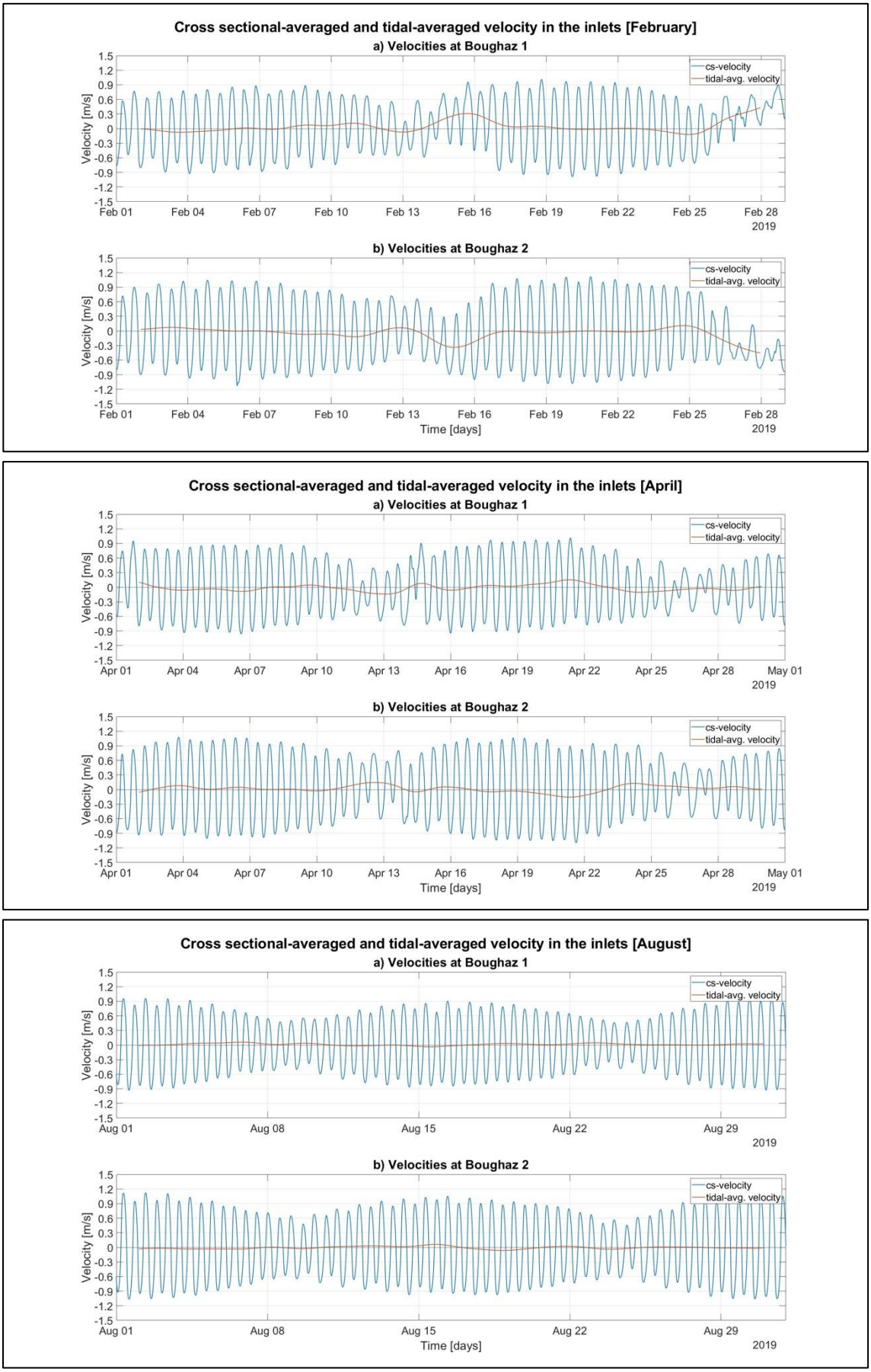

Figure 36: Timeseries of the instantaneous and tidal-averaged velocity [m/s] in the inlets during the status quo simulations. From top to bottom the months of February, April, and August are shown.

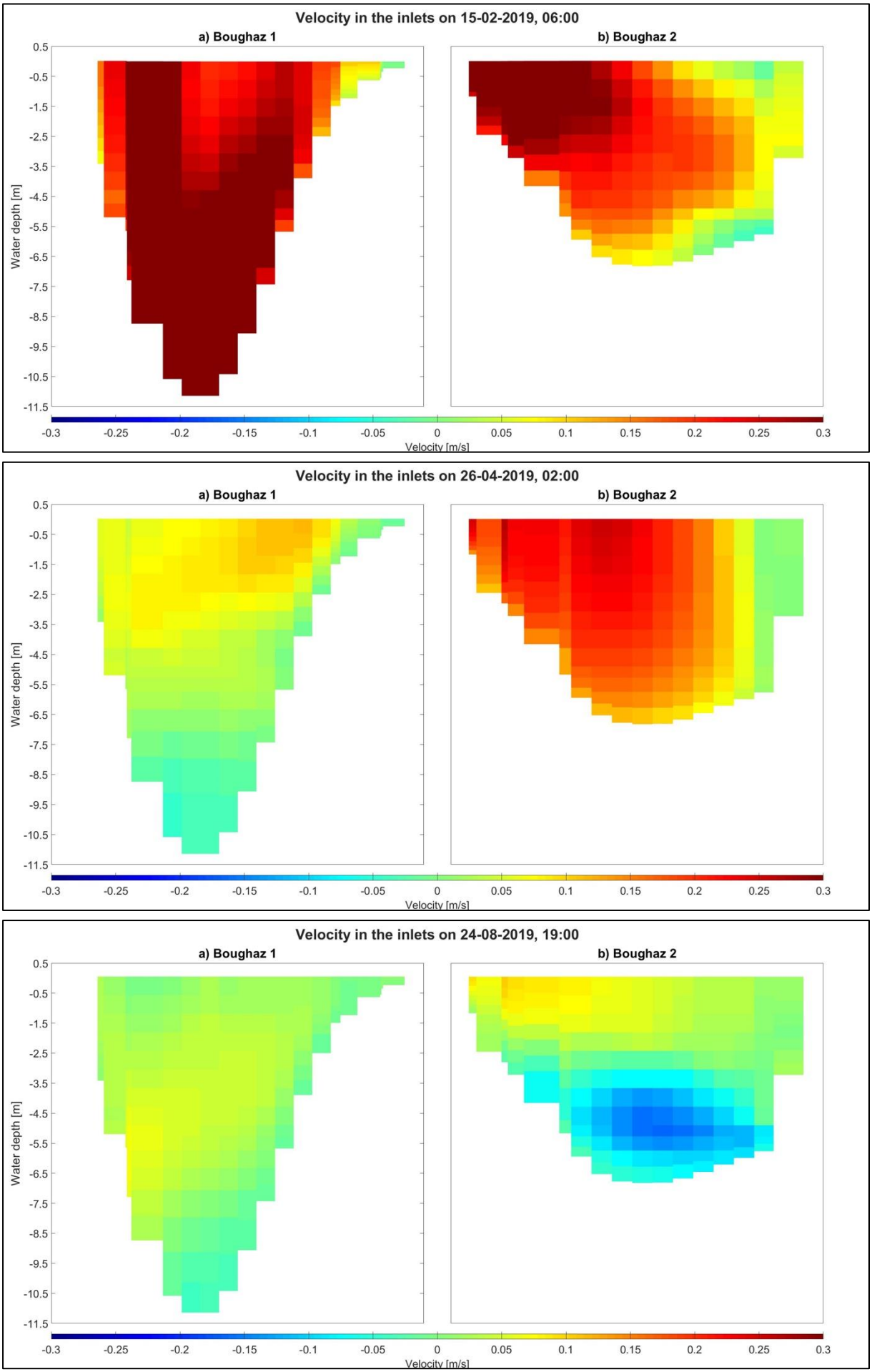

Figure 37: Cross-sectional plot of the inlet velocity [m/s] at individual points in time for February, April, and August (top to bottom). Situations presented always show a point in time after flood.